Abstract

Contents

Introduction

Chapter 1

Lattice field theory

(Something about the fact that in the strong coupling case we cannot apply perturbation theory. It depends on what I will write in the general introduction)

1.1 Quantum field theory and statistical mechanics

We can build a non-perturbative tool for quantum field theory by exploiting the strong similarity between quantum field theory and statistical mechanics. This gives us the possibility of applying Monte Carlo simulations, an intrinsically non-perturbative method, to quantum field theory.

In the path-integral formulation of quantum field theory, the generating functional of correlation functions is defined as:

$$Z[J] = \int \mathcal{D}\phi \exp\left[i \int \mathrm{d}^4x \left(\mathcal{L}[\phi] + J(x)\phi(x) \right) \right], \tag{1.1}$$

where ϕ generically represents the field content of the theory, $\mathcal{L}$ is the Lagrangian and $J(x)$ is an external source field. n-point functions are obtained by applying the functional derivative $\delta/\delta J(x)$ to $Z[J]$ as follows:

$$\begin{aligned} \langle 0| \,\mathrm{T}\phi(x_1)\dots\phi(x_n)\,|0\rangle =& \frac{1}{Z[0]} \prod_{i=1}^{n} \left(-i \frac{\delta}{\delta J(x_i)} \right) Z[J] \Big|_{J=0} = \\ &= \frac{1}{Z[0]} \int \mathcal{D}\phi \; \phi(x_1)\dots\phi(x_n) \exp\left[i \int \mathrm{d}^4x \, \mathcal{L}[\phi] \right], \end{aligned} \tag{1.2}$$

where $|0\rangle$ represents the vacuum state and T the time-ordered product. By performing a Wick rotation, we can make the generating functional 1.1 to be formally equal to the partition function of a statistical mechanical model.

As a concrete example, we consider a complex scalar field theory, with action:

$$S[\phi, \phi^*] = \int \mathrm{d}^4x \, \mathcal{L}[\phi, \phi^*] = \int \mathrm{d}^4x \big(\partial_\mu \phi^* \partial^\mu \phi - m^2 |\phi|^2 - \lambda |\phi|^4 \big), \tag{1.3}$$

and generating functional:

$$Z[J, J^*] = \int \mathcal{D}\phi \mathcal{D}\phi^* \exp\left[iS[\phi, \phi^*] + i \int \mathrm{d}^4x \; J^*(x)\phi(x) + i \int \mathrm{d}^4x \; \phi^*(x) J(x) \right] . \tag{1.4}$$

After performing a Wick rotation ($x^0 = -ix^0_E$, $x^i = x^i_E$), the following changes occur:

$$\begin{aligned} i\mathrm{d}^4x &= \mathrm{d}^4x_E \\ \partial_\mu \phi^* \partial^\mu \phi &= -\delta_{\mu\nu} \partial^\mu_E \phi^* \partial^\nu_E \phi \; . \end{aligned} \tag{1.5}$$

We define the Euclidean action as:

$$S_E[\phi, \phi^*] = \int \mathrm{d}^4x_E \left(\delta_{\mu\nu} \partial^\mu_E \phi^* \partial^\nu_E \phi + m^2 |\phi|^2 + \lambda |\phi|^4 \right) , \tag{1.6}$$

and we find that the generating functional

$$Z[J, J^*] = \int \mathcal{D}\phi \mathcal{D}\phi^* \exp\left[-\left(S_E[\phi, \phi^*] - \int \mathrm{d}^4x_E J(x_E)\phi(x_E) - \int \mathrm{d}^4x_E J^*(x_E)\phi^*(x_E) \right) \right] \tag{1.7}$$

is now formally equal to the partition function of a statistical mechanical system.

1.2 Monte Carlo simulations

In statistical mechanics, the probability for a system in thermal equilibrium to be found in the microscopical configuration ϕ is given by:

$$P[\phi] = \frac{e^{-H[\phi]/k_B T}}{Z} , \tag{1.8}$$

$Z = \sum_\phi \exp[-H[\phi]/k_B T]$ being the partition function, $H[\phi]$ the total energy of the system in the configuration ϕ, k_B the Boltzmann constant and T the temperature. Monte Carlo simulations are a numerical method for generating configurations distributed according to the probability distribution $P[\phi]$.

In the previous section, we argued that a quantum field theory, defined by the action $S[\phi]$, is equivalent to a statistical mechanical model with partition function

$$Z = \int \mathcal{D}\phi \, e^{-S_E[\phi]} \tag{1.9}$$

(here for simplicity we consider the case of zero external source). We can apply the Monte Carlo method for generating configurations distributed according to:

$$P[\phi] = \frac{e^{-S_E[\phi]}}{Z} . \tag{1.10}$$

Once we have an ensemble of such configurations, n-point functions are calculated by averaging products of fields over the configurations:

$$\frac{1}{Z}\int \mathcal{D}\phi\, \phi(x_1)\dots\phi(x_n)e^{-S_E[\phi]} \longrightarrow \frac{1}{N}\sum_{i=1}^{N}\phi_i(x_1)\dots\phi_i(x_n)\ , \tag{1.11}$$

where $\phi_i(x_j)$ is the value of the field ϕ at the space-time point x_j, in the i-th configuration.

In order to construct a Monte Carlo simulation, we consider a stochastic process generating a sequence of configurations. We start from an initial configuration ϕ_0 at "Monte-Carlo time" (MC-time) $t = 0$, and move to a new configuration ϕ_1 with transition probability $W(\phi_0 \to \phi_1)$. The following normalisation condition holds for the transition probability W:

$$\sum_{\phi'} W(\phi \to \phi') = 1\ . \tag{1.12}$$

We repeat this procedure many times, thus generating a sequence of configurations. The probability $P[\phi; t]$ of being in the configuration ϕ at MC-time t fulfils the following condition:

$$P[\phi; t] = \sum_{\phi'} P[\phi'; t-1]W(\phi' \to \phi)\ . \tag{1.13}$$

We want the stochastic process to have the Boltzmann distribution $P_B[\phi] = \exp[-S_E[\phi]]/Z$ as an attractive fixed point. This means that, after some thermalisation time t_T, the probability distribution stops changing with MC-time, and it equals the Boltzmann distribution: $P[\phi; t > t_T] = P_B[\phi]$. If we are able to build such a stochastic process, then we can obtain an ensemble of Boltzmann-distributed configurations on which we can apply equation 1.11 for calculating n-point functions.

It follows from equation 1.13 that, if P_B is a fixed point of the stochastic process, then:

$$P_B[\phi] = \sum_{\phi'} P_B[\phi']W(\phi' \to \phi)\ . \tag{1.14}$$

We define the detailed-balance relation as:

$$P_B[\phi]W(\phi \to \phi') = P_B[\phi']W(\phi' \to \phi)\ ; \tag{1.15}$$

this relation implies the fixed-point condition 1.14 (this can be shown by summing equation 1.15 over ϕ', and using the normalisation condition 1.12), and it is easier to verify in a specific stochastic process. A process satisfying the detailed balance relation can be parametrised as follows:

$$W(\phi \to \phi') = F\left(\frac{P_B[\phi']}{P_B[\phi]}\right)\ , \tag{1.16}$$

where F is a generic function satisfying the functional equation

$$\frac{F(z)}{F(1/z)} = z\ . \tag{1.17}$$

There are many possible choices for the function F, each of whom defines a viable algorithm for a Monte Carlo simulation. One of the most widely used is $F(z) = \min[1, z]$, leading to the transition probability:

$$W(\phi \to \phi') = \min\left[1, \frac{P_B[\phi']}{P_B[\phi]}\right] = \min\left[1, e^{-(S_E[\phi'] - S_E[\phi])}\right] . \tag{1.18}$$

This particular implementation of the Monte Carlo method is known as Metropolis algorithm [1].

The stochastic process described above can be implemented numerically. To make this possible, we must define the theory on a lattice of finite volume, so that each field configuration is represented by a discrete and finite set of real numbers. Specifically, one configuration is completely defined by the value of each field at each point of the discretised space-time. In section 1.3 we will discuss the definition of a gauge theory on a space-time lattice.

To conclude, Monte Carlo simulations are a powerful non-perturbative method for studying quantum field theories. The price to be paid is the introduction of different sources of error that must be carefully treated: discretisation errors, finite-volume effects and statistical errors due to conducting the analysis on a finite set of configurations.

1.3 Lattice action

As previously pointed out, in order to apply the Monte Carlo method to a quantum field theory, we must first define the theory on a discretised space-time. In this section we discuss the lattice discretisation of a gauge theory coupled to fermions.

We define the discretised space-time as the set of points:

$$\Lambda = \{\, x_\mu = n_\mu a \mid n_\mu = 0, \ldots, L_\mu - 1,\ \mu = 0, \ldots, 3 \,\} \ , \tag{1.19}$$

where a is the lattice spacing and L_μ the number of lattice points in direction μ. We denote by $\hat{\mu}$ the unit vector in direction μ. As discussed in section 1.1, we are interested in defining the theory on a Euclidean space-time . However, for some purposes (such as measuring masses via the exponential falloff of correlators) it is useful to maintain the notion of time direction on the lattice. We consider $\mu = 0$ as time direction, i.e. the one that must be Wick-rotated in order to analytically continue the Euclidean theory to Minkowski space.

When we define a quantum field theory on a lattice with a finite number of points, the functional integral becomes the product of a finite number of ordinary integrals. For example, in the case of a real scalar field theory we have:

$$\int \mathcal{D}\phi \to \int_{-\infty}^{\infty} \prod_{x \in \Lambda} \mathrm{d}\phi_x \ , \tag{1.20}$$

where ϕ_x is the value of the field ϕ at the lattice point x.

1.3.1 Gauge action

We consider a theory with SU(N) gauge symmetry, whose continuum action is defined in equations (?)(?). In order to define a discretised version of this theory, we assign to each link on the lattice Λ an element of the gauge group:

$$U_\mu(x) = \exp\left[iagA^b_\mu(x)T^b\right] \in \mathrm{SU(N)}\ , \tag{1.21}$$

where T^b, $b \in [1, \ldots, \mathrm{N}^2 - 1]$, are the generators of the fundamental representation of SU(N) and g is the gauge coupling. The following relation holds for the link variables U_μ:

$$U_{-\mu}(x) = U_\mu(x - a\hat{\mu})^\dagger\ . \tag{1.22}$$

We define a gauge transformation by assigning to each lattice site an independent element of the gauge group, $\Omega(x) \in \mathrm{SU(N)}$, and transforming the link variables as follows:

$$U_\mu(x) \to U'_\mu(x) = \Omega(x)U_\mu(x)\Omega(x + a\hat{\mu})^\dagger\ . \tag{1.23}$$

The Wilson plaquette action [2] is the first proposed lattice discretisation of the Yang-Mills action. It is defined as:

$$S_W[U] = \frac{2\mathrm{N}}{g^2}\sum_{x\in\Lambda}\sum_{\mu<\nu}\left[1 - \frac{1}{\mathrm{N}}\mathrm{Re\,tr}[U_{\mu\nu}]\right]\ , \tag{1.24}$$

where the plaquette $U_{\mu\nu}$ is the ordered product of the link variables around an elementary loop on the lattice:

$$U_{\mu\nu}(x) = U_\mu(x)U_\nu(x + a\hat{\mu})U_\mu(x + \hat{\nu})^\dagger U_\nu(x)^\dagger\ . \tag{1.25}$$

$S_W[U]$ is invariant under the gauge transformation 1.23, and, in the limit $a \to 0$, it reduces to the Euclidean Yang-Mills action. This can be shown by expanding the link variables 1.21 in powers of a, and by making use of the Baker-Campbell-Hausdorff formula for expanding the products of link variables:

$$e^A e^B = e^{A+B+\frac{1}{2}[A,B]+\ldots} \tag{1.26}$$

where A and B are generic matrices, and we are omitting higher powers of the matrices in the right-hand side. Moreover, we can relate a finite difference on the lattice to a continuum derivative as follows:

$$A_\mu(x + a\hat{\nu}) - A_\mu(x) = a\,\partial_\nu A_\mu(x) + \mathcal{O}(a^2)\ . \tag{1.27}$$

We find:

$$S_W[U] = \frac{a^4}{2}\sum_{x\in\Lambda}\sum_{\mu,\nu}\mathrm{tr}\left[F_{\mu\nu}(x)^2\right] + \mathcal{O}(a^2) \underset{a\to 0, V\to\infty}{\longrightarrow} \frac{1}{4}\int \mathrm{d}^4x\,(F^a_{\mu\nu})^2 = S^E_{YM}[A]\ , \tag{1.28}$$

where $V = \prod_{\mu=0}^{3} L_\mu$ is the total number of lattice points, μ and ν are Euclidean indices, and $F_{\mu\nu}$ is the field strength tensor, as defined in equation (?).

It must be noticed that, as we discretise the Yang-Mills action, the Poincaré symmetry of the continuum theory is reduced to the smaller group of symmetries of an hypercubic lattice. However, the discretised action that we defined has the remarkable property of being exactly gauge invariant even at finite lattice spacing.

1.3.2 Fermion action

The continuum Dirac action in Euclidean space is defined by:

$$S_D^E[\psi, \bar{\psi}, A] = \int \mathrm{d}^4x \; \bar{\psi}(\not{D} + m\mathbb{1})\psi = \int \mathrm{d}^4x \; \bar{\psi}\big[\gamma_\mu^E(\partial_\mu + igA_\mu) + m\mathbb{1}\big]\psi \,, \quad (1.29)$$

where $\mathbb{1}$ is the identity matrix in Dirac space, and γ_μ^E are the Euclidean gamma matrices, related to the Minkowskian ones by: $\gamma_0^E = \gamma_0$, $\gamma_j^E = -i\gamma^j$ $(j = 1, 2, 3)$. In the following we will omit the superscript E, and it will be understood that, whenever we are discussing a lattice model, gamma matrices assume their Euclidean form.

We start by discretising in the most naive way the free-fermion action. We define the forward and backward lattice derivatives as:

$$\begin{aligned} \nabla_\mu \psi(x) &= \frac{\psi(x + a\hat{\mu}) - \psi(x)}{a} \\ \nabla_\mu^* \psi(x) &= \frac{\psi(x) - \psi(x - a\hat{\mu})}{a} \,, \end{aligned} \quad (1.30)$$

and we use the symmetrised combination:

$$\frac{1}{2}\big(\nabla_\mu + \nabla_\mu^*\big)\psi(x) = \frac{\psi(x + a\hat{\mu}) - \psi(x - a\hat{\mu})}{2a} \quad (1.31)$$

in the definition of the lattice fermion action, which is:

$$S_F[\psi, \bar{\psi}] = a^4 \sum_{x\in\Lambda} \bar{\psi}(x)\left[\sum_{\mu=0}^{3} \gamma_\mu \left(\frac{\psi(x + a\hat{\mu}) - \psi(x - a\hat{\mu})}{2a}\right) + m\mathbb{1}\psi(x)\right] . \quad (1.32)$$

We rewrite equation 1.32 in the more compact form:

$$S_F[\psi, \bar{\psi}] = a^4 \sum_{x,y\in\Lambda} \bar{\psi}(x) D(x|y) \psi(y) \,, \quad (1.33)$$

where the Dirac operator $D(x|y)$ is defined as:

$$D(x|y) = \sum_{\mu=0}^{3} \gamma_\mu \frac{\delta_{y,x+a\hat{\mu}} - \delta_{y,x-a\hat{\mu}}}{2a} + m\mathbb{1}\delta_{x,y} \,. \quad (1.34)$$

This formulation of the lattice fermion action leads to the problem known as fermion doubling. In order to explicitly show what the problem is, we consider the Fourier transform of the Dirac operator:

$$\tilde{D}(p|q) = \frac{1}{V}\sum_{x,y\in\Lambda} e^{-ip\cdot x} D(x|y) e^{iq\cdot y} = \delta(p-q)\tilde{D}(q) \tag{1.35}$$

where

$$\tilde{D}(q) = \frac{i}{a}\sum_{\mu}\gamma_\mu \sin(q_\mu a) + m\mathbb{1}\,. \tag{1.36}$$

See appendix A.2 for the definition of Fourier transforms on the lattice.

By inverting the operator in equation 1.36 and transforming back to coordinate space, we obtain the fermion propagator:

$$\langle\psi(x)\bar{\psi}(y)\rangle = D^{-1}(x|y) = \int_{-\frac{\pi}{a}}^{\frac{\pi}{a}} \frac{\mathrm{d}^4 q}{(2\pi)^4} e^{iq\cdot(x-y)} \frac{m\mathbb{1} - i/a\sum_\mu \gamma_\mu \sin(q_\mu a)}{m^2 + \sum_\mu \sin^2(q_\mu a)/a^2}\,. \tag{1.37}$$

Here for simplicity we consider the infinite-volume limit, where lattice momenta have a continuum spectrum. In the limit $a \to 0$, the dominant contributions to the integral 1.37 arise from momentum ranges where

$$\frac{1}{a}\sin(q_\mu a) \sim 0\,. \tag{1.38}$$

This happens around $q = (0,0,0,0), (\pi/a,0,0,0), \ldots, (\pi/a,\pi/a,\pi/a,\pi/a)$. Of all these contributions, only the one arising from the integration around $q = (0,0,0,0)$ corresponds to the continuum propagator

$$\langle\psi(x)\bar{\psi}(y)\rangle_{\mathrm{cont}} = \int_{-\infty}^{\infty} \frac{\mathrm{d}^4 q}{(2\pi)^4} e^{iq\cdot(x-y)} \frac{m\mathbb{1} - i/a\sum_\mu \gamma_\mu q_\mu}{m^2 + q^2}\,, \tag{1.39}$$

while the other fifteen contributions have no continuum analogue, and are not defined in the continuum limit. These are lattice artefacts known as doublers.

One of the possible solutions to the doubling problem is to add an extra term to the Dirac operator, known as Wilson term [3]. The Wilson-Dirac operator in momentum space is defined by:

$$\tilde{D}(q) = \frac{i}{a}\sum_{\mu}\gamma_\mu \sin(q_\mu a) + m\mathbb{1} + \mathbb{1}\frac{1}{a}\sum_\mu \big(1-\cos(q_\mu a)\big)\,, \tag{1.40}$$

leading to the fermion propagator:

$$\langle\psi(x)\bar{\psi}(y)\rangle = \int_{-\frac{\pi}{a}}^{\frac{\pi}{a}} \frac{\mathrm{d}^4 q}{(2\pi)^4} e^{iq\cdot(x-y)} \frac{\big[m + a^{-1}\sum_\mu\big(1-\cos(q_\mu a)\big)\big]\mathbb{1} - ia^{-1}\sum_\mu \sin(q_\mu a)}{\big[m + a^{-1}\sum_\mu\big(1-\cos(q_\mu a)\big)\big]^2 + a^{-2}\sum_\mu \sin^2(q_\mu a)}. \tag{1.41}$$

We define $q^{(\pi)}$ as a momentum vector with n_π components equal to π/a and the other $4-n_\pi$ components equal to zero. In the vicinity of $q^{(\pi)}$, the denominator in equation 1.41 is given by:

$$\left[m+\frac{1}{a}\sum_{\mu}\big(1-\cos(q_\mu a)\big)\right]^2+\frac{1}{a^2}\sum_{\mu}\sin^2(q_\mu a)\underset{q\sim q^{(\pi)}}{\sim}\left[m+\frac{2n_\pi}{a}\right]^2+\frac{1}{a^2}\sum_{\mu}\sin^2(q_\mu a)\,. \tag{1.42}$$

This expression is finite in the $a\to 0$ limit only if $n_\pi=0$, otherwise it diverges. Thus the contributions from the doublers are eliminated. The price to be paid is that the Wilson fermion action is not chirally symmetric in the limit $m\to 0$.

The Wilson term $\tilde{D}_W(q)=\mathbb{1}a^{-1}\sum_\mu\big(1-\cos(q_\mu a)\big)$ has the following form in coordinate space:

$$D_W(x|y)=-\mathbb{1}a\sum_{\mu}\frac{\delta_{y,x+a\hat{\mu}}-2\delta_{x,y}+\delta_{y,x-a\hat{\mu}}}{2a^2}\underset{a\to 0}{\to}-\mathbb{1}\frac{a}{2}\partial_\mu\partial_\mu\,. \tag{1.43}$$

Equation 1.43 shows that D_W is a discretisation of the Laplace operator $\partial_\mu\partial_\mu$, multiplied by a factor a, which makes it clear that the Wilson term goes to zero in the limit of vanishing lattice spacing.

We now introduce the gauge interaction by inserting link variables in the products of neighbouring fermion fields:

$$\begin{aligned}&\bar{\psi}(x)\psi(x+a\hat{\mu})\to\bar{\psi}(x)U_\mu(x)\psi(x+a\hat{\mu})\\&\bar{\psi}(x)\psi(x-a\hat{\mu})\to\bar{\psi}(x)U_{-\mu}(x)\psi(x-a\hat{\mu})=\bar{\psi}(x)U_\mu^\dagger(x-a\hat{\mu})\psi(x-a\hat{\mu})\,.\end{aligned} \tag{1.44}$$

Now the fermion fields carry a colour index along with the Dirac index, and they transform as:

$$\begin{aligned}\psi(x)&\to\Omega(x)\psi(x)\\\bar{\psi}(x)&\to\bar{\psi}(x)\Omega^\dagger(x)\end{aligned} \tag{1.45}$$

under the gauge transformation 1.23, which shows that the products defined in equation 1.44 are gauge invariant.

To conclude, the interacting Wilson-Dirac operator is given by:

$$D(x|y)=\left(m+\frac{4}{a}\right)\mathbb{1}\times\mathbb{1}_C\delta_{x,y}-\frac{1}{2a}\left[\sum_\mu(\mathbb{1}-\gamma_\mu)U_\mu(x)\delta_{y,x+a\hat{\mu}}+\sum_\mu(\mathbb{1}+\gamma_\mu)U_\mu^\dagger(x-a\hat{\mu})\delta_{y,x-a\hat{\mu}}\right]. \tag{1.46}$$

where $\mathbb{1}_C$ represents the identity matrix in colour space.

We have thus defined Wilson's formulation of a lattice gauge theory coupled to fermions. The action is given by:

$$S[U,\psi^{(i)},\bar{\psi}^{(i)}]=\frac{2\mathrm{N}}{g^2}\sum_{x\in\Lambda}\sum_{\mu<\nu}\big[1-\frac{1}{\mathrm{N}}\mathrm{Re}\,\mathrm{tr}[U_{\mu\nu}]\big]+\sum_{i=1}^{N_f}a^4\sum_{x,y\in\Lambda}\bar{\psi}^{(i)}(x)D^{(i)}(x|y)\psi^{(i)}(y)\,, \tag{1.47}$$

where $U_{\mu\nu}$ is the plaquette, defined in equation 1.25, $D(x|y)$ is the Wilson-Dirac operator defined in equation 1.46, and N_f is the number of fermion flavours. The partition function of this model is:

$$Z = \int \prod_{x\in\Lambda} \left[\prod_{\mu} \mathrm{d}U_\mu(x) \right] \left[\prod_{i} \mathrm{d}\psi^{(i)}(x) \mathrm{d}\bar{\psi}^{(i)}(x) \right] e^{-S[U,\psi^{(i)},\bar{\psi}^{(i)}]} \,, \tag{1.48}$$

where $\mathrm{d}U_\mu(x)$ is the Haar measure for the integration over the gauge group.

The action 1.47 is not a unique choice. There exist other formulations, which for example have smaller discretisation errors, or implement a lattice version of chiral symmetry in the fermion action. For the study described in this thesis, Wilson's formulation 1.47 is used.

1.3.3 Pseudofermions

Fermion fields are represented in the path integral formalism by anticommuting Grassmann variables. Unfortunately, it is not possible to define Grassmann variables on a computer. This problem can be solved by using following trick: the Gaussian integral over the fermion fields is explicitly calculated:

$$\int \prod_{x\in\Lambda} \mathrm{d}\psi(x) \mathrm{d}\bar{\psi}(x) \exp\left[- \sum_{x,y\in\Lambda} \bar{\psi}(x) D(x|y) \psi(y) \right] = \det[-D] \,, \tag{1.49}$$

and then the fermionic determinant $\det[-D]$ is rewritten as an integral over new bosonic variables, known as pseudofermions.

But first of all it must be shown that the fermions' contribution to the partition function is real and nonnegative. The minus sign inside the determinant is actually irrelevant, since it simply provides an overall factor $(-1)^N$ in front of the path integral, where N is the dimension of the matrix D. If $\det[D]$ is a nonnegative real number in each gauge configuration, then it can be seen as a part of the Boltzmann weight in the partition function

$$Z = \int \prod_{x\in\Lambda} \left[\prod_{\mu} \mathrm{d}U_\mu(x) \right] \det[D] e^{-S_W[U]} \,, \tag{1.50}$$

otherwise it cannot be interpreted as probability density.

The Wilson-Dirac operator is γ_5-hermitian: $\gamma_5 D = D^\dagger \gamma_5$. We can use this property for defining an hermitian operator:

$$Q = \gamma_5 D \,, \tag{1.51}$$

whose determinant is a real number. Since $\det[\gamma_5] = 1$, the determinants of D and Q are equal, implying that the determinant of the Wilson-Dirac operator is real. But this does not guarantee that $\det[D]$ is nonnegative.

A possible strategy for ensuring the positivity of the integrand in the partition function is to have couples of mass-degenerate fermion fields in the theory. Two mass-degenerate fermions are coupled to identical Dirac operators, and contribute to the partition function with a factor $\det[D]^2 \geq 0$.

We can now define the lattice fermion action in terms of pseudofermion fields.We consider a theory with two mass-degenerate fermions, and we rewrite the fermionic contribution as an integral over bosonic degrees of freedom, ϕ and $\phi^\dagger$:

$$\det[D]^2 = \det[Q]^2 = \det\left[Q^2\right] = \pi^{-N} \int \prod_{x\in\Lambda} \mathrm{d}\phi(x)\mathrm{d}\phi^\dagger(x) \exp\left[-\sum_{x,y\in\Lambda} \phi^\dagger(x) Q^{-2}(x|y)\phi(y)\right]. \tag{1.52}$$

The factor π^{-N} can be neglected, since it is an overall factor in the path integral. The lattice action can now be expressed as a function of bosonic variables:

$$S[U,\phi,\phi^\dagger] = \frac{2\mathrm{N}}{g^2} \sum_{x\in\Lambda}\sum_{\mu<\nu}\left[1 - \frac{1}{\mathrm{N}}\mathrm{Re}\,\mathrm{tr}[U_{\mu\nu}]\right] + a^4 \sum_{x,y\in\Lambda} \phi^\dagger(x) Q^{-2}(x|y)\phi(y)\,, \tag{1.53}$$

and is suitable for the implementation of a Monte Carlo simulation.

1.4 Hybrid Monte Carlo

The lattice action 1.53 is highly nonlocal, due to the inverse Q operator in the pseudofermion term. It may be inefficient in this case to use algorithms based on local updates of the configurations. By local update we mean that just one or a few link variables are changed when generating a new configuration.

For example, we imagine to update the gauge field by changing the value of one link variable, and then to accept or reject the new configuration according to Metropolis transition probability 1.18. Even though only one link variable has been changed, the variation of the action appearing in equation 1.18 depends on all the link variables in the lattice. With this method, subsequent configurations are highly correlated to each other, and at the same time each Metropolis step is computationally expensive.

In this case it is a better solution to change all the link variables at once. The Hybrid Monte Carlo (HMC) algorithm is based on the idea of updating the configurations via a molecular dynamics evolution, in such a way that all the link variables are changed, but at the same time the change in the action is very small, so that the new configuration is very likely to be accepted in a Metropolis step. In this section we describe the general idea behind the HMC method by using a scalar field theory as a concrete example. In section 2.3.2 we will give the details for the application of the method to a gauge theory coupled to fermions and scalars.

We consider a scalar field theory, with action $S[\phi]$, and we write the expectation value of an observable O as:

$$\langle O\rangle = \frac{\int \prod_x \mathrm{d}\phi(x)\, O[\phi] \exp[-S[\phi]]}{\int \prod_x \mathrm{d}\phi(x)\ \exp[-S[\phi]]} = \frac{\int \prod_x \mathrm{d}\phi(x)\mathrm{d}\pi(x)\, O[\phi] \exp\left[-\frac{1}{2}\sum_y \pi(y)^2 - S[\phi]\right]}{\int \prod_x \mathrm{d}\phi(x)\mathrm{d}\pi(x)\ \exp\left[-\frac{1}{2}\sum_y \pi(y)^2 - S[\phi]\right]}, \tag{1.54}$$

where in the last step we multiplied both numerator and denominator by the factor $\int \prod_x \mathrm{d}\pi(x) \exp\left[-\frac{1}{2}\sum_y \pi(y)^2\right]$. We interpret $H[\pi,\phi] = \frac{1}{2}\sum_x \pi(x)^2 + S[\phi]$ as an Hamiltonian, whose Hamilton's equations are given by:

$$\begin{aligned} \dot{\pi}(x) &= -\frac{\partial H}{\partial \phi(x)} = -\frac{\partial S}{\partial \phi(x)} \\ \dot{\phi}(x) &= \frac{\partial H}{\partial \pi(x)} = \pi(x)\,, \end{aligned} \tag{1.55}$$

where the dot denotes the derivative with respect to molecular-dynamics time. If we were able to exactly solve these equations, we would have a trajectory in configuration space characterised by a constant value of the Hamiltonian.

The HMC method is based on solving numerically Hamilton's equations 1.55, thus generating a molecular dynamics trajectory. The system is let evolve for a finite number of steps of the numerical integrator and the final configuration is accepted or rejected in a Metropolis step, with acceptance probability

$$W_M(\pi,\phi \to \pi'\phi') = \min\left[1, \frac{e^{-H[\pi',\phi']}}{e^{-H[\pi,\phi]}}\right]. \tag{1.56}$$

In appendix A.3 we show that, when the numerical integrator meets certain requirements, the algorithm described above respects the detailed balance relation 1.15.

To conclude, the HMC algorithm is very useful for simulating gauge theories coupled to dynamical fermions. It reduces the correlation between subsequent configurations in the Monte Carlo evolution, and at the same time the acceptance can be kept high by tuning the parameters of the numerical integrator.

1.5 Mass measurements on the lattice

Among the many interesting observables that can be measured on the lattice, there is the energy spectrum of the theory. The energy levels can be measured from the study of correlation functions.

We define the correlation function in Euclidean time of two generic operators A and B as:

$$C_{AB}(t) = \langle A(t)B(0)\rangle = \frac{1}{Z}\,\mathrm{tr}\left[e^{-(T-t)\hat{H}} A(0) e^{-t\hat{H}} B(0)\right], \tag{1.57}$$

where the partition function Z is expressed in the operator formalism as:

$$Z = \mathrm{tr}\left[e^{-T\hat{H}}\right]. \tag{1.58}$$

$T \equiv L_0$ is the number of lattice points in the time direction, and $t \equiv x^0$ is the Euclidean time coordinate. $\hat{H}$ is the Hamiltonian operator generating time translations, and the trace is intended over the Hilbert space of physical states.

We choose a basis of eigenstates of $\hat{H}$, $\hat{H}\,|n\rangle = E_n\,|n\rangle$, and we rewrite equations 1.57 and 1.58 as:

$$C_{AB}(t) = \frac{1}{Z}\sum_n \langle n|\, e^{-(T-t)\hat{H}} A(0) e^{-t\hat{H}} B(0)\,|n\rangle \ , \tag{1.59}$$

$$Z = \sum_n \langle n|\, e^{-T\hat{H}}\,|n\rangle \ . \tag{1.60}$$

By inserting a completeness relation, $\sum_m |m\rangle\langle m| = \mathbb{1}$, we obtain:

$$\begin{aligned} C_{AB}(t) &= \frac{1}{Z}\sum_{n,m} \langle n|\, e^{-(T-t)\hat{H}} A(0)\,|m\rangle\langle m|\, e^{-t\hat{H}} B(0)\,|n\rangle = \\ &= \frac{\sum_{n,m} e^{-(T-t)E_n} e^{-tE_m}\,\langle n|\, A(0)\,|m\rangle\langle m|\, B(0)\,|n\rangle}{\sum_n e^{-TE_n}} \ . \end{aligned} \tag{1.61}$$

In the limit of large lattice time extent, $T \to \infty$, and large time separations, $t \to \infty$, we find:

$$C_{AB}(t) \underset{\substack{T\to\infty \\ t\to\infty}}{\sim} \frac{e^{-(T-t)E_0} e^{-tE_{AB}} c_{AB}}{e^{-TE_0}} + \frac{e^{-(T-t)E_{BA}} e^{-tE_0} c_{BA}}{e^{-TE_0}} \ , \tag{1.62}$$

where E_0 is the energy of the vacuum state and E_{AB}, E_{BA} are the energies of the states $|m_{AB}\rangle$, $|n_{BA}\rangle$, defined as the lightest states such that:

$$\begin{aligned} c_{AB} &\equiv \langle 0|\, A(0)\,|m_{AB}\rangle\langle m_{AB}|\, B(0)\,|0\rangle \neq 0 \\ c_{BA} &\equiv \langle 0|\, B(0)\,|n_{BA}\rangle\langle n_{BA}|\, A(0)\,|0\rangle \neq 0 \ . \end{aligned} \tag{1.63}$$

If $B = A^\dagger$, the coefficients c_{AB}, c_{BA} are real and positive, and equal to each other: $c_{AB} = c_{BA} \equiv c$, and the correlator is given by:

$$C_{AA^\dagger}(t) \underset{\substack{T\to\infty \\ t\to\infty}}{\sim} c\left(e^{-t(E_{m_0}-E_0)} + e^{-(T-t)(E_{m_0}-E_0)} \right) \ , \tag{1.64}$$

where E_{m_0} is the energy of the lightest state $|m_0\rangle$ with nonzero overlap with $A^\dagger\,|0\rangle$, i.e. $c = \left|\langle m_0|\, A^\dagger(0)\,|0\rangle\right|^2 \neq 0$.

In this setup, the energy of the state $|m_0\rangle$ can be measured by studying the exponential decay of the correlator $C_{AA^\dagger}(t)$ for large Euclidean time separations. The energy is measured with respect to the energy of the vacuum state E_0. The goal is then to find operators with a good overlap with the states whose energy we want to to measure. In the following we describe the operators used for the mass measurements done in this thesis.

1.5.1 Meson masses

In order to measure meson masses, we need operators that generate states with the quantum numbers of the desired mesons. We consider a theory with two fermion

flavours, and, in analogy with the first quark family of the Standard Model, we denote the fermion fields by u (up) and d (down). These two fermions belong to an isospin doublet, with $I = 1/2$, and $I_3 = +1/2$ (u), $I_3 = -1/2$ (d).

In this thesis we will measure the mass of the isospin-triplet pseudoscalar mesons (analogue to pions in QCD) and the isospin-triplet vector mesons (analogue to ρ mesons in QCD). For the pseudoscalar isospin triplet, the following operators are used:

- $(I = 1, I_3 = +1)$: $O_{\pi^+}(x) = \bar{d}(x)\gamma_5 u(x)$
- $(I = 1, I_3 = 0)$: $O_{\pi^0}(x) = \frac{1}{\sqrt{2}}\big(\bar{u}(x)\gamma_5 u(x) - \bar{d}(x)\gamma_5 d(x)\big)$
- $(I = 1, I_3 = -1)$: $O_{\pi^-}(x) = \bar{u}(x)\gamma_5 d(x)$.

These operators have spin zero and negative parity, O_{π^0} is an eigenstate of charge conjugation, with eigenvalue $+1$, while O_{π^+} and O_{π^-} are mapped into each other by charge conjugation. When the fermion masses are degenerate and there are no electroweak interactions, the three states $\pi^{\pm,0}$ have the same mass, therefore it is sufficient to study only one of these operators.

In order to measure the mass of the pseudoscalar meson state, the correlator $C_{\pi^-}(t) = \sum_{\vec{x}} \langle O_{\pi^-}(\vec{x}, t) O_{\pi^-}(\vec{0}, 0)^\dagger \rangle$ is used in this thesis. The sum over the spacial coordinates $\vec{x}$ is introduced for projecting to states with zero spacial momentum. In fact, if there exists a one-particle state with the quantum numbers of the operator $O^\dagger_{\pi^-}$, then the energy of the lowest-energy state with zero spacial momentum is simply given by the mass of the particle.

The operators chosen for studying the isospin-triplet vector mesons are very similar to $O_{\pi^\pm}$ and O_{π^0}, with the only difference that γ_5 is replaced with γ_i, $i = 1, 2, 3$. These operators generate states with spin one and negative parity. Again, in the absence of electroweak effects and if u and d have the same mass, the three states in the isospin triplet have equal masses.

To summarise, we define the operator $O_\Gamma(x) = \bar{u}(x)\Gamma d(x)$, where Γ stands in general for a product of gamma matrices, and the cases of our interest are $\Gamma = \gamma_5$ (pseudoscalar meson) and $\Gamma = \gamma_i$ (vector meson). We measure isospin-triplet meson masses by studying the exponential decay of the correlator:

$$C_\Gamma(t) = \sum_{\vec{x}} \langle O_\Gamma(\vec{x}, t) O_\Gamma(\vec{0}, 0)^\dagger \rangle \, . \tag{1.65}$$

More specifically, we define the effective mass $m_\Gamma^{eff}(t)$ via the equation:

$$\frac{C_\Gamma(t-1)}{C_\Gamma(t)} = \frac{e^{-m_\Gamma^{eff}(t)(T-(t-1))} + e^{-m_\Gamma^{eff}(t)(t-1)}}{e^{-m_\Gamma^{eff}(t)(T-t)} + e^{-m_\Gamma^{eff}(t)t}} \, , \tag{1.66}$$

and we find the meson mass as the large-t limit of $m_\Gamma^{eff}(t)$.

1.5.2 PCAC mass

In this thesis we will also measure the fermion mass via the Partially Conserved Axial Current (PCAC) relation. The PCAC relation, or axial Ward identity, is a

consequence of the transformation properties of the fermion action under chiral rotations in flavour space. In order to derive it, we consider the partition function 1.48, and a field redefinition:

$$\begin{aligned} \psi^{(i)} &\to \psi^{(i)} + \delta\psi^{(i)} \\ \bar{\psi}^{(i)} &\to \bar{\psi}^{(i)} + \delta\bar{\psi}^{(i)} \, . \end{aligned} \tag{1.67}$$

The partition function doesn't change under this transformation, and, if the integration measure is also symmetric, it follows that:

$$\langle \delta S \rangle = 0 \, , \tag{1.68}$$

where δS is the infinitesimal shift in the action.

We now consider the continuum fermion action for a two-flavour theory:

$$S_{\text{cont}}[\psi, \bar{\psi}] = \int \mathrm{d}^4x \; \bar{\psi}(x)(\gamma_\mu D_\mu + M\mathbb{1})\psi(x) \, , \tag{1.69}$$

where $\psi = (u \; d)^T$, M is the two-by-two diagonal mass matrix and $\mathbb{1}$ the identity in Dirac space. As in the previous section, we denote the two fermion fields by u and d. We consider the following infinitesimal transformation in flavour space:

$$\begin{aligned} \psi(x) &\to \psi(x) + i\epsilon(x)\gamma_5\sigma^a\psi(x) \\ \bar{\psi}(x) &\to \bar{\psi}(x) + i\epsilon(x)\bar{\psi}(x)\gamma_5\sigma^a \, , \end{aligned} \tag{1.70}$$

where σ^a are the Pauli matrices, with $a = 1, 2, 3$, and $\epsilon(x)$ is a generic smooth function, which is nonzero only inside a bounded region. For this specific transformation, equation 1.68 reads:

$$\langle \partial_\mu \big(\bar{\psi}(x)\gamma_\mu\gamma_5\sigma^a\psi(x) \big) \rangle = \langle \bar{\psi}(x) \big\{ M, \sigma^a \big\} \gamma_5 \psi(x) \rangle \, . \tag{1.71}$$

If the two fermions have equal masses, $m_u = m_d = m$, equation 1.71 becomes:

$$\langle \partial_\mu A^a_\mu(x) \rangle = 2m \langle P^a(x) \rangle \, , \tag{1.72}$$

where we have defined the axial vector current as $A^a_\mu = 1/2 \; \bar{\psi}\gamma_\mu\gamma_5\sigma^a\psi$, and the pseudoscalar interpolator as $P^a = 1/2 \; \bar{\psi}\gamma_5\sigma^a\psi$. P^a is related to the $O_{\pi^{\pm,0}}$ operators of the previous section by:

$$\begin{aligned} P^1 - iP^2 &= \bar{d}\gamma_5 u = O_{\pi^+} \\ P^1 + iP^2 &= \bar{u}\gamma_5 d = O_{\pi^-} \\ P^0 &= \frac{1}{2}\big(\bar{u}\gamma_5 u - \bar{d}\gamma_5 d \big) = \frac{1}{\sqrt{2}} O_{\pi^0} \, . \end{aligned} \tag{1.73}$$

Equation 1.72 is known as PCAC relation, and it implies that, when $m = 0$, the axial vector current is conserved, due to the symmetry of the action under chiral flavour rotations. On the lattice however, the Wilson fermion action is not chirally

symmetric even when the fermion mass is zero, and the analogue of the PCAC relation involves additional terms.

The PCAC relation can be used to measure the fermion mass on the lattice by studying the long-distance behaviour of the following ratio of correlators:

$$\frac{1}{2}\frac{\sum_{\vec{x}}\langle\partial_t A_0^-(\vec{x},t)^\dagger O_{\pi^-}(0)\rangle}{\sum_{\vec{x}}\langle O_{\pi^-}(\vec{x},t)^\dagger O_{\pi^-}(0)\rangle} \underset{t\to\infty}{\sim} m_{PCAC}\,, \tag{1.74}$$

where $A_\mu^- = A_\mu^1 + iA_\mu^2$, and, due to the zero-momentum projection, only the time derivative survives. m_{PCAC} is identified with the unrenormalised fermion mass. Due to the fact that the lattice fermion action is not chirally symmetric, m_{PCAC} is not equal to the bare mass used as parameter in the fermion action, and in general is not zero when the bare mass is zero. The chiral limit of the lattice theory is identified by finding the values of the bare lattice parameters such that $m_{PCAC} = 0$.

1.6 The continuum limit

Lattice calculations make it possible to study non-perturbatively the discretised version of a quantum field theory. Information on the continuum theory can be obtained by performing the continuum limit.

We have previously observed that, in the limit $a \to 0$, the lattice action 1.47 reduces to the continuum Euclidean action of a gauge theory coupled to fermions. However, this is not enough to ensure that meaningful continuum results can be extracted from the lattice theory. In order to illustrate this, we consider the mass of some physical state, measured on the lattice from the exponential decay of a correlator, as described in section 1.5. The lattice calculation results in a dimensionless quantity $\hat{M}$, which is the inverse of a correlation length, and is related to the physical value of the mass M by: $M = \hat{M}/a$. If we want M to be finite in the continuum limit, we need $\hat{M}$ to go to zero as a goes to zero. This means that the bare parameters of the lattice theory must be tuned to a critical point, where correlation lengths diverge.

When we say that $M = \hat{M}/a$ is the physical value of the mass, we are implicitly assuming that we can express the lattice spacing a in physical units, say in fm. This information is not contained in the lattice theory itself, and it must be deduced by using some external input. For example, if we are studying lattice QCD, we can pick any observable, such as the mass of a bound state, and set its experimental value to be equal to the value measured on the lattice. From this equality we can extract the value of the lattice spacing measured in physical units.

Once we have a measure for the lattice spacing, the goal is to extrapolate continuum physics out of the lattice results by moving to smaller and smaller values of the lattice spacing. As pointed out earlier, in order to have finite values for the observables in the continuum limit, we have to change the bare lattice couplings as functions of a, in such a way that when a goes to zero we move towards a critical point where correlation lengths diverge. In particular, in a pure gauge theory the gauge coupling g must change as a function of a in such a way that:

$$O(a, g(a)) \underset{a\to 0}{\longrightarrow} O_{ph}\,, \tag{1.75}$$

where O is a generic observable and O_{ph} is its physical value. The functional form of $g(a)$ may depend on the specific observable if a is not small enough. However, when we get close to the continuum limit, there must be a unique function $g(a)$ that ensures the finiteness of any observable. We can obtain information on $g(a)$ by using the renormalisation group equation:

$$\left[a\frac{\partial}{\partial a} - \beta(g)\frac{\partial}{\partial g}\right]O(a, g(a)) = 0\,, \tag{1.76}$$

where $\beta(a) = -a\,\partial g/\partial a$. We obtain this equation by assuming to be close enough to the continuum limit, so that equation 1.75 can be rewritten as an equality, and by deriving with respect to a the right- and left-hand-side. The beta function $\beta(g)$ can be computed perturbatively by expanding $O(a, g)$ in powers of g, and by inserting the expansion in equation 1.76. The result up to $\mathcal{O}(g^3)$ is the same for any observable O, and it is given by:

$$\beta(g) = -\frac{11N}{3}\frac{g^3}{(4\pi)^2} + \mathcal{O}(g^5)\,, \tag{1.77}$$

where we assumed the gauge group to be SU(N). With the help of equation 1.77, we can solve the differential equation $\beta(a) = -a\,\partial g/\partial a$ and express a as a function of g:

$$a = \frac{1}{\Lambda_L}e^{-\frac{(4\pi)^2}{2\beta_0 g^2}}\,, \tag{1.78}$$

where $\beta_0 = 11N/3$, and Λ_L is a constant with the dimension of an energy. Equation 1.78 shows that the lattice spacing goes to zero when g goes to zero, and therefore we have to move in parameter space towards $g = 0$ in order to take the continuum limit.

When studying a lattice gauge theory coupled to fermions, there is one extra parameter to consider: the fermion mass m. We consider here the case of Wilson fermions, whose action is defined in section 1.3.2, and we define the bare fermion mass measured in lattice units as $\hat{m} = ma$. The typical procedure for ensuring that in the continuum limit we describe the desired theory (for example QCD), is to repeat the lattice measurements for different values of g, and for each value of g to tune $\hat{m}$ in such a way that some dimensionless ratio of observables assumes its physical value. This way a line of constant physics in the space of bare lattice parameters is defined. The physical value of the lattice spacing is determined by equalling one observable to its experimental value, and then all the other observables can be expressed in physical units, representing the real independent lattice measurements. The continuum value of these observables is extrapolated by moving towards $g = 0$ along the line of constant physics.

One more important point to consider when taking the continuum limit is the lattice volume. As the lattice spacing becomes smaller, the number of lattice points must be increased, so that the physical volume doesn't shrink. Typically the extrapolation to $a = 0$ is performed by keeping the physical lattice volume fixed, which implies increasing the number of lattice points as $g \to 0$.

Chapter 2

Lattice study of a gauge-fermion-scalar theory

The Standard Model electroweak theory is very successful in describing experimental results. However, some theoretical concerns suggest that a more consistent theory should be found. Specifically, the search for an alternative mechanism for the generation of masses is an active research field. Composite Higgs models belong to this branch of Beyond the Standard Model (BSM) research.

In this chapter we discuss the lattice study of an SU(2) gauge theory coupled to fermions and scalars. This theory is intended as a minimal scenario for composite Higgs models, in which the problem of the generation of fermion masses is addressed via the fundamental partial compositeness mechanism [4].

The chapter is organised as follows. We start by exposing some of the reasons why the Standard Model Higgs mechanism turns out to be theoretically unappealing. Then we introduce composite Higgs models, and we explain what makes the generation of fermion masses a bit problematic in this setup. We then describe the mechanism of fundamental partial compositeness. After setting these theoretical motivations, we move to the description of the specific theory under analysis, starting with some continuum aspects and then moving to the lattice setup. Finally, we present the results obtained on the spectrum and phase space of the lattice theory. Some of these results have been published in [5], while others are reported here for the first time.

2.1 Composite Higgs models and fundamental partial compositeness

2.1.1 The naturalness and triviality problems

The Standard Model Higgs boson is an elementary scalar field. There exist some theoretical problems related to elementary scalars, known as naturalness and triviality problem.

The naturalness problem is due to the fact that the Higgs mass is extremely sensitive to corrections arising from new physics, which may appear at a very high energy scale. We know the Standard Model to be an effective field theory, valid up

to some ultraviolet cutoff Λ_{SM}, whose UV-completion is yet unknown. Λ_{SM} will be at most equal to the Planck scale $M_{PL} = 10^{19}$ GeV, where a complete quantum theory of gravity should appear. When we consider the Standard Model (SM) as an effective theory, we do not restrict ourselves to the renormalisable operators of the SM Lagrangian, but we consider an effective Lagrangian containing all possible operators built with the SM elementary fields, which respect the symmetries of the SM:

$$\mathcal{L}_{eff} = \sum_{d=1}^{\infty} \frac{c_{(d)}}{\Lambda_{SM}^{d-4}} O^{(d)} \,, \tag{2.1}$$

where d is the energy dimension of the operator $O^{(d)}$. For dimensional reasons, the coefficients of $d > 4$ operators are suppressed by a factor $\Lambda_{SM}^{-|d-4|}$, while the coefficients of $d < 4$ operators are enhanced by a factor $\Lambda_{SM}^{|d-4|}$. If we knew the UV-completion of the SM, i.e. a theory valid up to arbitrarily high energy scales, of which the SM is a low-energy effective description, then we could in principle compute the coefficients $c_{(d)}$ as functions of the parameters of the UV-complete theory. The quadratic term in the Higgs potential is the only $d < 4$ operator present in $\mathcal{L}_{eff}$, specifically it is a $d = 2$ operator. The tree-level Higgs mass is proportional to the coefficient of this operator. The fact that the Higgs is "light", together with the fact that new physics may come at a very high energy scale, contributes to creating a theoretically problematic scenario. If new physics appeared at a scale which is significantly larger than the TeV, then reconstructing the experimental value of 125 GeV for the Higgs mass would require the coefficient $c_{(2)}$ to be extremely small. As a consequence, the UV-completion accounting for the new physics would be constrained by the fact that $c_{(2)}$ must assume the required very small value. This scenario, in which the low-energy parameters of the theory constrain to a very high degree the UV-completion, defined at a much higher scale, is considered to be unnatural.

Elementary scalars may also be affected by the triviality problem [6]. This problem is related to the running of the scalar quartic self-coupling. In a pure scalar field theory, defined by the Lagrangian

$$\mathcal{L}[\phi] = \frac{1}{2}\partial_\mu\phi\,\partial^\mu\phi - \frac{1}{2}m^2\phi^2 - \frac{\lambda}{4!}\phi^4 \,, \tag{2.2}$$

the renormalised quartic coupling at the momentum scale p, at lowest order in perturbation theory, is given by:

$$\bar{\lambda}(p) = \frac{\lambda_R}{1 - \frac{3}{16\pi^2}\lambda_R \log\frac{p}{\mu}} \,, \tag{2.3}$$

where λ_R is the renormalised coupling at the scale $p = \mu$. If $\lambda_R \neq 0$, there exists a finite momentum scale at which the renormalised coupling diverges, thus making the theory inconsistent. It seems that the only consistent theory is the noninteracting one, characterised by $\lambda_R = 0$. Should this be the case also for the SM Higgs field, the Higgs mechanism would be invalidated, since it is strongly based on the existence of the scalar self-interactions. This argument however does not directly apply to the SM Higgs scalar, since gauge and Yukawa interactions must be also taken into

account in order to compute the running of λ. The quartic coupling of the SM Higgs actually becomes negative at high energies, thus leading to problems related to the stability of the SM vacuum [7]. A scalar field theory is trivial whenever an ultraviolet fixed point for the quartic coupling is absent. In this case, the theory is ill-defined at high energies, unless the renormalised coupling is set to zero, thus eliminating scalar self-interactions. This supports the interpretation of the SM as an effective field theory, defined up to an ultraviolet cutoff, and discourages the introduction of elementary scalars in a UV-complete theory.

2.1.2 Composite Higgs models

Composite Higgs models constitute an alternative to the Higgs mechanism for the generation of masses, in which no elementary scalars are included. The first inspiration for composite Higgs models came from the fact that the Higgs vacuum expectation value is not the only source of electroweak symmetry breaking in the Standard Model. In fact, QCD pions contribute to the mass of the W and Z gauge bosons. This is due to the fact that electroweak symmetry is embedded in the chiral $\mathrm{SU}(2)_L \times \mathrm{SU}(2)_R$ symmetry of QCD, which is spontaneously broken by the strong dynamics.

It is shown in [8] that, in a theory with the SM gauge symmetry $\mathrm{SU}(2)_L \times \mathrm{U}(1)_Y \times \mathrm{SU}(3)_C$, containing one family of massless quarks and no Higgs doublet, the electroweak gauge bosons become massive. Specifically, the $W^\pm$ bosons acquire a mass $M_W = (g/2) f_\pi \simeq 30\,\mathrm{MeV}$, where g is the $\mathrm{SU}(2)_L$ gauge coupling, and f_π the pion decay constant. Moreover, the photon is massless and the ratio of the W and Z masses is the same as in the SM. In order to obtain these results, the gauge couplings are assumed to run in the same way as in the SM. In particular, the $\mathrm{SU}(3)_C$ gauge coupling becomes ~ 1 at 1 GeV, and the electroweak sector is treated as a small perturbation. The value of $g/2$ can be deduced from the relation between the Fermi constant G_F and the W boson mass:

$$\frac{G_F}{\sqrt{2}} = \left(\frac{g}{2\sqrt{2}}\right)^2 \frac{1}{M_W^2}\,, \tag{2.4}$$

while the pion decay constant is given by $f_\pi = 93\,\mathrm{MeV}$ [9].

The W boson mass thus generated is clearly too small with respect to the experimental value of 80 GeV, and indeed in the SM the almost unique source of electroweak symmetry breaking is the Higgs vacuum expectation value. However, one may imagine a "scaled-up" version of QCD, where the pion decay constant is big enough to provide a realistic mass for W and Z bosons. This is the idea behind Technicolor (TC) models [10, 8]. In these models, all the SM particles are included except for the Higgs doublet, and on top of that a new strongly interacting sector is added. The new sector contains fermionic matter, which we will refer to as TC-fermions, and a new non-Abelian gauge interaction. The TC sector in isolation is symmetric under a global flavour symmetry, which is assumed to be spontaneously broken by the formation of the TC-fermion condensate. The flavour symmetry is required to have an $\mathrm{SU}(2) \times \mathrm{U}(1)$ subgroup, so as to allow the embedding of electroweak interactions. Specifically, the $\mathrm{SU}(2)_L \times \mathrm{U}(1)_Y$ generators are identified

with some of the broken generators of the TC flavour symmetry. As a consequence, the W and Z bosons acquire a mass proportional to the TC-pion decay constant. In these models the Higgs boson is identified with the lightest scalar resonance of the TC-sector. In general it is not automatic to obtain both a Higgs mass and W and Z masses in good agreement with experimental values. In particular, unless some care is taken, the Higgs boson will end up being heavier than the measured 125 GeV. Walking Technicolor models [11, 12, 13, 14] address this kind of issue.

Another composite Higgs scenario is the one of composite Goldstone Higgs models [15, 16]. In these models a new strongly interacting sector analogous to the TC one is introduced (we will continue to call it TC sector), but the embedding of electroweak symmetry is substantially different. In fact, the $\mathrm{SU}(2)_L \times \mathrm{U}(1)_Y$ generators are identified with some of the unbroken generators of the TC flavour symmetry, so that W and Z bosons remain massless. The Higgs is identified with one of the Goldstone bosons of the broken flavour symmetry. Unless some explicit breaking of this symmetry is introduced, the Goldstone-Higgs is a massless particle. In order to generate the correct Higgs mass and to give masses to W and Z, some new interactions are introduced, which explicitly break the TC flavour symmetry. The explicit form of possible symmetry-breaking interactions will be discussed in the next section, in the case of a specific model. In the setup of composite Goldstone Higgs models, the Higgs boson is naturally light and a large separation occurs between the electroweak scale and the scale at which the TC gauge coupling becomes strong. Therefore the masses of non-Goldstone TC-hadrons are expected to be large with respect to the electroweak scale, and possibly beyond the range explored so far in accelerator experiments.

To conclude, we remark that in composite Higgs models electroweak symmetry is broken as a consequence of the dynamics of the theory. In this respect, these models are more theoretically satisfactory than the SM, where electroweak symmetry breaking is simply modelled and no dynamical reason is given for its occurrence. In the next section we analyse in some more detail the SU(2) gauge theory with two fermions in the fundamental representation, which can serve as setup for both Technicolor and composite Goldstone Higgs scenarios [17].

2.1.3 SU(2) + 2 fermions as minimal composite Higgs model

In this section, following the lines of [17], we discuss a specific model: the SU(2) gauge theory with two fermions in the fundamental representation. This is a good candidate for being the TC sector in both a Technicolor and a composite Goldstone Higgs scenario.

The Lagrangian of this model is given by:

$$\mathcal{L} = -\frac{1}{4} F^a_{\mu\nu} F^{a\mu\nu} + \bar{u}(i \not{D} - m)u + \bar{d}(i \not{D} - m)d \,, \tag{2.5}$$

where u and d are the two TC-fermion fields with equal mass m, $F^a_{\mu\nu}$ is the non-Abelian field strength tensor and D_μ is the covariant derivative. In the case $m = 0$, this Lagrangian has a larger flavour symmetry than the $\mathrm{SU}(2)_L \times \mathrm{SU}(2)_R$ generally expected for an SU(N) gauge theory with two fundamental fermions. This is due

to the fact that the fundamental representation of SU(2) is pseudo-real, i.e. there is a relation between a matrix of SU(2) and its complex conjugate:

$$U = (-i\sigma^2)U^*(i\sigma^2)\,, \quad U \in \mathrm{SU}(2)\,, \tag{2.6}$$

where σ^2 is the second Pauli matrix. Due to this property, we can define an enlarged flavour multiplet of left-handed fields transforming under the fundamental representation of SU(2):

$$Q = \begin{pmatrix} u_L \\ d_L \\ \tilde{u}_L \\ \tilde{d}_L \end{pmatrix}\,, \tag{2.7}$$

where the left- and right-handed spinors are defined by:

$$u_L = \frac{\mathbb{1}-\gamma_5}{2}u\,, \quad u_R = \frac{\mathbb{1}+\gamma_5}{2}u\,, \quad d_L = \frac{\mathbb{1}-\gamma_5}{2}d\,, \quad d_R = \frac{\mathbb{1}+\gamma_5}{2}d\,, \tag{2.8}$$

and we have defined some new left-handed fields $\tilde{u}_L$ and $\tilde{d}_L$ as:

$$\tilde{u}_L = -i\sigma^2 C\bar{u}_R^T\,, \quad \tilde{d}_L = -i\sigma^2 C\bar{d}_R^T\,. \tag{2.9}$$

In equation 2.9, the matrix $-i\sigma^2$ acts on the colour indices of the spinors, while C is the charge conjugation operator, acting on Dirac indices (see appendix A.1.2). As a consequence of equation 2.6, $\tilde{u}_L$ and $\tilde{d}_L$ transform under the fundamental representation of the TC group SU(2):

$$\begin{gathered} u_R \to u'_R = Uu_R, \quad U \in \mathrm{SU}(2) \\ \Downarrow \\ \tilde{u}'_L = -i\sigma^2 C\bar{u'}_R^T = -i\sigma^2 U^* C\bar{u}_R^T = U\tilde{u}_L\,. \end{gathered}$$

The Lagrangian 2.5 can be rewritten in terms of Q as follows:

$$\mathcal{L} = -\frac{1}{4}F^a_{\mu\nu}F^{a\mu\nu} + i\bar{Q}\not{D}Q + \frac{m}{2}Q^T(-i\sigma^2)CEQ + \frac{m}{2}(Q^T(-i\sigma^2)CEQ)^\dagger\,, \tag{2.10}$$

where

$$E = \begin{pmatrix} 0 & 0 & 1 & 0 \\ 0 & 0 & 0 & 1 \\ -1 & 0 & 0 & 0 \\ 0 & -1 & 0 & 0 \end{pmatrix}\,. \tag{2.11}$$

If $m = 0$, this Lagrangian is symmetric under global SU(4) transformations of the multiplet Q, while if $m \neq 0$ the symmetry is reduced to the subgroup Sp(4), defined as being the group of transformations such that the following condition is verified:

$$ET_n + T_n^T E = 0\,, \tag{2.12}$$

where T_n are the fifteen generators of the fundamental representation of SU(4).

After defining the TC sector in isolation, we embed electroweak symmetry by assigning the following transformation properties:

- $Q_L = (u_L, d_L)^T$ is an $\mathrm{SU}(2)_L$ doublet with zero hypercharge
- $\tilde{u}_L$ and $\tilde{d}_L$ are two $\mathrm{SU}(2)_L$ singlets with hypercharges -1/2 and +1/2 respectively.

With these assignments, we can identify the electroweak generators among the generators of flavour symmetry. First of all, we list the generators of SU(4), and, for future purposes, we split them into two groups, denoted by S^i, $i = 1, \ldots, 10$, and X^j, $j = 1, \ldots, 5$:

$$\begin{aligned} S^{1,2,3} &= \frac{1}{2}\begin{pmatrix} \sigma^i & 0 \\ 0 & 0 \end{pmatrix}, \quad S^{4,5,6} = \frac{1}{2}\begin{pmatrix} 0 & 0 \\ 0 & -\sigma^{iT} \end{pmatrix}, \\ S^{7,8,9} &= \frac{1}{2\sqrt{2}}\begin{pmatrix} 0 & i\sigma^i \\ -i\sigma^i & 0 \end{pmatrix}, \quad S^{10} = \frac{1}{2\sqrt{2}}\begin{pmatrix} 0 & 1 \\ 1 & 0 \end{pmatrix}, \end{aligned} \tag{2.13}$$

$$\begin{aligned} X^1 = \frac{1}{2\sqrt{2}}\begin{pmatrix} 0 & \sigma^3 \\ \sigma^3 & 0 \end{pmatrix}, \quad X^2 = \frac{1}{2\sqrt{2}}\begin{pmatrix} 0 & -i \\ -i & 0 \end{pmatrix}, \quad X^3 = \frac{1}{2\sqrt{2}}\begin{pmatrix} 0 & \sigma^1 \\ \sigma^1 & 0 \end{pmatrix}, \\ X^4 = \frac{1}{2\sqrt{2}}\begin{pmatrix} 0 & \sigma^2 \\ \sigma^2 & 0 \end{pmatrix}, \quad X^5 = \frac{1}{2\sqrt{2}}\begin{pmatrix} 1 & 0 \\ 0 & -1 \end{pmatrix}, \end{aligned} \tag{2.14}$$

where, as usual, σ^i, $i = 1, 2, 3$, are the Pauli matrices. Due to the transformation properties of Q_L, $\tilde{u}_L$ and $\tilde{d}_L$ under the electroweak gauge group, $S^{1,2,3}$ are identified with the generators of $\mathrm{SU}(2)_L$, while S^6 is the generator of $\mathrm{U}(1)_Y$.

We now assume that the TC sector in isolation, in the SU(4)-symmetric case $m = 0$, undergoes spontaneous flavour symmetry breaking due to the formation of the TC-fermion condensate:

$$\langle Q^T(-i\sigma^2)C\Sigma_0 Q + (Q^T(-i\sigma^2)C\Sigma_0 Q)^\dagger \rangle \neq 0\,. \tag{2.15}$$

The SU(4) flavour symmetry is broken down to the subgroup spanned by the unbroken generators, which fulfil the following condition:

$$\Sigma_0 T_n + T_n^T \Sigma_0 = 0\,. \tag{2.16}$$

Σ_0 is a yet unspecified matrix in flavour space, whose alignment with respect to the electroweak generators will be determined by minimising the effective potential of the theory in interaction with the electroweak group, taking into account also possible symmetry-breaking perturbations.

We rewrite Σ_0 as the superposition:

$$\Sigma_0 = \cos\theta\, \Sigma_B + \sin\theta\, \Sigma_H\,, \tag{2.17}$$

where

$$\Sigma_B = \begin{pmatrix} i\sigma^2 & 0 \\ 0 & -i\sigma^2 \end{pmatrix} , \quad \Sigma_H = E = \begin{pmatrix} 0 & \mathbb{1} \\ -\mathbb{1} & 0 \end{pmatrix} . \tag{2.18}$$

If $\Sigma_0 = \Sigma_B$, the unbroken generators are the S^i's defined in equation 2.13, while the broken generators are the X^j's of equation 2.14. In particular, electroweak symmetry is preserved. If $\Sigma_0 = \Sigma_H$, the unbroken generators are:

$$S^1 + S^4 , \quad S^2 + S^5 , \quad S^3 + S^6 , \quad S^{7,9,10} , \quad X^{1,2,3,5} , \tag{2.19}$$

and the broken ones:

$$S^1 - S^4 , \quad S^2 - S^5 , \quad S^3 - S^6 , \quad S^8 , \quad X^4 . \tag{2.20}$$

In this case electroweak symmetry is broken. Moreover, we will see in the following that, for $\theta = \pi/2$, the mass of the $W^\pm$ bosons is directly determined by the Goldstone-boson decay constant and the $\mathrm{SU}(2)_L$ coupling constant, as in Technicolor models. It follows that a model with $\theta = \pi/2$ is a good candidate for Technicolor, while a model with $\theta \sim 0$ could work as composite Goldstone Higgs scenario.

For a generic alignment θ, the broken generators are given by the following combinations:

$$\begin{gathered} Y^1 = c_\theta X^1 - s_\theta \frac{S^1 - S^4}{\sqrt{2}} , \quad Y^2 = c_\theta X^2 + s_\theta \frac{S^2 - S^5}{\sqrt{2}} , \quad Y^3 = c_\theta X^3 + s_\theta \frac{S^3 - S^6}{\sqrt{2}} , \\ Y^4 = X^4 , \quad Y^5 = c_\theta X^5 - s_\theta S^8 , \end{gathered} \tag{2.21}$$

where $c_\theta = \cos\theta$ and $s_\theta = \sin\theta$. In order to study the phenomenology of the low-energy excitations of this model, the effective Lagrangian approach can be used. We define the Goldstone matrix as:

$$\Sigma = e^{i\frac{\phi^a}{f}Y^a}\Sigma_0 , \tag{2.22}$$

where $\phi^a(x)$, $a = 1, \ldots, 5$, are the Goldstone boson fields and f the Goldstone boson decay constant. The kinetic term of the effective Lagrangian, where the electroweak interactions are introduced via the covariant derivative D_μ, is given by:

$$f^2 \operatorname{tr}\left[(D_\mu\Sigma)^\dagger D^\mu \Sigma\right] , \tag{2.23}$$

where

$$D_\mu\Sigma = \partial_\mu\Sigma - i(G_\mu^T\Sigma + \Sigma G_\mu) , \tag{2.24}$$

$$G_\mu = gW_\mu^i S^i + g' B_\mu S^6 , \quad i = 1, 2, 3 . \tag{2.25}$$

In the previous equation, g is the $\mathrm{SU}(2)_L$ coupling, g' the $\mathrm{U}(1)_Y$ coupling and W_μ^i, B_μ their respective gauge boson fields.

In [17], computations are carried on in the unitary gauge, i.e. by fixing to zero the Goldstone boson fields which provide the longitudinal degrees of freedom of W

and Z. In our case this means: $\phi^{1,2,3} = 0$. The remaining Goldstone bosons are renamed as: $\phi^4 \equiv h$, $\phi^5 \equiv \eta$. The Goldstone matrix in the unitary gauge reads:

$$\Sigma = e^{\frac{i}{f}(hY^4+\eta Y^5)}\Sigma_0 \,. \tag{2.26}$$

By inserting 2.26 in 2.23, and expanding in powers of η/f, h/f, one finds the masses and couplings of the fields $W^\pm$, Z, h and η. W^i and B are expressed in terms of $W^\pm$, A and Z as in equations (*must be added in the introduction*). The resulting gauge boson masses are:

$$m_W^2 = 2g^2 f^2 s_\theta^2 \,, \tag{2.27}$$

$$m_Z^2 = 2(g^2 + g'^2) f^2 s_\theta^2 = \frac{m_W^2}{\cos^2\theta_W} \,, \tag{2.28}$$

where θ_W is the Weinberg angle. The Goldstone bosons h and η are massless (at tree level), and their couplings to the electroweak gauge bosons are given by:

$$g_{hWW} = \sqrt{2} g^2 f s_\theta c_\theta = g m_W c_\theta = g_{hWW}^{SM} c_\theta \,, \tag{2.29}$$

$$g_{hZZ} = \sqrt{2}(g^2 + g'^2) f s_\theta c_\theta = \sqrt{g^2 + g'^2}\, m_Z c_\theta = g_{hZZ}^{SM} c_\theta \,, \tag{2.30}$$

$$g_{hhWW} = \frac{1}{4} g^2 c_{2\theta} = g_{hhWW}^{SM} c_{2\theta} \,, \tag{2.31}$$

$$g_{hhZZ} = \frac{g_{hhWW}}{2\cos^2\theta_W} = g_{hhZZ}^{SM} c_{2\theta} \,, \tag{2.32}$$

$$g_{\eta\eta WW} = -\frac{1}{4} g^2 s_\theta^2 \,, \tag{2.33}$$

$$g_{\eta\eta ZZ} = \frac{g_{\eta\eta WW}}{2\cos^2\theta_W} \,. \tag{2.34}$$

It can be seen that for $\theta \sim 0$ the couplings of h to W and Z are very similar to the ones of the Standard Model Higgs, while the couplings of η are suppressed by a factor s_θ^2. Moreover, if $\theta \sim 0$, the scale hierarchy $f \gg m_W$ is realised, according to which the TC-hadron masses are expected to be much larger than the electroweak scale. This is the limit in which the composite Goldstone Higgs scenario is realised. If θ is significantly larger than zero, the h particle stops looking similar to the Higgs, and the Higgs role is assumed by the lightest scalar resonance of the TC sector, as in Technicolor. If $\theta = \pi/2$, the two scalar particles h and η become degenerate (their couplings to W and Z are equal), and the associated complex state is stable and can play a role as dark matter candidate [17].

Unless flavour symmetry is explicitly broken, all the possible alignments of Σ_0 are equivalent. The introduction of electroweak interactions via partial gauging of SU(4) results in the explicit breaking of flavour symmetry. Gauge boson loops induce a potential for the Goldstone bosons, which is minimised by a specific value of the alignment angle θ. Moreover, also other possible symmetry-breaking

contributions, such as interactions with SM fermions and mass terms for the TC-fermions, contribute to the potential, and influence the alignment of Σ_0. It is shown in [17] that the contribution of gauge boson loops to the one-loop potential contains mass terms for h and η, and is minimised at $\theta = 0$, corresponding to preserved electroweak symmetry.

A complete model of composite Higgs will contain some extra interactions on top of the ones mentioned until now, which are meant to generate masses for the SM fermions. For example, concentrating on the top quark mass, one could add to the Lagrangian 2.10 an effective four-fermion operator of the form:

$$\frac{y_t}{\Lambda_t^2}\bar{q}_L t_R \bar{u}_R Q_L + \text{h.c.}\,, \tag{2.35}$$

where q_L is the left-handed doublet containing the SM top and bottom quarks, $q_L = (t_L\, b_L)^T$, and t_R is the right-handed top quark. u_R and $Q_L = (u_L\, d_L)^T$ are TC-fermion fields. This is just an effective operator, which indicates that the theory should be extended by including some new interactions at energies larger than Λ_t. The contribution of this operator to the one-loop potential is minimised at $\theta = \pi/2$, i.e the Technicolor-like alignment [17].

The last source for the Goldstone boson potential analysed in [17] is a mass term for the TC-fermions. This term is assumed to be symmetric under $\text{SU}(2)_L \times \text{U}(1)_Y$, and therefore proportional to Σ_B: $M = \mu\Sigma_B$. It is found that, at the price of some fine tuning between the contributions of the top loop and the TC-fermion mass term, a small value of θ can be obtained, thus realising the composite Goldstone Higgs scenario.

The construction made until now is based on the assumption that the spontaneous symmetry breaking pattern $\text{SU}(4) \to \text{Sp}(4)$ is realised in the TC sector in isolation. This assumption must be verified via lattice simulations. Lattice studies of the SU(2) gauge theory with two fundamental fermions have found clear signs of symmetry breaking [18]: Goldstone boson states have been observed whose mass vanishes in the limit of vanishing fermion mass while the associated decay constant remains finite. Moreover, lattice simulations are the only way for measuring the mass spectrum of the theory, indicating in which energy range new particles are to be expected. In the case of the SU(2) model with two fundamental fermions, the lightest resonances have been found to lie beyond the present LHC limits, even in the Technicolor limit $\theta = \pi/2$ [18].

2.1.4 Fermion masses and partial compositeness

The setup of composite Higgs models must be extended in order to include massive fermion states. This is usually done by introducing in the Lagrangian operators which couple the SM fermions to the TC-fermions. The couplings can involve SM fermion bilinears, as in extended Technicolor [19, 20]:

$$\frac{\lambda_t}{\Lambda_{UV}^{d-1}}\bar{q}_L \mathcal{O} t_R + \text{h.c.}\,, \tag{2.36}$$

or can be linear in the SM fermions, as in partial compositeness [21]:

$$\frac{\lambda_t}{\Lambda_{UV}^{d_L-5/2}}\bar{q}_L\mathcal{O}^L + \frac{\bar{\lambda}_t}{\Lambda_{UV}^{d_R-5/2}}\bar{t}_R\mathcal{O}^R + \text{h.c.}\,. \tag{2.37}$$

In the previous equations we only listed the operators participating in the generation of the top quark mass. $q_L = (t_L b_L)$ represents the SM third quark family left-handed doublet, t_R the right-handed top quark and $\mathcal{O}$, $\mathcal{O}^L$, $\mathcal{O}^R$ composite operators of the TC sector. Generally the operators of equations 2.36, 2.37 are non-renormalisable, and the theory must be extended with new interactions at energies larger than Λ_{UV}. The operators 2.36, 2.37 thus arise as low-energy effective operators, accompanied by a power of Λ_{UV} dictated by the scaling dimension of $\mathcal{O}$, $\mathcal{O}^L$, $\mathcal{O}^R$ (d, d_L, d_R). The particle content of the TC sector must be chosen in such a way that the composite operators can have the correct quantum numbers for coupling with SM fermions. In particular the operator $\mathcal{O}$ of equation 2.36 must have the same quantum numbers as the SM Higgs, while $\mathcal{O}^L$ and $\mathcal{O}^R$ of equation 2.37 must have spin 1/2 and, on top of the electroweak quantum numbers, must also carry $\text{SU}(3)_C$ charge. This means that, in the partial compositeness setup, the $\text{SU}(3)_C$ symmetry must be embedded in the TC-fermion flavour symmetry, in such a way that it is not broken by the TC-fermion condensate.

We now discuss the partial compositeness mechanism in some more detail, since it is relevant for the study done in this thesis. In this scenario, fermion masses are generated via mixing between SM fermions and fermionic composite states of the TC sector. We denote by $\Lambda_{TC} < \Lambda_{UV}$ the scale at which the TC gauge coupling becomes strong, and we consider the effective theory arising when the ultraviolet cutoff is fixed to Λ_{TC}. In the model considered in [21], the operators $\mathcal{O}^L$, $\mathcal{O}^R$ mediate the coupling of the top quark to the same fermionic resonance B. The interactions in the effective Lagrangian look like:

$$\mathcal{L}_{eff}^{int} = c\Lambda_{TC}\big(\lambda_t(\Lambda_{TC})\bar{t}_L B_R + \bar{\lambda}_t(\Lambda_{TC})\bar{t}_R B_L\big) - m_B\bar{B}_L B_R + \text{h.c.}\,, \tag{2.38}$$

where c is an unknown coefficient and $\lambda_t(\Lambda_{TC})$, $\bar{\lambda}_t(\Lambda_{TC})$ are the coefficients appearing in equation 2.37 evolved down to the scale Λ_{TC}. Under the assumption $(c\Lambda_{TC})^2\lambda_t(\Lambda_{TC})\bar{\lambda}_t(\Lambda_{TC})/m_B^2 \ll 1$, the mass matrix has one light eigenvalue with mass

$$m_t \sim \frac{\lambda_t(\Lambda_{TC})\bar{\lambda}_t(\Lambda_{TC})}{m_B}(c\Lambda_{TC})^2\,, \tag{2.39}$$

and one heavier eigenvalue with mass $\sim m_B$. The physical top quark is identified with the light eigenstate, which is a superposition of the SM top and a TC composite state. This is the reason for the name partial compositeness: physical states are superpositions of elementary and composite states. The model proposed in [21], when extended to three families of SM quarks and leptons, is able to generate a large hierarchy of masses among the three families, having the first and second families much lighter than the third, even though a very general flavour structure is assumed in the underlying microscopic theory.

In the context of partial compositeness (and extended Technicolor as well), it is difficult to generate a realistic top quark mass, without at the same time introducing flavour changing neutral currents (FCNC) incompatible with experimental

constraints. In fact, the microscopic interactions that generate the operators 2.37, 2.36 in general generate also couplings among four SM fermions, which may lead to large FCNC. For this reason, it is desirable to have a very large scale for the new microscopic interactions $\Lambda_{UV} \gtrsim 1000\,\text{TeV}$, thus suppressing the contribution from unwanted FCNC. However, this constraint suppresses the value of the top mass as well.

This problem can be solved by assuming "walking" dynamics for the TC gauge coupling, in combination with large anomalous dimensions for the composite operators. The walking dynamics is realised when the TC gauge coupling has an approximate fixed point, so that is stays approximately constant between Λ_{UV} and Λ_{TC} (this point will be discussed in more detail in section 3.1). This implies:

$$\frac{\lambda_t}{\Lambda_{UV}^{d_L-5/2}} = \frac{\lambda_t(\Lambda_{TC})}{\Lambda_{TC}^{d_L-5/2}}\,, \quad \frac{\bar{\lambda}_t}{\Lambda_{UV}^{d_R-5/2}} = \frac{\bar{\lambda}_t(\Lambda_{TC})}{\Lambda_{TC}^{d_R-5/2}}\,. \tag{2.40}$$

It follows that the couplings relevant for the generation of the top quark mass are suppressed by a power of $\Lambda_{TC}/\Lambda_{UV}$:

$$\lambda_t(\Lambda_{TC}) = \lambda_t\left(\frac{\Lambda_{TC}}{\Lambda_{UV}}\right)^{d_L-\frac{5}{2}}\,, \quad \bar{\lambda}_t(\Lambda_{TC}) = \bar{\lambda}_t\left(\frac{\Lambda_{TC}}{\Lambda_{UV}}\right)^{d_R-\frac{5}{2}}\,. \tag{2.41}$$

One may obtain results compatible with experiments if the scaling dimensions of $\mathcal{O}^L$ and $\mathcal{O}^R$ are such that $d_L, d_R \sim 5/2$. We consider for example a model in which the fermionic operators $\mathcal{O}^L$, $\mathcal{O}^R$ are given by the product of three TC-fermion fields. In this case:

$$d_L = \frac{9}{2} - \gamma_L\,, \quad d_R = \frac{9}{2} - \gamma_R\,, \tag{2.42}$$

where $\gamma_{L,R}$ are the anomalous dimensions. Large anomalous dimensions $\gamma_{L,R} \sim 2$ would make it possible to have a large top mass, and at the same time suppressed FCNC. In fact, operators containing four SM fermions, responsible for FCNC, are not expected to develop large anomalous dimensions, since SM fermions are not coloured under the TC gauge interaction [21].

Recent studies indicate that the required large anomalous dimensions are hard to achieve. In particular, in [22] the SU(3) gauge theory with fundamental fermions is considered. The number of fermions is chosen in such a way that the theory is inside the conformal window, i.e. it has a nontrivial infrared fixed point. It is observed that the anomalous dimension of baryonic operators remains small down to the lowest point in the conformal window that can be analysed in perturbation theory. For a more detailed discussion of the conformal window see section 3.1

2.1.5 Fundamental Partial Compositeness

In order to overcome the difficulties related to the generation of fermion masses in composite Higgs scenarios, models of fundamental partial compositeness have recently been introduced [4]. In these models, the TC sector contains as matter fields not only fermions but also scalars. The Lagrangian can be written schematically as follows:

$$\mathcal{L} = \mathcal{L}_{SM}^{H=0} + \mathcal{L}_{TC}^{kin} + \mathcal{L}_Y - V_S \ , \tag{2.43}$$

where $\mathcal{L}_{SM}^{H=0}$ is the SM Lagrangian without the Higgs sector, $\mathcal{L}_{TC}^{kin}$ is the kinetic Lagrangian of the TC sector, containing eventual mass terms of TC-fermions and TC-scalars, $\mathcal{L}_Y$ contains Yukawa interactions among SM fermions, TC-fermions and TC-scalars, and V_S is the TC-scalar quartic potential.

The interactions between SM fermions and TC-fermions are mediated by Yukawa couplings with TC-scalars. At energies lower than Λ_{TC}, interactions between SM fermions and composite fermionic states formed by one TC-fermion and one TC-scalar are thus generated, and SM fermion masses arise via the partial compositeness mechanism. The name "fundamental" is due to the fact that only renormalisable operators appear in the Lagrangian. The low-energy effective field theory arising from this setup has been studied in detail in [23]. The implications for flavour physics and the compatibility with precision measurements of a minimal realisation of this scenario, i.e. containing the minimal number of new elementary particles, have been analysed in [24].

One may argue that, due to the presence of elementary scalars, models of fundamental partial compositeness are affected by the naturalness and triviality problems in the same way as the SM. While it is true that the naturalness problem is reintroduced, the scalars of fundamental partial compositeness may be free from the triviality problem. In fact, an ultraviolet fixed point may be present in the flow of the scalar quartic couplings. We will discuss this point in more detail in section 2.2. Moreover, the constraint $d_{L,R} \sim 5/2$ on the scaling dimensions of the operators $\mathcal{O}^{L,R}$ of equation 2.37 seems to indicate that operators with the scaling dimension of elementary scalars $d \sim 1$ must be present in the TC sector, which should mediate Yukawa-like couplings between SM fermions and TC-fermions. Therefore one may expect any purely fermionic realisation of partial compositeness to look at the effective level as the model described here [4] . Another interesting feature of the fundamental partial compositeness setup is that a complete theory of flavour is realised in a relatively self-contained way. This scenario offers a complete alternative to the Higgs mechanism of the SM.

As in the case of ordinary composite Higgs models, the pattern of global symmetry breaking assumed for the TC sector in isolation must be verified via lattice simulations. Specifically, in the model described in [23], the symmetry breaking pattern $\mathrm{SU}(2N_f) \to \mathrm{Sp}(2N_f)$ is assumed in the fermion sector, N_f being the number of Dirac TC-fermion fields. The enlarged flavour symmetry $\mathrm{SU}(2N_f)$ can be defined due to the fact that the gauge group is chosen in a pseudo-real representation. Moreover, the scalar sector is characterised by a global $\mathrm{Sp}(2N_S)$ symmetry, where N_S is the number of TC-scalars. In the model described in [23], the scalar flavour symmetry is assumed to be unbroken. This should also be tested on the lattice. However, this feature cannot be tested in a model with a single scalar field, because in this case there is no possibility of spontaneous symmetry breaking. In fact, the gauge-symmetric scalar bilinears, which may break flavour symmetry, are also flavour-symmetric. This is shown explicitly in appendix A.4, in the case of an SU(2) gauge group. Lattice measurements of the Wilson coefficients determined by the strong dynamics would also be of great interest in the context of

the low-energy effective theory [23].

With these motivations, we started a lattice study of the SU(2) gauge theory with two fundamental fermions and one fundamental scalar. While this is not a realistic TC sector for a fundamental partial compositeness model, which would require multiple scalar fields, it is a good setup for a preliminary analysis of the impact of scalar fields on the symmetry breaking pattern and on the spectrum of the theory.

2.2 Perturbative aspects of the continuum theory

The object of our lattice analysis is the SU(2) theory with two fundamental fermions and one fundamental scalar. Before entering in the details of the lattice study, we mention some interesting aspects of the continuum theory, related to the running of the scalar quartic couplings.

For these first considerations, we analyse a more general model, with SU(N) gauge group, and N_f fermions and N_S scalars in the fundamental representation. We organise the scalar and fermion fields into matrices carrying a colour index α and a flavour index i: $S_{\alpha i}$, $Q_{\alpha i}$, and we write the Lagrangian as:

$$\mathcal{L} = -\frac{1}{4}F^a_{\mu\nu}F^{a\mu\nu} + \mathrm{tr}\big[\bar{Q}i\not{D}Q\big] + \mathrm{tr}\big[(D_\mu S)^\dagger D^\mu S\big] - V_S \,, \tag{2.44}$$

where V_S is the scalar quartic potential. The most general quartic operators invariant under both SU(N) and a global SU(N_S) flavour symmetry are:

$$\big(\mathrm{tr}\big[S^\dagger S\big]\big)^2 = S^*_{i\alpha}S_{\alpha i}S^*_{j\beta}S_{\beta j} \,, \quad \mathrm{tr}\big[S^\dagger S S^\dagger S\big] = S^*_{i\alpha}S_{\alpha j}S^*_{j\beta}S_{\beta i} \,. \tag{2.45}$$

It follows that the scalar quartic potential, respecting colour and flavour symmetries, is given by:

$$V_S = \lambda_1\big(\mathrm{tr}\big[S^\dagger S\big]\big)^2 + \lambda_2\,\mathrm{tr}\big[S^\dagger S S^\dagger S\big] \,. \tag{2.46}$$

If $N_S = 1$, the two operators of equation 2.45 are equal, and one single scalar quartic coupling $\lambda = \lambda_1 + \lambda_2$ is present in the Lagrangian. Since it is of interest for the model studied in this thesis, we specialise the following considerations to the case $N_S = 1$. A complete analysis with generic N_S has been carried out in [25].

The one-loop beta functions of the gauge coupling g and the scalar quartic coupling λ are given by [4]:

$$\begin{aligned}
(4\pi)^2\beta_g &= -\left(\frac{11}{3}N - \frac{2}{3}N_f - \frac{1}{6}\right)g^3 \,, \\
(4\pi)^2\beta_\lambda &= 4(N+4)\lambda^2 - \frac{6(N^2-1)}{N}g^2\lambda + \frac{3N^3+3N^2-12N+6}{4N^2}g^4 \,.
\end{aligned} \tag{2.47}$$

The running of g and λ as functions of the energy scale μ is determined by solving the renormalisation group equations:

$$\frac{\mathrm{d}g}{\mathrm{d}\ln\mu} = \beta_g(g) \,, \quad \frac{\mathrm{d}\lambda}{\mathrm{d}\ln\mu} = \beta_\lambda(\lambda, g) \,. \tag{2.48}$$

Depending on the choice of N and N_f, the solutions may display complete asymptotic freedom, i.e. both g and λ go to zero in the limit of large μ. In this case the theory is well defined at high energies and does not suffer from the triviality problem, even though it contains elementary scalars. As an example, we report in figure 2.1 the running of g^2 and λ in the case $N = 5$, $N_f = 26$. It can be seen that, while g^2 always goes to zero at high energies, the initial condition of λ can be chosen such that also λ flows to zero, thus realising complete asymptotic freedom. In table 2.1 we report, for different values of N, the ranges in N_f such that there exist completely asymptotically free solutions. It can be noticed that for $N = 2$, the object of our lattice study, there is no possible choice of N_f leading to complete asymptotic freedom. Nevertheless the case $N = 2$ is of great interest. In fact, as shown in section 2.1.3, the SU(2) gauge theory with two fundamental fermions offers a minimal setup for composite Higgs models, and for this reason it has been extensively studied on the lattice [18]. Adding a fundamental scalar to this setup seems to be the first mandatory step to be taken, in order to observe the impact of TC-scalars on the dynamics of the TC sector in a fundamental partial compositeness scenario.

Figure 2.2 shows the running of g^2 and λ in the SU(2) gauge theory with two fundamental fermions and one fundamental scalar. Two different initial conditions are chosen for λ: $\lambda_0 = \lambda(\mu_0) = 0$, and $\lambda_0 = \lambda(\mu_0) = 0.2$. While in both cases the coupling λ diverges at high energies, this happens at an energy scale which is very large compared to the scale at which $g^2 = 1$. Specifically, if we assume that $g^2 = 1$ at $\mu_0 \sim 10^3$ GeV, then the singularity is located beyond the Planck scale ($\ln(\mu_{Pl}/\mu_0) \sim 37$) for both choices of initial conditions.

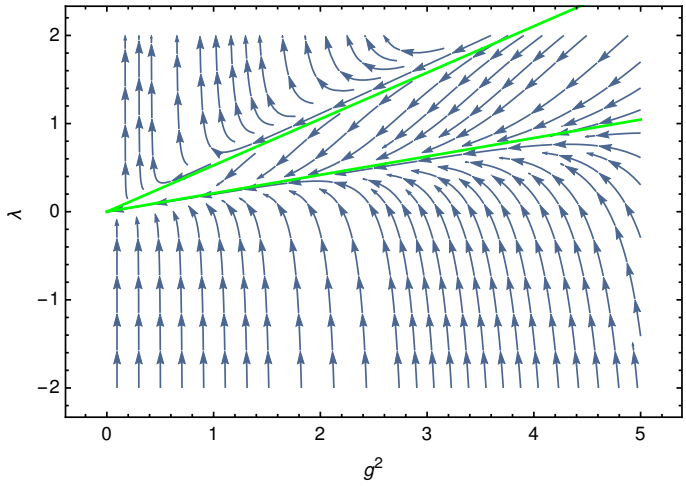

Figure 2.1: Running of the squared gauge coupling g^2 and of the scalar quartic coupling λ for a theory with SU(5) gauge group, $N_f = 26$ fundamental fermions and $N_S = 1$ fundamental scalars. The arrows indicate the direction of increasing energy. The green lines represent the fixed flow solutions of the renormalisation group equations, characterised by a constant ratio λ/g^2. This picture has already been published in [5].

One more comment must be made regarding the case $N = 2$. As previously pointed out, the fundamental representation of SU(2) is pseudo-real. One may

Table 2.1: For different values of N, ranges in N_f such that there exist completely asymptotically free solutions, in a theory with SU(N) gauge group, N_f fundamental fermions and $N_S = 1$ fundamental scalars.

N	N_f
2	No solutions
3	$15.93 < N_f < 16.25$
4	$19.8 < N_f < 21.75$
5	$23.56 < N_f < 27.25$
6	$27.27 < N_f < 32.75$
7	$30.94 < N_f < 38.25$
8	$34.6 < N_f < 43.75$
9	$38.24 < N_f < 49.25$
10	$41.88 < N_f < 54.75$

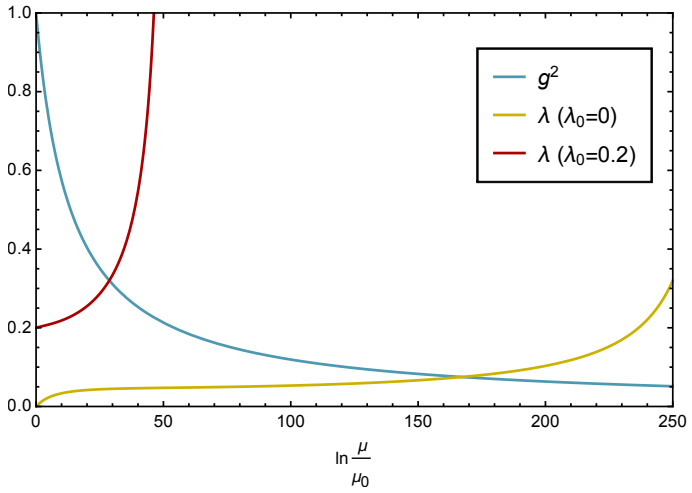

Figure 2.2: Running of g^2 and λ as functions of $\ln(\mu/\mu_0)$ in an SU(2) gauge theory with $N_f = 2$ fundamental fermions and $N_S = 1$ fundamental scalars. λ is plotted for two different initial conditions: $\lambda_0 = \lambda(\mu_0) = 0$, and $\lambda_0 = \lambda(\mu_0) = 0.2$. This picture has already been published in [5].

wonder whether in this case there exist more quartic operators than the ones listed in equation 2.45. It is shown in appendix A.4 that, also in the case of an SU(2) gauge group, the most general quartic potential takes the form 2.46.

2.3 Lattice setup

We now move to the lattice study of the SU(2) gauge theory with two fundamental fermions and one fundamental scalar. In section 2.2, we discussed the running of the scalar quartic coupling, and we concluded that the SU(2) theory is not well defined at high energies because the quartic coupling diverges. Because of this, it is impossible to define the continuum limit of the lattice theory. In fact, due to the universality of the first two coefficients of the beta function, the running of the

lattice bare couplings as functions of the lattice spacing is the same as shown in figure 2.2, with $\mu \propto 1/a$. It follows that, at least in the region where perturbation theory is valid, there is no critical point in the space of bare lattice parameters, and the program of taking the lattice spacing to zero while moving on lines of constant physics cannot be undertaken. Instead, one can take the lattice spacing down to some small but finite value, and match the lattice theory to an effective theory with an ultraviolet cutoff. Given the running of the scalar quartic coupling shown in figure 2.2, we expect the lattice theory to present a good scaling window when changing the lattice spacing, so that valuable input for phenomenological models can be provided.

For our lattice study, we generated gauge and scalar field configurations with the HiRep code, first introduced in [26], which we extended in order to simulate the scalar field in addition to gauge and fermions. In the following we describe the lattice action and the resulting forces needed for the implementation of the Hybrid Monte Carlo algorithm.

2.3.1 Action

For the gauge and fermion action we use the Wilson discretisation, as defined in equation 1.53. For simplicity, we fix the lattice spacing to one, and we use the standard notation $\beta = 2N/g^2 = 4/g^2$. As for the scalar field S, we consider the Euclidean continuum action:

$$S_S^{cont}[A, S^\dagger, S] = \int d^4x \left((D_\mu S)^\dagger D_\mu S + m_S^2 |S|^2 + \lambda |S|^4 \right) , \tag{2.49}$$

and we discretise it by assigning

$$\int \mathrm{d}^4x (D_\mu S)^\dagger D_\mu S \to - \sum_{x,\mu} S^\dagger \nabla_\mu^* \nabla_\mu S \, , \tag{2.50}$$

where

$$\begin{aligned} \nabla_\mu S(x) &= U_\mu(x) S(x+\hat{\mu}) - S(x) \\ \nabla_\mu^* S(x) &= S(x) - U_\mu(x-\hat{\mu})^\dagger S(x-\hat{\mu}) \, . \end{aligned} \tag{2.51}$$

The resulting discretised action is:

$$\begin{aligned} S_S[U, S^\dagger, S] = \sum_x \Big[- \sum_\mu \Big(S^\dagger(x) U_\mu(x) S(x+\hat{\mu}) + S^\dagger(x) U_\mu(x-\hat{\mu})^\dagger S(x-\hat{\mu}) \Big) + \\ M^2 S^\dagger(x) S(x) + \lambda \big(S^\dagger(x) S(x) \big)^2 \Big] \, , \end{aligned} \tag{2.52}$$

where $M^2 = m_S^2 + 8$. For future purposes, we write the action of our lattice model as:

$$S[U,\phi^\dagger,\phi,S^\dagger,S] = S_G[U] + S_F[U,\phi^\dagger,\phi] + S_S[U,S^\dagger,S]\,, \tag{2.53}$$

where S_S is the scalar contribution given by equation 2.52, S_G is the gauge contribution:

$$S_G[U] = \beta \sum_{x\in\Lambda}\sum_{\mu<\nu}\left[1 - \frac{1}{\mathrm{N}}\mathrm{Re}\,\mathrm{tr}[U_{\mu\nu}]\right], \tag{2.54}$$

and S_F the pseudofermion contribution (for two mass-degenerate fermion flavours):

$$S_F[U,\phi^\dagger,\phi] = \sum_{x,y\in\Lambda} \phi^\dagger(x) Q^{-2}(x|y)\phi(y) \equiv \phi^\dagger Q^{-2}\phi\,, \tag{2.55}$$

where we introduced a short-hand notation that will be useful in the following.

2.3.2 Forces

In order to implement the Hybrid Monte Carlo algorithm, we introduce the Hamiltonian:

$$H = \frac{1}{2}T_R \sum_{x,\mu}\sum_{a=1}^{N^2-1} \pi_a(x,\mu)^2 + \sum_x \sum_{i=1}^{N} P_i(x)P_i^*(x) + S[U,\phi^\dagger,\phi,S^\dagger,S]\,, \tag{2.56}$$

where $\pi_a(x,\mu)$ and $P_i(x)$ are the momenta associated to the gauge and scalar fields, and S is the action 2.53. Here, to be more general, we are referring to an SU(N) gauge group. T_R is the normalisation of the SU(N) generators in the representation R, defined by: $\mathrm{tr}(T^aT^b) = T_R\delta^{ab}$. In this setup, only gauge and scalar fields evolve dynamically along the molecular dynamics trajectory. The pseudofermions are updated before starting every new trajectory according to the following rule: a field χ is extracted out of a Gaussian distribution, with probability $P[\chi] \propto \exp\left[-\chi^\dagger\chi\right]$, and then the pseudofermion field is defined as: $\phi = D\chi$, where D is the Wilson-Dirac operator 1.46. The field ϕ defined in this way is correctly distributed according to:

$$\det\left[Q^2\right] = \det[D]^2 = \det\left[DD^\dagger\right] = \pi^{-N}\int \prod_{x\in\Lambda} \mathrm{d}\phi(x)\mathrm{d}\phi^\dagger(x)\exp\left[-\phi^\dagger(DD^\dagger)^{-1}\phi\right]. \tag{2.57}$$

We express the link variables as:

$$U_\mu(x) = \exp\left[\frac{i}{T_R}q_a(x,\mu)T^a\right], \tag{2.58}$$

and we assign the conjugate momenta as follows:

$$\begin{aligned} &q_a(x,\mu) \to \pi_a(x,\mu) \\ &S_i(x) \to P_i(x)\,. \end{aligned} \tag{2.59}$$

Hamilton's equations are given by:

$$\begin{aligned}
\dot{q}_a(x,\mu) &= \frac{\partial H}{\partial \pi_a(x,\mu)} = T_R \pi_a(x,\mu) \\
\dot{\pi}_a(x,\mu) &= -\frac{\partial H}{\partial q_a(x,\mu)} = -\frac{\partial S_G}{\partial q_a(x,\mu)} - \frac{\partial S_F}{\partial q_a(x,\mu)} - \frac{\partial S_S}{\partial q_a(x,\mu)} \\
\dot{S}_i(x) &= \frac{\partial H}{\partial P_i(x)} = P_i^*(x) \\
\dot{P}_i(x) &= -\frac{\partial H}{\partial S_i(x)} = -\frac{\partial S_S}{\partial S_i(x)} \,,
\end{aligned} \tag{2.60}$$

where the dot indicates the derivative with respect to molecular dynamics time. For brevity we omitted the equations for $\dot{S}^*$ and $\dot{P}^*$, which are simply given by the complex conjugate of the last two lines in 2.60. The first line of 2.60 can be rewritten in terms of the link variables as follows:

$$\dot{U_\mu}(x) = i\pi_a(x,\mu) T^a U_\mu(x) \,. \tag{2.61}$$

The driving forces are given by:

- $$\frac{\partial S_G}{\partial q_a(x,\mu)} = -\frac{\beta}{N}\frac{1}{T_R}\mathrm{Re\ tr}\Big[iT^a U_\mu(x) V_\mu^\dagger(x)\Big] \tag{2.62}$$

where $V_\mu(x) = \sum_{\nu\neq\mu}\big[U_\nu(x)U_\mu(x+\hat{\nu})U_\nu^\dagger(x+\hat{\mu}) + U_\nu^\dagger(x-\hat{\nu})U_\mu(x-\hat{\nu})U_\nu(x-\hat{\nu}+\hat{\mu})\big]$ is the sum of the staples around the link $U_\mu(x)$,

- $$\frac{\partial S_F}{\partial q_a(x,\mu)} = -\left[\phi^\dagger Q^{-2}\frac{\partial Q}{\partial q_a(x,\mu)}Q^{-1}\phi + \phi^\dagger Q^{-1}\frac{\partial Q}{\partial q_a(x,\mu)}Q^{-2}\phi\right] \tag{2.63}$$

where

$$\frac{\partial Q(x|y)}{\partial q_a(z,\mu)} = \gamma_5\left(-\frac{i}{2T_R}(\mathbb{1}-\gamma_\mu)T^a U_\mu(z)\delta_{y,z+\hat{\mu}}\delta_{x,z} + \frac{i}{2T_R}(\mathbb{1}+\gamma_\mu)U_\mu^\dagger(z)T^a\delta_{y,z}\delta_{x-a\hat{\mu},z}\right), \tag{2.64}$$

- $$\frac{\partial S_S}{\partial q_a(x,\mu)} = -\frac{2}{T_R}\,\mathrm{Re}\Big[S^\dagger(x) iT^a U_\mu(x) S(x+\hat{\mu})\Big] \tag{2.65}$$

- $$\begin{aligned}\frac{\partial S_S}{\partial S_i(x)} = &-\sum_\mu\Big(S_k^*(x-\hat{\mu})U_\mu(x-\hat{\mu})_{ki} + S_k^*(x+\hat{\mu})U_\mu(x)^\dagger_{ki}\Big) + \\ &+ M^2 S_i^*(x) + 2\lambda S_k^*(x)S_k(x)S_i^*(x) \,.\end{aligned} \tag{2.66}$$

Hamilton's equations 2.60 are to be solved numerically, thus generating the molecular dynamics trajectory. In this work we used a second-order Omelyan integrator [27, 28] for the numerical integration.

2.4 Spectrum

2.4.1 Mesons

In this section, we present our results on the meson spectrum of the SU(2) gauge theory with two fundamental fermions and one fundamental scalar. We measured the mass of the isospin-triplet pseudoscalar (m_{PS}) and vector (m_V) mesons. The interpolating operators for these observables are defined in section 1.5.1. We also measured the fermion mass m_{PCAC} via the PCAC relation, as described in section 1.5.2. Moreover, we measured the Goldstone boson decay constant f_{PS}. This observable (once renormalised) can be used to express the lattice spacing in physical units. In fact, as discussed in section 2.1.3, the W boson mass is given by[1]:

$$m_W = \frac{g_{EW}}{2}(f_{PS})_0^{ren} \sin\theta \,, \tag{2.67}$$

where g_{EW} is the $\mathrm{SU}(2)_L$ electroweak gauge coupling and θ the alignment angle. $(f_{PS})_0^{ren}$ denotes the renormalised Goldstone boson decay constant in the chiral limit ($m_{PCAC} \to 0$). It follows that the experimental value of m_W is recovered by fixing $(f_{PS})_0^{ren} \sin\theta = v$, $v = 246\,\mathrm{GeV}$ being the Higgs vacuum expectation value. f_{PS} is computed as:

$$f_{PS} = \frac{2m_{PCAC}}{m_{PS}^2} G_{PS} \,, \tag{2.68}$$

where G_{PS} is obtained from the large-t behaviour of the correlator $C_{\gamma_5}(t)$, defined in section 1.5.1:

$$C_{\gamma_5}(t) \underset{t\to\infty}{\sim} -\frac{G_{PS}^2}{m_{PS}} e^{-m_{PS}t} \,. \tag{2.69}$$

Renormalisation has not been addressed in our work yet, and the values of m_{PCAC} and f_{PS} that we quote are unrenormalised. Moreover, all our results, listed in table 2.2, are expressed in lattice units. For our measurements, we chose values of the inverse gauge coupling β and of the bare fermion mass m_f that have already been studied in the SU(2) gauge theory with two fundamental fermions [18]. In particular, at the current status of our analysis, we considered one single value of β ($\beta = 2$) and two values of the bare fermion mass: $m_f = -0.94, -0.952$. For each choice of m_f, we simulated several values of the squared scalar mass m_S^2, and, in the case of $m_f = -0.94$, we repeated the analysis for two different values of the scalar quartic coupling λ. In a few cases, we repeated the measurements with the same bare parameters at two different lattice volumes. We consider lattices with the same extent in all spacial directions $L_1 = L_2 = L_3 \equiv L$, and we denote the lattice time extent by $T \equiv L_0$.

Since we will use quite often the SU(2) theory with two fundamental fermions as a comparison, we will shortly refer to it as the SU(2)-2F model, and we will make reference to the most recent results published in [18]. In figure 2.3, we plot the PCAC mass, the meson masses and the Goldstone boson decay constant as

[1]Here we use a different normalisation for the Goldstone boson decay constant with respect to section 2.1.3. The two conventions are related by: $f = f_{PS}/(2\sqrt{2})$.

functions of the squared scalar mass m_S^2. Together with our data points, we report the results for the same observables obtained in the SU(2)-2F model (dashed lines). We observe that, provided m_S^2 is large enough, the results of the SU(2)-2F model are recovered, while for $m_S^2 \lesssim 1$ deviations from those results can be observed in all the considered observables. Moreover, for $\lambda = 2$ and $m_f = -0.94$, we observe a sharp change of behaviour around $m_S^2 \simeq -3.2$, presumably corresponding to a phase transition. In particular, at (m_f, λ, m_S^2) = (-0.94, 2, -3.6), the PCAC mass is negative, m_{PS} and m_V are almost degenerate and f_{PS} is compatible with zero. For $m_f = -0.94$, $\lambda = 2$ and $m_S^2 \leq -3.2$, the simulations become significantly more time-consuming than for larger values of m_S^2, and require a very fine integration step in the molecular dynamics trajectories. In the case of $m_f = -0.94$ and $\lambda = 0$, we were not able to run simulations at $m_S^2 < -1$. We believe that this is due to instability of the scalar potential. It will be shown in the next section that a similar situation occurs in the SU(2) model with one fundamental scalar and no fermions (SU(2)-Higgs model).

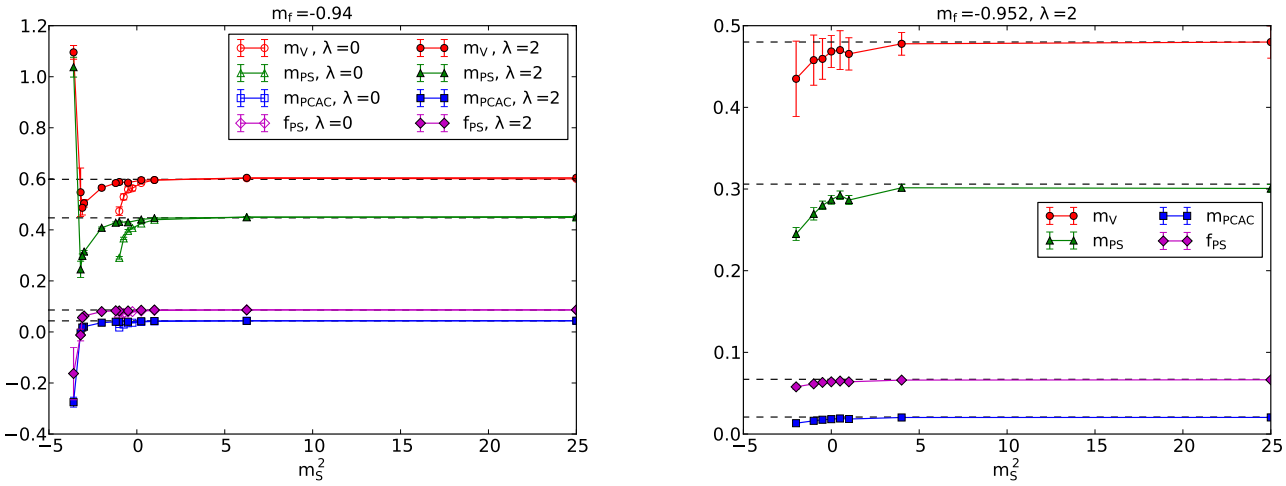

Figure 2.3: Fermion mass (m_{PCAC}), pseudoscalar meson mass (m_{PS}), vector meson mass (m_V) and Goldstone boson decay constant (f_{PS}) as functions of the squared scalar mass m_S^2. Together with our data points, we report the results for the same observables obtained in the SU2-2F model (dashed lines). In the left panel we plot the results for $m_f = -0.94$ and two different values of λ, while in the right panel there appear the results for $m_f = -0.952$ and $\lambda = 2$.

In figure 2.4, we plot m_{PS}, m_V and f_{PS} as functions of m_{PCAC}, for $m_f = -0.94$. In the left panel we report all our data points, while in the right panel we omit two points, corresponding to (λ, m_S^2) = (2, -3.6), (2, -3.2). Together with our data, we report fits to the data of the SU(2)-2F model. The forms of the fitting functions for m_{PS} and f_{PS} are motivated by chiral perturbation theory, and are given by:

$$\frac{m_{PS}^2}{m_{PCAC}} = M_0\left[1 + M_1 m_{PCAC}\log(m_{PCAC}) + M_2 m_{PCAC}\right], \tag{2.70}$$

$$f_{PS} = F_0\left[1 + F_1 m_{PCAC}\log(m_{PCAC}) + F_2 m_{PCAC}\right], \tag{2.71}$$

while for m_V the following polynomial ansatz is used:

$$m_V = V_0 + V_1 m_{PCAC} + V_2 m_{PCAC}^2 \,. \tag{2.72}$$

It can be observed that, once the points (λ, m_S^2) = (2, -3.6), (2, -3.2) are excluded, there is very good agreement between our data and the fits in the SU(2)-2F model. We stress the fact that the curves in figure 2.4 are obtained in the SU(2)-2F model by fitting data at fixed β and varying m_f, while our data points shown in the figure are obtained at fixed β and m_f, and varying m_S^2, for two different values of λ. In the right panel of figure 2.4, the black points represent measurements obtained in larger lattice volumes. It can be observed from the data in table 2.2, that large finite volume corrections in the PCAC mass and pseudoscalar meson mass occur at (m_f, λ, m_S^2) = (-0.94, 0, -1). The same effect is not observed at (m_f, λ, m_S^2) = (-0.94, 0, 0.0625), where we also repeated the measurements in two different volumes.

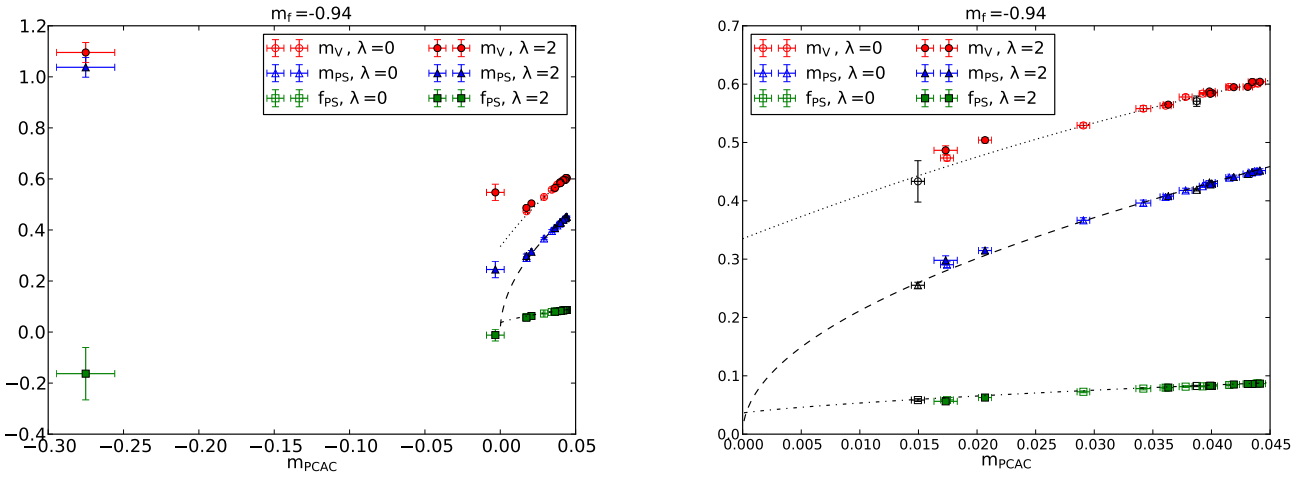

Figure 2.4: Pseudoscalar meson mass (m_{PS}), vector meson mass (m_V) and Goldstone boson decay constant (f_{PS}) as functions of m_{PCAC}, at $m_f = -0.94$. In the left panel all the available data are included, while in the right panel we excluded the points (λ, m_S^2) = (2, -3.6), (2, -3.2). The dotted, dashed and dash-dotted lines are fits to the data of the SU(2)-2F model, obtained by fitting data at fixed $\beta = 2$ and varying m_f, by using the functional forms 2.72, 2.70, 2.71. The black data points in the right panel represent measurements obtained in a larger volume $L = 24$, $T = 48$. All the other points correspond to $L = 16$, $T = 32$.

In figure 2.5 we plot m_{PS}, m_V and f_{PS} as functions of m_{PCAC}, for $\lambda = 2$ and the two available values of m_f. The points (m_f, λ, m_S^2) = (-0.94, 2, -3.6), (-0.94, 2, -3.2) are excluded. The curves are the same as in figure 2.4. We again observe an impressive agreement with the data of the SU(2)-2F model. As the PCAC mass becomes lighter, the data at $m_f = -0.94$ start to show small deviations with respect to the curves, as the presumed phase transition approaches, while the $m_f = -0.952$ data are still in very good agreement with the curves. We presume that the phase transition will occur also in the case $m_f = -0.952$, $\lambda = 2$, even though we have not yet reached the critical value of m_S^2 in our analysis.

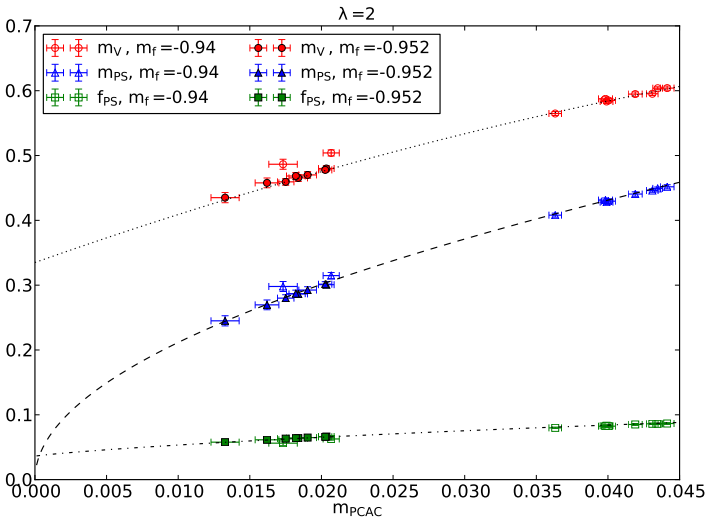

Figure 2.5: Same as the right panel of figure 2.4, but for fixed $\lambda = 2$ and two different values of m_f.

To conclude, our somewhat preliminary analysis of the meson spectrum of the SU(2) gauge theory with two fundamental fermions and one fundamental scalar already shows some interesting results. First of all, there seems to exist a phase with broken fermion-flavour symmetry, with Goldstone boson states (the pseudoscalar mesons) whose mass goes to zero in the limit of vanishing m_{PCAC} and whose decay constant remains finite in the same limit. This seems to indicate that additional scalar fields may not dramatically affect the symmetry breaking pattern of a gauge-fermion theory, and it is encouraging from the point of view of composite Higgs models based on the fundamental partial compositeness paradigm. However, we found two kinds of obstacles in moving towards small values of the PCAC mass: at $m_f = -0.94$, $\lambda = 0$, we found a critical value of the squared scalar mass, $m_S^2 = -1$, below which the simulations do not work, due presumably to instability of the scalar potential (we will discuss this point in more detail in the next section). At $m_f = -0.94$, $\lambda = 2$, we observed an abrupt change of behaviour of the meson observables around $m_S^2 = -3.2$, presumably due to a phase transition. In particular, we find a point with zero PCAC mass and nonzero m_{PS}, (m_S^2 = -3.2) and one point with negative PCAC mass and degenerate m_{PS} and m_V ($m_S^2 = -3.6$). An extension of our analysis to smaller values of the bare fermion mass and larger values of β will give us a better understanding of the phase structure of the model.

Another interesting result is the impressive agreement between our results and the results of the SU(2) theory with two fundamental fermions [18], once the meson masses and Goldstone boson decay constant are expressed as functions of m_{PCAC}. In particular, our data fall pretty accurately on top of the curves obtained by fitting the data of the SU(2)-2F model, provided we exclude some of the data which presumably belong to a different phase. This seems to indicate that the main influence of the scalar field on the meson observables is due to a shift of the PCAC mass. The last interesting observation, for which we have no explanation at the

moment, is the occurrence of large finite volume effects in m_{PCAC} and m_{PS} at (m_f, λ, m_S^2) = (-0.94, 0, -1).

2.4.2 Bound states with the scalar

In fundamental partial compositeness models, as discussed in section 2.1.5, fermionic bound states made by one fermion and one scalar are involved in the generation of Standard Model fermion masses, and it is therefore very interesting to measure their mass spectrum. In this section, we report our very preliminary analysis of the spectrum of bound states involving the scalar field. Our analysis did not lead to any results yet, and we will need to apply more refined techniques in order to measure this part of the spectrum.

To measure the mass of spin-zero states formed by a scalar-antiscalar pair, we consider the correlator:

$$C(t) = \frac{1}{T}\sum_{\tau=0}^{T-1}\sum_{\vec{x},\vec{y}}\langle S^\dagger(\vec{x},\tau+t)S(\vec{x},\tau+t)S^\dagger(\vec{y},\tau)S(\vec{y},\tau)\rangle \ . \tag{2.73}$$

In order to subtract the contributions from disconnected diagrams, we study $C(t)-C(t+1)$ as a function of t, as shown in figure 2.6. We observe that the decay with increasing t is very fast, which suggests that no light states are present in this channel. The data are very noisy, and do not allow us to extract the coefficient of the exponential decay at large t.

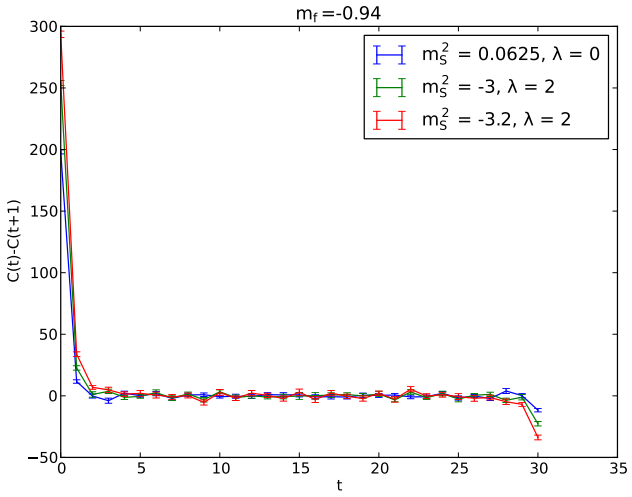

Figure 2.6: Decay of $C(t) - C(t+1)$ as a function of the Euclidean time t, at $m_f = -0.94$ and different values of m_S^2 and λ. The correlator $C(t)$ is defined in equation 2.73. We observe a very fast decay, which suggests the absence of light states in this channel. The data are too noisy to extract any quantitative information.

To study fermionic bound states made by one fermion and one scalar, we consider two kinds of correlators:

m_f	λ	m_S^2	L	T	m_{PCAC}	m_{PS}	f_{PS}	m_V	$\mathcal{Q}_L$	$\mathcal{Q}_C$
-0.94	0	25	16	32	0.0435(2)	0.449(1)	0.0860(6)	0.600(3)		
-0.94	0	6.25	16	32	0.0439(2)	0.450(1)	0.0868(7)	0.602(2)	$2.03(3) \times 10^{-6}$	0.1626(7)
-0.94	0	1	16	32	0.0415(3)	0.440(2)	0.084(1)	0.595(5)		
-0.94	0	0.25	16	32	0.0392(3)	0.425(2)	0.082(1)	0.584(5)		
-0.94	0	0.0625	16	32	0.0385(4)	0.420(3)	0.082(1)	0.571(8)	$1.15(2) \times 10^{-5}$	0.174(2)
-0.94	0	0.0625	24	48	0.0387(3)	0.419(2)	0.083(1)	0.57(1)	$2.24(5) \times 10^{-6}$	0.0729(3)
-0.94	0	0	16	32	0.0378(6)	0.418(4)	0.081(2)	0.578(8)		
-0.94	0	-0.25	16	32	0.0361(5)	0.407(3)	0.080(1)	0.56(1)		
-0.94	0	-0.5	16	32	0.0342(6)	0.396(5)	0.078(2)	0.56(1)		
-0.94	0	-0.75	16	32	0.0291(5)	0.367(4)	0.073(2)	0.53(1)		
-0.94	0	-1	16	32	0.0174(6)	0.290(5)	0.059(4)	0.47(2)	$1.01(4) \times 10^{-4}$	0.233(2)
-0.94	0	-1	24	48	0.0150(6)	0.255(5)	0.058(2)	0.43(4)	$2.0(1) \times 10^{-5}$	0.117(1)
-0.94	2	25	16	32	0.0441(5)	0.452(3)	0.087(1)	0.604(8)		
-0.94	2	6.25	16	32	0.0435(3)	0.449(2)	0.086(1)	0.604(6)		
-0.94	2	1	16	32	0.0431(4)	0.446(3)	0.086(1)	0.595(7)		
-0.94	2	0.25	16	32	0.0419(5)	0.441(3)	0.085(1)	0.60(1)		
-0.94	2	-0.5	16	32	0.0400(5)	0.430(4)	0.082(2)	0.59(1)		
-0.94	2	-1	16	32	0.0398(5)	0.431(3)	0.082(2)	0.59(1)		
-0.94	2	-1.2	16	32	0.0399(4)	0.428(3)	0.083(1)	0.583(8)		
-0.94	2	-2	16	32	0.0363(4)	0.408(3)	0.080(1)	0.565(8)		
-0.94	2	-3	16	32	0.0207(6)	0.315(5)	0.063(2)	0.50(1)		
-0.94	2	-3.1	16	32	0.017(1)	0.298(8)	0.056(3)	0.49(3)	$1.02(3) \times 10^{-4}$	0.233(4)
-0.94	2	-3.2	16	32	-0.003(6)	0.25(3)	-0.01(2)	0.5(1)	$3.8(7) \times 10^{-4}$	0.34(2)
-0.94	2	-3.6	16	32	-0.28(2)	1.04(4)	-0.2(1)	1.10(3)	0.2166(1)	1.0965(3)
-0.952	2	25	32	32	0.0203(5)	0.301(5)	0.066(2)	0.48(2)	$7.1(2) \times 10^{-8}$	0.0472(3)
-0.952	2	4	32	32	0.0203(5)	0.302(4)	0.066(1)	0.48(1)	$3.07(5) \times 10^{-7}$	0.0466(3)
-0.952	2	1	32	32	0.0184(6)	0.286(6)	0.064(2)	0.47(2)	$5.4(1) \times 10^{-7}$	0.0486(3)
-0.952	2	0.5	32	32	0.0190(6)	0.292(5)	0.065(2)	0.47(2)	$6.1(1) \times 10^{-7}$	0.0480(3)
-0.952	2	0	32	32	0.0182(7)	0.287(5)	0.064(2)	0.47(2)	$7.1(2) \times 10^{-7}$	0.0486(4)
-0.952	2	-0.5	32	32	0.0175(6)	0.280(5)	0.063(2)	0.46(3)	$8.9(2) \times 10^{-7}$	0.0501(4)
-0.952	2	-1	32	32	0.0162(8)	0.270(8)	0.061(3)	0.46(3)	$1.10(3) \times 10^{-6}$	0.0509(6)
-0.952	2	-2	32	32	0.013(1)	0.245(8)	0.058(3)	0.43(5)	$1.8(2) \times 10^{-6}$	0.0560(7)

Table 2.2: In this table we report our results, obtained at a fixed value of the inverse gauge coupling $\beta = 2$, and different values of m_f, λ and m_S^2. The observables under analysis are: the fermion mass m_{PCAC}, the pseudoscalar meson mass m_{PS}, the vector meson mass m_V, the Goldstone boson decay constant f_{PS} and the gauge-dependent order parameters $\mathcal{Q}_L$ and $\mathcal{Q}_C$. The latter have only been measured in some of the ensembles. All the results are expressed in lattice units. The values of m_{PCAC} and f_{PS} are unrenormalised.

$$C_F(t) = \frac{1}{L^3}\sum_{\vec{x},\vec{y}}\langle S^\dagger(\vec{x},t)\psi_i(\vec{x},t)\bar{\psi}_i(\vec{y},0)S(\vec{y},0)\rangle\ , \tag{2.74}$$

$$C_F^\pm(t) = \frac{1}{L^3}\sum_{\vec{x},\vec{y}}\langle(\mathbb{1}\pm\gamma_0)_{ij}S^\dagger(\vec{x},t)\psi_j(\vec{x},t)\bar{\psi}_k(\vec{y},0)S(\vec{y},0)(\mathbb{1}\pm\gamma_0)_{ki}\rangle\ , \tag{2.75}$$

where all the repeated spin indices i, j, k are summed over. The correlator $C_F^\pm$ is built by using the parity-eigenstate operators $O_i^\pm(x) = (\mathbb{1}\pm\gamma_0)_{ij}S^\dagger(x)\psi_j(x)$. In figures 2.7, 2.8, 2.9, we report our cleanest results for these correlators. The decay is again very fast, indicating the absence of light states. For the computation of the term $\sum_{\vec{y}}\langle\psi_i(x)\bar{\psi}_j(\vec{y},0)\rangle S(\vec{y},0) = \sum_{\vec{y}} D^{-1}(x|\vec{y},0)_{ij}S(\vec{y},0)$, we use the scalar field as a source in the inversion of the Dirac operator, i.e. we invert the equation:

$$\sum_{y,\vec{z}}\sum_{b,c,\beta,\gamma} D(x|y)^{\alpha\beta}_{ab}D^{-1}(y|\vec{z},0)^{\beta\gamma}_{bc}S_c(\vec{z},0)\delta^{\gamma\gamma_0} = S_a(\vec{x},0)\delta^{\alpha\gamma_0}\ , \tag{2.76}$$

where $D(x|y)$ is the Wilson-Dirac operator 1.46, a, b and c are colour indices and α, β and γ are spin indices.

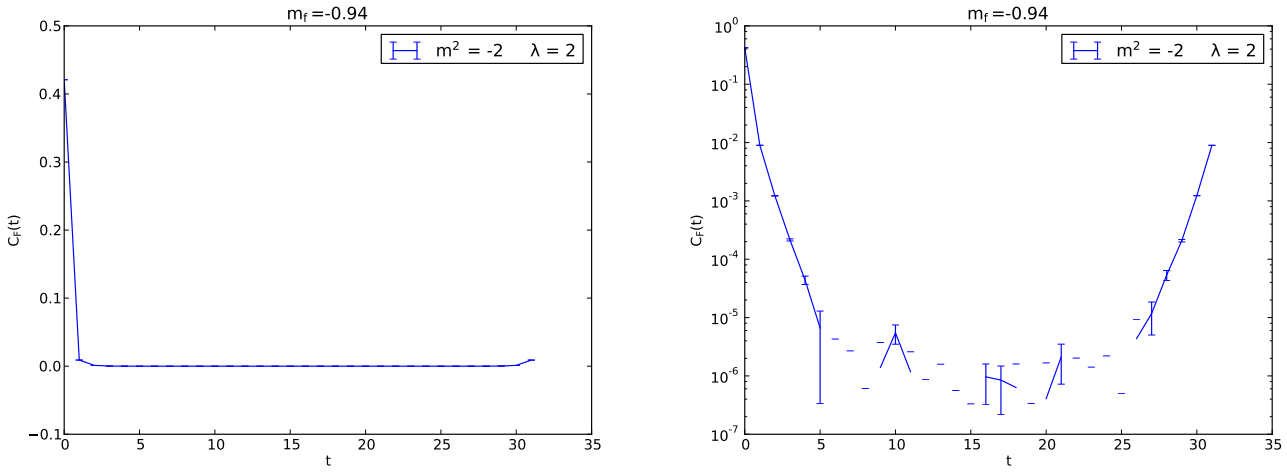

Figure 2.7: Correlator $C_F(t)$, defined in equation 2.74, as a function of t, for $m_f = -0.94$, $\lambda = 2$, $m_S^2 = -2$, both in a regular scale (left panel) and in a log-scale (right panel).

The results of our very preliminary analysis of the spectrum of bound states of the scalar field can be summarised by saying that no light states have been observed, and more refined techniques must be used to obtain quantitative results. In particular, we may need to consider a larger operator basis and to introduce some smearing of the operators. Probably larger statistics would also help. For example, in [32] the spectrum of the SU(2)-Higgs theory is computed on an ensemble of 20000 configurations, while we used ensembles of $\sim$ 2000 configurations for our measurements.

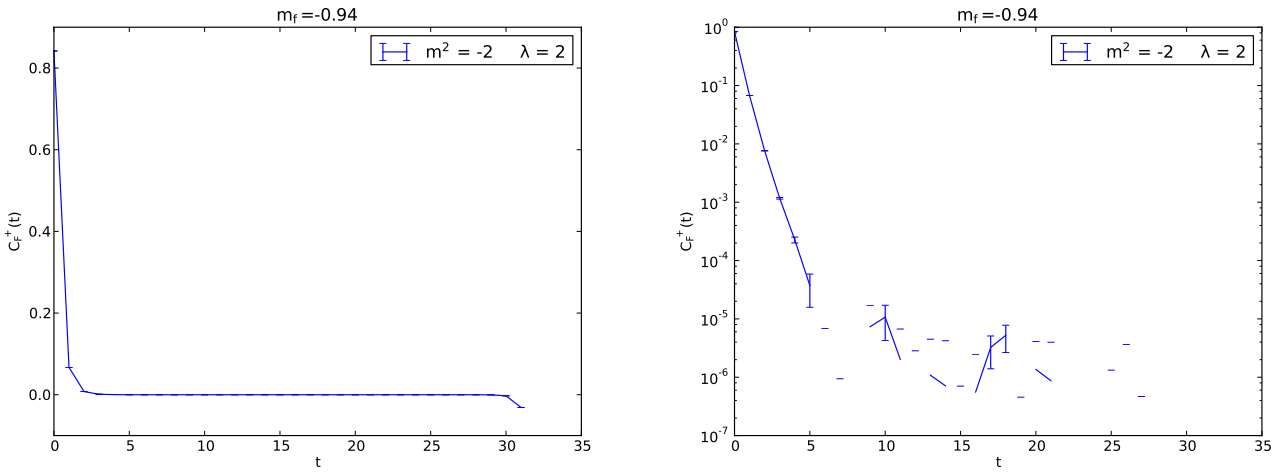

Figure 2.8: Correlator $C_F^+(t)$, defined in equation 2.75, as a function of t, for $m_f = -0.94$, $\lambda = 2$, $m_S^2 = -2$, both in a regular scale (left panel) and in a log-scale (right panel).

2.5 Higgs phase

In this section, we address the question of whether the scalar field can induce spontaneous gauge symmetry breaking in the SU(2) gauge theory with two fundamental fermions and one fundamental scalar. We take inspiration from [29], where the phase diagram of the SU(2)-Higgs model is analysed in relation to the question of spontaneous gauge symmetry breaking. In studies of the SU(2)-Higgs model, the scalar field action is usually expressed as:

$$S_S = \sum_x \left[S^\dagger(x)S(x) + \tilde{\lambda}\left(S^\dagger(x)S(x)-1\right)^2 - \gamma \sum_\mu \left(S^\dagger(x)U_\mu(x)S(x+\hat{\mu}) + S^\dagger(x)U_\mu(x-\hat{\mu})^\dagger S(x-\hat{\mu}) \right) \right] , \tag{2.77}$$

where the coefficients $\tilde{\lambda}$ and γ are related to our λ and m_S^2 by the following equations:

$$\begin{cases} \lambda = \tilde{\lambda}/\gamma^2 \\ m_S^2 = (1-2\tilde{\lambda})/\gamma - 8 \end{cases} . \tag{2.78}$$

A schematic picture of the phase diagram of the SU(2)-Higgs model, in the infinite-$\tilde{\lambda}$ limit, is given in the upper panel of figure 2.10. The infinite-$\tilde{\lambda}$ limit corresponds to a fixed-length scalar field: $S^\dagger S \equiv 1$. For $(\beta, \gamma) \ll 1$, the system is in a confinement-like phase, with a linear potential between static colour sources (up to a maximal distance where string breaking occurs due to the formation of scalar-antiscalar pairs) and a rich spectrum of QCD-like bound states. For $(\beta, \gamma) \gg 1$, the system is in a Higgs-like phase, with Yukawa-type potential between static sources and a spectrum of three massive vector bosons and a single scalar particle. The two phases are partially separated by a line of first order phase transitions, which terminates in the middle of the diagram. The Higgs and confinement phases are analytically connected [30, 31]: any two points in the phase diagram can be connected by a

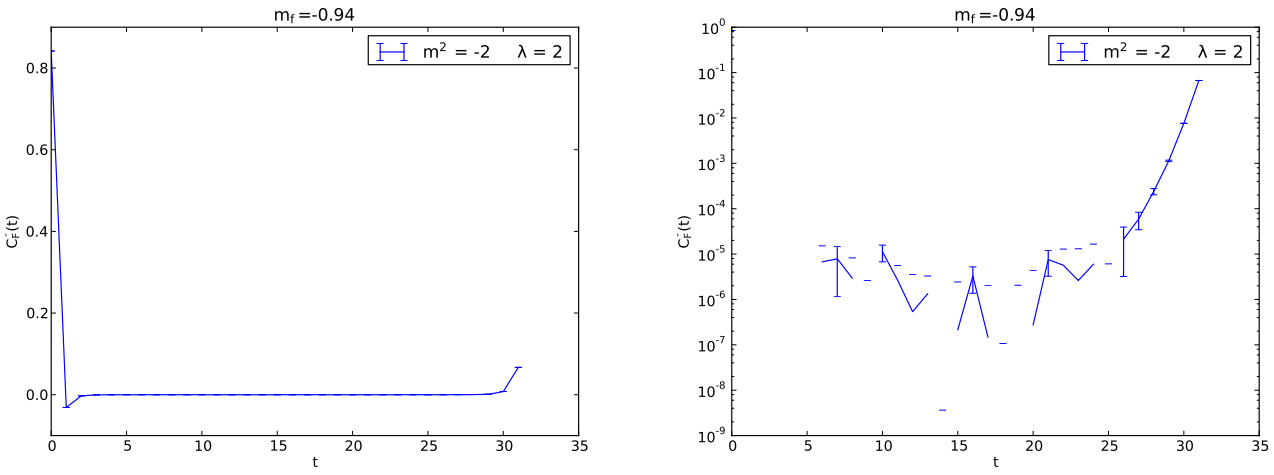

Figure 2.9: Correlator $C_F^-(t)$, defined in equation 2.75, as a function of t, for $m_f = -0.94$, $\lambda = 2$, $m_S^2 = -2$, both in a regular scale (left panel) and in a log-scale (right panel).

path over which the expectation value of any local gauge-invariant observable varies analytically. Also the spectrum, which appears to be qualitatively very different in the two phases, changes smoothly along this analytical path. In [32], the spectrum of the SU(2)-Higgs model is measured in the Higgs phase, and the observed states are found to be consistent with collections of almost noninteracting Higgs and W bosons. The same gauge-invariant operators with all possible quantum numbers are to be used to measure the spectrum in both the Higgs and the confinement phase. While these operators generate hadron-like and "W-ball" states in the confinement phase, they correspond to weakly-interacting multi-particle states in the Higgs phase, and the transition between the two regimes occurs smoothly.

The authors of [29] address the question of whether the concept of gauge symmetry breaking can be used to distinguish between the Higgs and the confinement phase, i.e. whether the phase diagram of the SU(2)-Higgs model can be unambiguously separated in a symmetric region and a broken-symmetry region. The first thing that they point out, is that gauge symmetries cannot be spontaneously broken, due to the Elitzur theorem [33]. As a consequence, unless the gauge is fixed, the vacuum expectation value of the scalar field is always zero. Only global subgroups of the gauge symmetry group can be spontaneously broken. "Global" refers to transformations depending on a finite number of parameters, which is independent of the volume. As a contrast, local transformations depend on a number of parameters which grows with the lattice volume. The breaking of some global subgroup can be studied by fixing a gauge which leaves the desired global subgroup unfixed, and then measuring an order parameter which transforms nontrivially under the remnant symmetry. In [29], the Landau and Coulomb gauges are considered. The Landau gauge is defined by:

$$\partial_\mu A_\mu = 0 \;\rightarrow \sum_{\mu=0}^{3} \big(A_\mu(x) - A_\mu(x-\hat{\mu})\big) = 0\,, \tag{2.79}$$

and the Coulomb gauge by:

$$\partial_i A_i = 0 \;\rightarrow \sum_{i=1}^{3} \big(A_i(x) - A_i(x - \hat{i}) \big) = 0 \,, \tag{2.80}$$

where we reported both the continuum and the discretised forms of the gauge conditions (and the lattice spacing is fixed to one). When the Landau gauge is fixed, there is a remnant symmetry under transformations constant in space: $\Omega(x) \equiv \Omega$. An order parameter $\mathcal{Q}_L$ can be defined as follows:

$$\bar{S} = \frac{1}{V} \sum_x S(x) \,, \tag{2.81}$$

$$\mathcal{Q}_L = \langle \bar{S}^\dagger \bar{S} \rangle \,. \tag{2.82}$$

The average scalar $\bar{S}$ transforms nontrivially under constant gauge transformations, and the scaling of $\mathcal{Q}_L$ with the lattice volume indicates whether the symmetry is broken or not. When the symmetry is broken, $\mathcal{Q}_L$ goes to a finite constant in the infinite-volume limit $V = TL^3 \rightarrow \infty$, while in the symmetric phase $\mathcal{Q}_L \rightarrow 0$ as $V \rightarrow \infty$. When the Coulomb gauge is fixed, on top of constant gauge transformations there is a larger remnant global symmetry, corresponding to transformations constant in space but not in time: $\Omega(x) \equiv \Omega(t)$. An order parameter $\mathcal{Q}_C$ for the breaking of this global subgroup is given by:

$$\tilde{U}(t) = \frac{1}{L^3} \sum_{\vec{x}} U_0(\vec{x}, t) \,, \tag{2.83}$$

$$\mathcal{Q}_C = \frac{1}{T} \sum_{t=0}^{T-1} \langle \mathrm{tr} \Big[\tilde{U}(t) \tilde{U}(t)^\dagger \Big] \rangle \,. \tag{2.84}$$

$\tilde{U}(t)$ is the average time-like link at fixed time t, and its trace $\mathrm{tr}\Big[\tilde{U}(t)\Big]$ is symmetric with respect to constant transformations, but not with respect to transformations depending on time $\Omega(x) \equiv \Omega(t)$. Therefore $\mathcal{Q}_L$ and $\mathcal{Q}_C$ probe two different global subgroups of the local symmetry group. In the infinite-volume limit, $\mathcal{Q}_C \rightarrow 0$ in the symmetric phase, while $\mathcal{Q}_C \rightarrow$ constant in the broken phase. As an example, in figure 2.11 we plot $\mathcal{Q}_L$ and $\mathcal{Q}_C$ as functions of the volume in the SU(2)-Higgs model, at $(\beta, \lambda) = (2.3, 10.8135)$, for one point in the symmetric phase (left panel) and one point in the broken-symmetry phase (right panel). The value of m_S^2 corresponding to the first order phase transition at these values of β and λ is: $m_S^2 = -11.2884$ [34].

The order parameters $\mathcal{Q}_L$ and $\mathcal{Q}_C$ test the breaking of two different global subgroups of the local symmetry group. The authors of [29] discuss the question of whether the two global subgroups break at the same points in parameter space, thus identifying unambiguously phases of broken and unbroken symmetry. Their results are reported in the lower panel of figure 2.10. Along the line of first order thermodynamic phase transitions, the two subgroups probed by $\mathcal{Q}_L$ and $\mathcal{Q}_C$ break simultaneously in parameter space, at the points of the thermodynamic transitions. Where a thermodynamic transition is absent, the spontaneous breaking of the

two different global subgroups happens at different points in parameter space. It follows that, to separate the phase diagram in a symmetric and a broken-symmetry phase, one should first specify which global subgroup of the gauge symmetry group is supposed to be spontaneously broken. The authors of [29] conclude that the spontaneous breaking of global gauge symmetries does not necessarily correspond to a change in physical state, and that there is no unambiguous distinction between a symmetric and non-symmetric phase in the phase diagram of the SU(2)-Higgs model.

We thought it interesting to analyse the behaviour of the gauge-dependent order parameters $\mathcal{Q}_L$ and $\mathcal{Q}_C$ in our model with SU(2) gauge group, two fundamental fermions and one fundamental scalar.

2.5.1 SU(2)-Higgs model

As a first step, we considered the SU(2)-Higgs model at $\beta = 2$ and the two different values of λ analysed in our study of SU(2) with two fermions and one scalar ($\lambda = 0, 2$). In order to locate the symmetry-breaking transition in parameter space, we simulated different values of the squared scalar mass m_S^2, gaugefixed the gauge and scalar configurations in both the Landau and Coulomb gauge, and measured the order parameters $\mathcal{Q}_L$ and $\mathcal{Q}_C$. In each ensemble, we also measured the scalar condensate $S^\dagger S$:

$$S^\dagger S = \frac{1}{V} \sum_x S^\dagger(x) S(x) \,, \tag{2.85}$$

and the plaquette:

$$U = \frac{1}{6V} \sum_x \sum_{\mu<\nu} \frac{1}{2} \mathrm{Re}\,\mathrm{tr}[U_{\mu\nu}(x)] \,. \tag{2.86}$$

The goal is to use this analysis of the SU(2)-Higgs model as a guideline for studying our model with fermions and scalars. For this reason, we did not attempt a scaling analysis of $\mathcal{Q}_L$ and $\mathcal{Q}_C$ for different lattice volumes, since this approach would become computationally quite expensive when applied to a model with dynamical fermions. Instead, we simply analysed the order parameters as functions of m_S^2, and we think that this allowed us to locate quite clearly the symmetry-breaking transition.

We start by reporting the results we obtained at $\lambda = 2$. Figure 2.12 shows the order parameters $\mathcal{Q}_L$ and $\mathcal{Q}_C$ as functions of the squared scalar mass. We observe a jump in both observables around $m_S^2 = -3.97$, corresponding to the symmetry-breaking transition. Even without analysing their volume scaling, $\mathcal{Q}_L$ and $\mathcal{Q}_C$ seem to look quite different in the symmetric and broken phase. $\mathcal{Q}_L$ is very close to zero in the symmetric phase, and it jumps to $\mathcal{Q}_L \simeq 0.25$ in the broken-symmetry phase. $\mathcal{Q}_C$ is approximately constant in the symmetric phase, assuming a value $\mathcal{Q}_C \simeq 0.05$, and it jumps to $\mathcal{Q}_C \simeq 0.9$ in the broken phase. In figure 2.13, we plot the scalar condensate $\langle S^\dagger S \rangle$ and the plaquette $\langle U \rangle$ as functions of m_S^2. Also these observables display a jump around $m_S^2 = -3.97$, which indicates that we are in the presence of

the thermodynamic first-order phase transition, accompanied by the spontaneous breaking of both the global subgroups probed by $\mathcal{Q}_L$ and $\mathcal{Q}_C$.

At $\lambda = 0$ we do not observe a symmetry-breaking transition. For all the values of m_S^2 that we simulated, the values of $\mathcal{Q}_L$ and $\mathcal{Q}_C$ seem to correspond to a symmetric phase. We could not run the simulations at $m_S^2 \leq -1.5$. The history of the scalar condensate in Monte Carlo time at $m_S^2 = -1.5$, shown in the right panel of figure 2.14, indicates that this could be due to instability of the scalar potential. The scalar condensate moves towards very large values with increasing Monte Carlo time, and the configurations stop being accepted. This is probably due to large values of the forces associated to the scalar field, and we presume that we could make the simulations work by using a much smaller integration step to generate the molecular dynamics trajectories. However, this system would never thermalise, and would keep on moving towards larger and larger values of $S^\dagger S$.

2.5.2 SU(2) with two fermions and one scalar

We repeat the same analysis in the SU(2) model with two fermions and one scalar. All the values of $\mathcal{Q}_L$ and $\mathcal{Q}_C$ that we measured are reported in table 2.2. We observe the symmetry-breaking transition at $(m_f,\ \lambda) =$ (-0.94, 2), and we presume that we will observe it also at $(m_f,\ \lambda) =$ (-0.952, 2), once we extend our analysis to smaller values of m_S^2. At $(m_f,\ \lambda) =$ (-0.94, 0), all the ensembles that we generated belong to the symmetric phase, and we found a minimum value $m_S^2 = -1$ below which the simulations do not work. In analogy with what observed in the SU(2)-Higgs model, we believe that this is due to instability of the scalar potential.

In figure 2.15, we plot $\mathcal{Q}_L$ and $\mathcal{Q}_C$ as functions of m_S^2, at $(m_f,\ \lambda) =$ (-0.94, 2). We observe a jump in these observables around $m_S^2 = -3.2$. The symmetry-breaking transition seems to happen simultaneously for both the gauge-dependent order parameters. The plaquette $\langle U \rangle$ and the scalar condensate $\langle S^\dagger S \rangle$ seem to indicate a first-order phase transition around $m_S^2 = -3.2$, as shown in figure 2.16. Moreover, as discussed in section 2.4.1, also the meson spectrum shows an abrupt change of behaviour around the same value of m_S^2. The value $m_S^2 = -3.2$ is somewhat in between the two phases. In fact, according to figures 2.15, 2.16, it seems to belong to the same phase as the points with larger values of m_S^2. In the meson spectrum however, $m_S^2 = -3.2$ already shows large qualitative deviations from the behaviour of the points with $m_S^2 > -3.2$.

2.6 Conclusions and outlook

In this chapter we discussed our lattice study of the SU(2) gauge theory with two fundamental fermions and one fundamental scalar. The theoretical motivation for this study is given by the recent proposal of fundamental partial compositeness models [4], featuring strongly interacting fermions and scalars.

We measured the meson spectrum of the lattice model, and we found a phase compatible with spontaneous breaking of the fermion flavour symmetry.

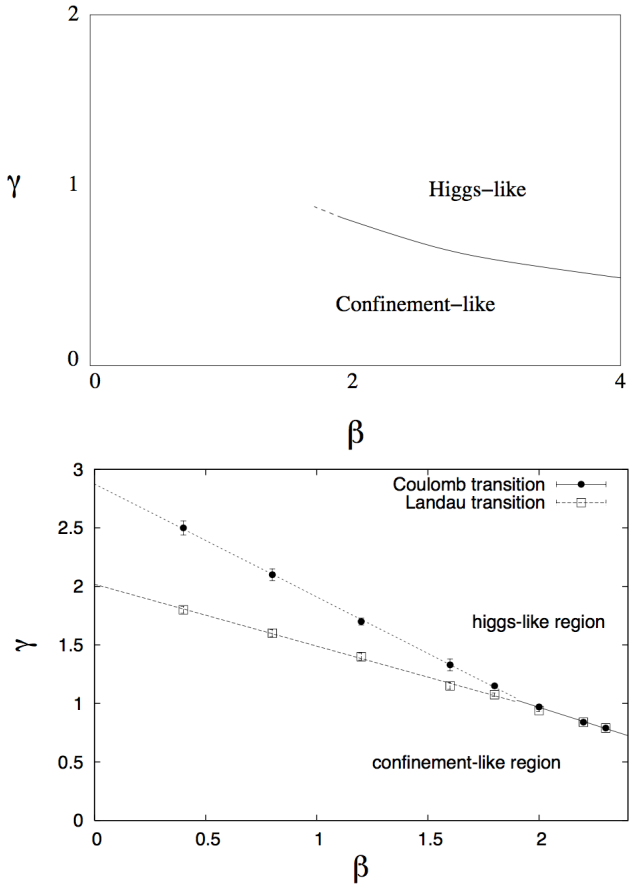

Figure 2.10: Upper panel: sketch of the phase diagram of the SU(2)-Higgs model in the infinite-$\tilde{\lambda}$ limit. The line of first order phase transitions terminates in the middle of the diagram, indicating that the Higgs and confinement phases are analytically connected. Lower panel: transition between the symmetric and broken-symmetry phase, probed by the two gauge-dependent order parameters $\mathcal{Q}_L$ and $\mathcal{Q}_C$. Where there exists a thermodynamic phase transition, the transition to the broken-symmetry phase occurs simultaneously for both order parameters, and together with the thermodynamic transition. In the absence of a thermodynamic phase transition, the two different global subgroups probed by $\mathcal{Q}_L$ and $\mathcal{Q}_C$ break at different points in parameter space, thus indicating that it is not possible to unambiguously separate the phase diagram in a symmetric and a non-symmetric phase. Both pictures are taken from [29].

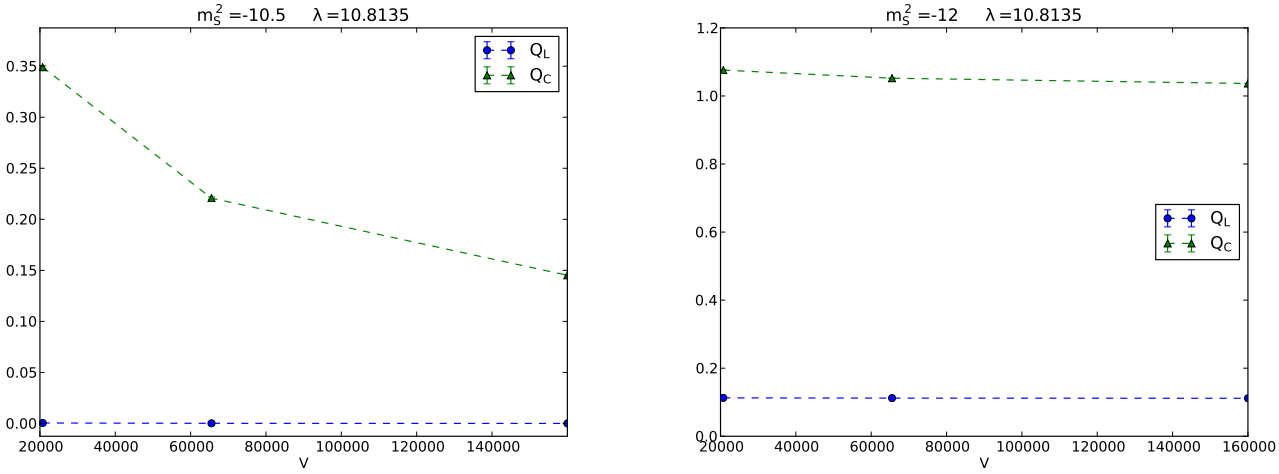

Figure 2.11: Gauge-dependent order parameters $\mathcal{Q}_L$ and $\mathcal{Q}_C$ in the SU(2)-Higgs model, at $\beta = 2.3$ and $\lambda = 10.8135$. We plot the data at three different lattice volumes (12^4, 16^4, 20^4), for one point in the confinement phase (left panel) and one point in the Higgs phase (right panel). The point corresponding to the first order phase transition, (β, λ, m_S^2) = (2.3, 10.8135, -11.2884), is given in reference [34]. $\mathcal{Q}_L$ and $\mathcal{Q}_C$ converge to a finite constant in the broken-symmetry phase, while they move towards zero as the volume increases in the symmetric phase.

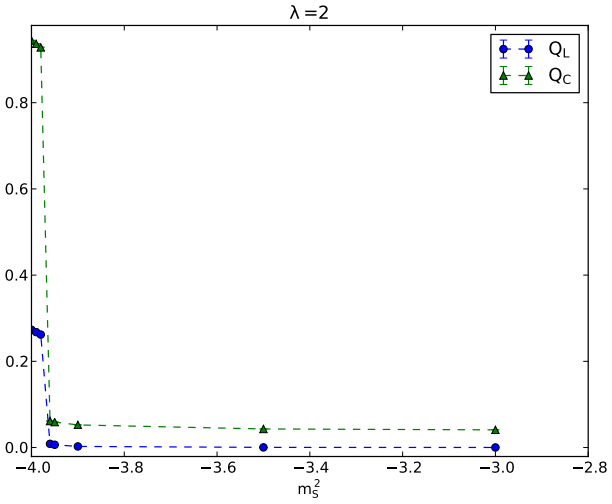

Figure 2.12: $\mathcal{Q}_L$ and $\mathcal{Q}_C$ as functions of the squared scalar mass, in the SU(2)-Higgs model, at $\beta = 2$ and $\lambda = 2$. We observe the transition to the broken-symmetry phase around $m_S^2 = -3.97$. The transition happens simultaneously for both $\mathcal{Q}_L$ and $\mathcal{Q}_C$. We made these measurements on a 12^4 lattice.

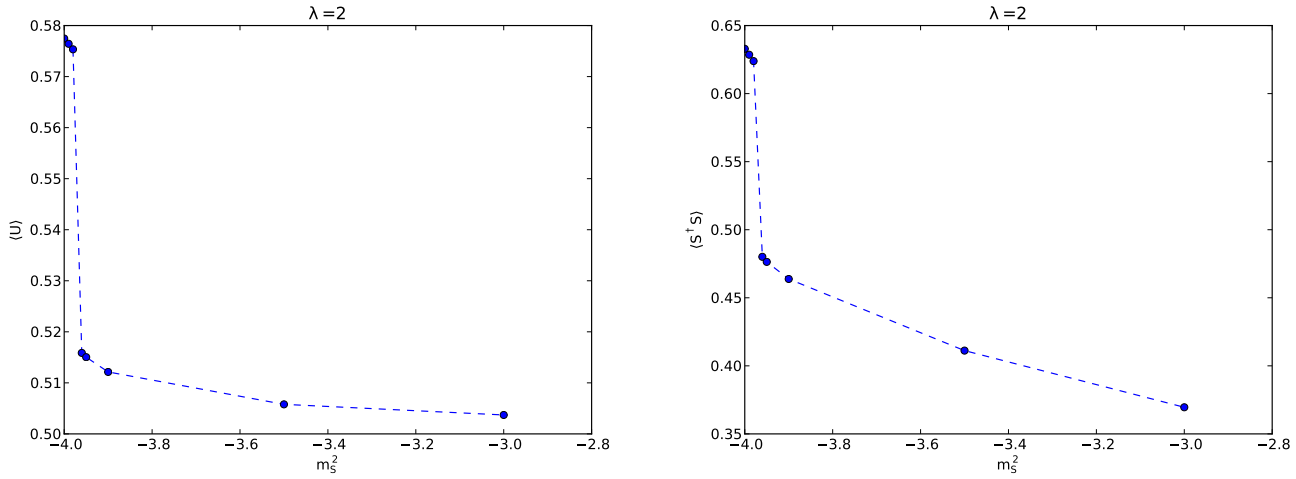

Figure 2.13: Plaquette $\langle U \rangle$ and scalar condensate $\langle S^\dagger S \rangle$ as functions of m_S^2, in the SU(2)-Higgs model, at $\beta = 2$ and $\lambda = 2$. Both observables display an abrupt jump around $m_S^2 = -3.97$, due to the thermodynamic first-order phase transition. We obtained these data on a 12^4 lattice.

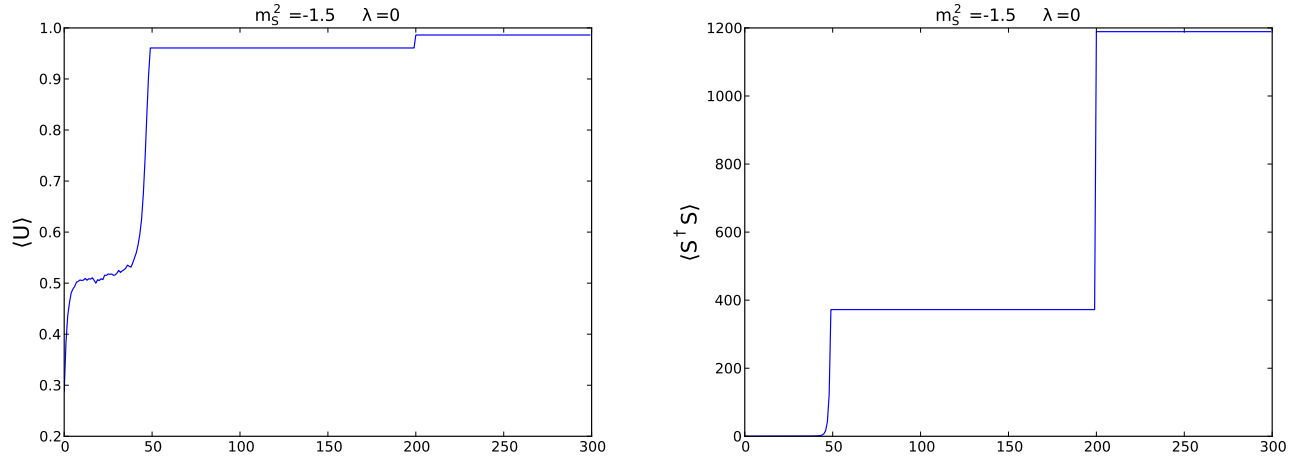

Figure 2.14: History of the plaquette $\langle U \rangle$ and of the scalar condensate $\langle S^\dagger S \rangle$, in the SU(2)-Higgs model, at $\beta = 2$, $\lambda = 0$ and $m_S^2 = -1.5$. The simulations get stuck with zero acceptance, apparently due to the scalar condensate's very big values. These data have been measured on an 8^4 lattice.

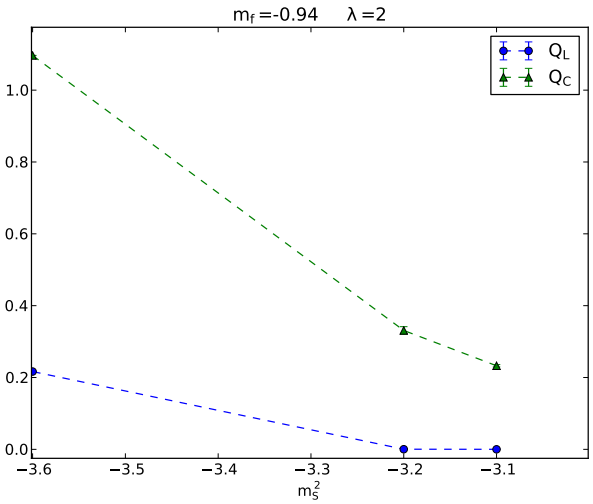

Figure 2.15: $\mathcal{Q}_L$ and $\mathcal{Q}_C$ as functions of m_S^2, in the SU(2) model with two fermions and one scalar, at $(m_f,\ \lambda)$ = (-0.94, 2). We observe the symmetry-breaking transition around $m_S^2 = -3.2$. The data shown in this figure can be found in table 2.2.

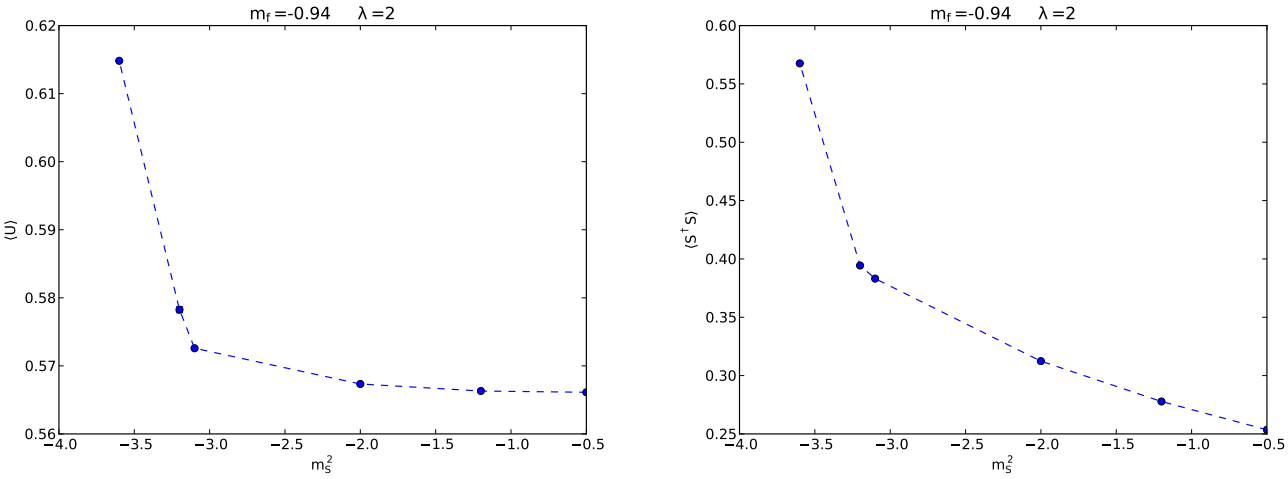

Figure 2.16: Plaquette $\langle U \rangle$ and scalar condensate $\langle S^\dagger S \rangle$ as functions of m_S^2, in the SU(2) model with two fermions and one scalar, at $(m_f,\ \lambda)$ = (-0.94, 2). This plot seems to evidence a first-order phase transition around $m_S^2 = -3.2$.

Chapter 3

Transport coefficients in the conformal window

Gauge theories with a nontrivial infrared (IR) fixed point are important in the context of model building Beyond the Standard Model [35]. These theories are characterised by scale invariance in the infrared and, in the case of four space-time dimensions, they are invariant under the larger group of conformal transformations. For this reason, the region in theory space, parametrised by the number of colours (N) and fermion flavours (N_f), such that a nontrivial IR fixed point exists, is called conformal window. Substantial effort has been taken in studying the properties of theories in the conformal window, both perturbatively and via lattice simulations (*references?*). In this chapter, we present a study of the transport coefficients of theories in the perturbative conformal window, which has been published in [36]. The chapter is organised as follows: we start by introducing the conformal window and the definition of the transport coefficients under analysis. We then describe the method used by the authors of [37] for calculating the transport coefficients of a high temperature gauge theory. Finally, we present the results obtained by applying the perturbative results of [37] to theories in the conformal window.

3.1 The conformal window

We consider a non-Abelian gauge theory, with gauge group SU(N) and N_f fermions in the representation r. The two-loop beta function for the gauge coupling g is given by:

$$\beta(g) = -\frac{\beta_0}{(4\pi)^2} g^3 - \frac{\beta_1}{(4\pi)^4} g^5 + \mathcal{O}(g^7) \,, \tag{3.1}$$

with

$$\beta_0 = \frac{11}{3} C_2[G] - \frac{4}{3} T[r] N_f \,, \tag{3.2}$$

$$\beta_1 = \frac{34}{3} C_2^2[G] - \left(\frac{20}{3} C_2[G] + 4 C_2[r] \right) T[r] N_f \,, \tag{3.3}$$

where G denotes the adjoint representation. The definition of the group theory factors C_2, T and d can be found in appendix A.1.3. If $\beta_0 > 0$, the theory is asymptotically free, i.e. $g = 0$ is an ultraviolet(UV)-stable fixed point of the renormalisation group (RG) flow. This happens provided the number of fermions is smaller than the upper limit:

$$N_f^{AF} = \frac{11}{4}\frac{C_2[G]}{T[r]} \,. \tag{3.4}$$

The number of flavours and colours can be chosen such that $\beta_0 > 0$ and $\beta_1 < 0$. In this case there exists an additional zero of the beta function:

$$g^* = -(4\pi)^2 \frac{\beta_0}{\beta_1} \,. \tag{3.5}$$

This is an IR-stable fixed point, which can be studied in perturbation theory in case g^* is small [38]. In particular, g^* goes to zero in the limit $N_f \to N_f^{AF}$. If g^* is small, the theory remains perturbative along the whole RG flow, from the UV, where it is dominated by the asymptotically free fixed point $g = 0$, down to the IR. If g^* is not small enough, then one has to consider higher-order terms in the beta function 3.1, and eventually, when g^* leaves the perturbative regime, apply non-perturbative methods such as lattice simulations. In theory space, parametrised by N and N_f, the upper boundary of the conformal window for every fixed N is given by $N_f = N_f^{AF}$, while the lower boundary is yet to be found via non-perturbative methods, since the value of g^* increases with decreasing N_f.

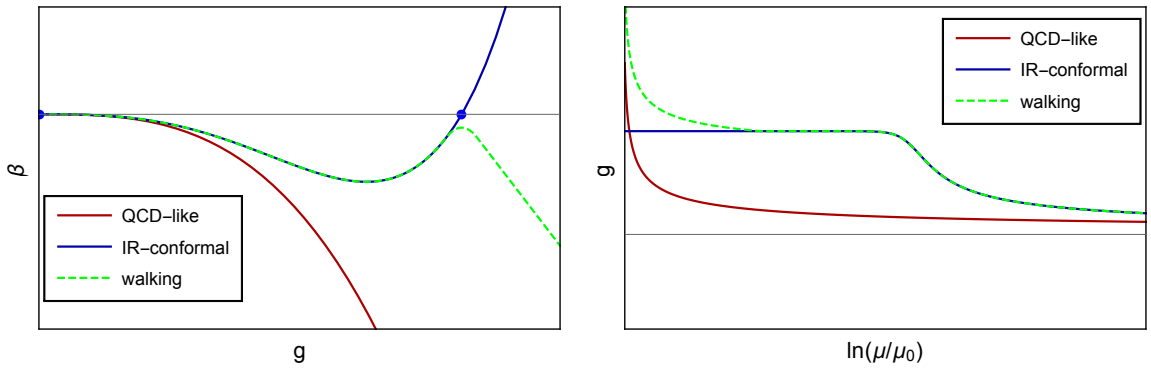

Figure 3.1: Beta function (left panel) and gauge coupling (right panel) for three different kinds of theories: a QCD-like theory (red line), a theory in the conformal window (blue line) and a theory with walking gauge coupling (green dashed line). In the right panel, the gauge coupling is plotted as a function of the energy scale μ over some reference scale μ_0.

Figure 3.1 shows three different regimes of the beta function, and the related running of the gauge coupling. The first one (red line) characterises a QCD-like theory. The beta function has one single zero at $g = 0$, and is negative for all other values of g. In this case, the coupling goes to zero in the UV (asymptotic freedom) and grows when moving towards the IR, until it diverges at some finite energy scale. This theory displays spontaneous chiral symmetry breaking in the IR. The second regime (blue line) characterises a theory in the conformal window. The beta

function has two zeros, $g = 0$ and $g = g^*$, and is negative in between. The gauge coupling goes to zero in the UV, and stabilises at the fixed point value $g = g^*$ in the IR. This theory is characterised by scale invariance in the IR, and does not display spontaneous chiral symmetry breaking. The third regime (green dashed line) is associated to "walking" dynamics. It is reasonable to assume that, close to the lower boundary of the conformal window, theories with an approximate IR fixed point can be found. Their beta function is very similar to the one of theories in the conformal window, with the difference that it gets very close to zero at $g \simeq g^*$, without actually reaching a fixed point, and then assumes a QCD-like behaviour for larger values of g. In this theory the gauge coupling goes to zero in the UV, then stabilises at an approximately constant value for a wide range of energies, and finally diverges at a finite energy scale, thus triggering chiral symmetry breaking. Theories with walking gauge coupling are very important in the context of composite Higgs models, as discussed in section 2.1.4. In fact these theories show an approximate conformal behaviour, which can lead to a nice separation of scales and good scaling properties of composite operators, and at the same time break chiral symmetry, which is a necessary ingredient in composite Higgs models. Lattice simulations can be used in order to find out whether a theory is in one of the three regimes shown in figure 3.1, see for example [39, 40].

Here we consider theories in the perturbative conformal window, i.e. $N_f \lesssim N_f^{AF}$, and we study their shear viscosity and fermion number diffusion coefficient by applying the perturbative results obtained in [37].

3.2 Transport coefficients

Transport coefficients characterise the response of a fluid to small deviations from thermodynamic equilibrium. The transport coefficients considered in our study are viscosity and diffusion coefficients. Viscosity describes the response to spacial variations of the flow velocity, in the presence of dissipative phenomena (internal friction). Diffusion coefficients describe the evolution of the density of conserved charges, when the charge concentration is not uniform over the fluid. In this section we introduce the equations of motion of a viscous fluid and the diffusion equation, which provide the definitions of the transport coefficients under analysis.

3.2.1 Viscosity

In this derivation we follow the lines of [41]. We start by considering the motion of an ideal fluid, which is described by the continuity equation:

$$\partial_t \rho + \partial_i(\rho v_i) = 0 \,, \tag{3.6}$$

and Euler's equation (given here in component form):

$$\partial_t v_i + v_j \partial_j v_i = -\frac{1}{\rho}\partial_i p \,, \tag{3.7}$$

where time is denoted by t, spacial coordinates by x_i $(i = 1, 2, 3)$, the fluid mass density by ρ, the flow velocity components by v_i, and the pressure by p. Sums over

repeated indices are understood. Euler's equation can be rewritten as:

$$\partial_t(\rho v_i) = -\partial_j \Pi_{ij} \,, \tag{3.8}$$

where the symmetric tensor $\Pi_{ij} = p\delta_{ij} + \rho v_i v_j$ represents the flux density of the momentum component i in all possible directions j. The momentum transfer described by Π_{ij} is reversible, and it is due to the mechanical transport of volumes of fluid and to pressure forces acting in the fluid. The motion of a viscous fluid is characterised by an extra, irreversible, transfer of momentum, occurring from points where the flow velocity is large to points where it is low. In the case of a viscous fluid, the tensor Π_{ij} can be parametrised as:

$$\Pi_{ij} = p\delta_{ij} + \rho v_i v_j - \sigma_{ik} \,, \tag{3.9}$$

where $-\sigma_{ik}$ is the contribution due to internal friction. Always following [41], we notice that σ_{ik} must depend on the spacial derivatives of the flow velocity, since internal friction occurs only when different layers of fluid move with respect to each other, and must vanish when the flow velocity is constant in space. Moreover, σ_{ij} must vanish when the fluid is in uniform rotational motion, because in this case there is no relative motion between different layers of fluid. The flow velocity of a uniformly rotating fluid is expressed as: $\vec{v} = \vec{\Omega} \times \vec{r}$, $\vec{r}$ being the distance from the centre of rotation and $\vec{\Omega}$ the constant angular velocity. If the velocity gradients are small, we may assume that σ_{ik} is a linear function of the first derivatives of the flow velocity. The most general function of this sort, which vanishes in case $\vec{v} =$ constant, or $\vec{v} = \vec{\Omega} \times \vec{r}$, is:

$$\sigma_{ij} = \eta\left(\partial_i v_j + \partial_j v_i - \frac{2}{3}\delta_{ij}\partial_k v_k\right) + \zeta\delta_{ij}\partial_k v_k \,, \tag{3.10}$$

where the coefficient η is the shear viscosity and ζ the bulk viscosity. The terms in equation 3.10 are organised so that the expression in parentheses vanishes when traced over i and j. To conclude, for a viscous fluid

$$\Pi_{ij} = p\delta_{ij} + \rho v_i v_j - \eta\left(\partial_i v_j + \partial_j v_i - \frac{2}{3}\delta_{ij}\partial_k v_k\right) - \zeta\delta_{ij}\partial_k v_k \,, \tag{3.11}$$

and Euler's equation is substituted by the Navier-Stokes equation, obtained by inserting 3.11 in 3.8.

Relativistic fluid equations describe a fluid whose flow velocity is relativistic, or whose microscopical components move at relativistic speed. In order to derive them, we introduce the energy-momentum tensor $T^{\mu\nu}$ of the relativistic fluid. The component T^{00} is the fluid energy density, $T^{i0} = T^{0i}$ is the momentum component density (equal to the energy flux density), and T^{ij} the momentum flux density, analogue to the non-relativistic Π_{ij}. The equations of motion

$$\partial_\mu T^{\mu\nu} = 0 \tag{3.12}$$

express the conservation of energy and momentum in the fluid. We start by defining $T^{\mu\nu}$ for an ideal fluid in the local rest frame. In the local rest frame, the momentum density is zero ($T^{0i} = 0$), and the force exerted by the fluid on some surface is the

same in all directions, and always perpendicular to the surface. The i-th component of the force exerted on an infinitesimal surface $\mathrm{d}\hat{\Sigma} = |\mathrm{d}\Sigma|\,\hat{n}$ is given by: $T^{ij}\mathrm{d}\hat{\Sigma}^j$, where $\hat{n}$ is the normal to the surface. It follows from the above argument that $T^{ij}\mathrm{d}\hat{\Sigma}^j = p\,\mathrm{d}\hat{\Sigma}^i$, and therefore $T^{ij} = \delta^{ij}p$. Consequently, in the local rest frame:

$$(T^{\mu\nu}) = \begin{pmatrix} e & 0 & 0 & 0 \\ 0 & p & 0 & 0 \\ 0 & 0 & p & 0 \\ 0 & 0 & 0 & p \end{pmatrix} , \tag{3.13}$$

where e is the energy density and p the pressure. This expression can be generalised to a generic reference frame by introducing the fluid four-velocity u^μ, given by $u^0 = 1$, $u^i = 0$ in the local rest frame, and by $u^0 = 1/\sqrt{1-v^2}$, $u^i = v^i/\sqrt{1-v^2}$ in a frame in which the fluid element moves with velocity $\vec{v}$. In a generic frame, $T^{\mu\nu}$ is expressed as:

$$T^{\mu\nu} = (e+p)u^\mu u^\nu - p\,\eta^{\mu\nu} , \tag{3.14}$$

where $\eta_{\mu\nu}$ is Minkowski metric. Equation 3.13 is recovered by fixing $u^0 = 1$, $u^i = 0$. In the presence of internal friction, further terms must be added to the energy momentum tensor 3.14. In the local rest frame, the spatial components of the energy momentum tensor of a viscous relativistic fluid are given by:

$$T_{ij} = p\delta_{ij} - \eta\left(\partial_i u_j + \partial_j u_i - \frac{2}{3}\delta_{ij}\partial_k u_k\right) - \zeta\delta_{ij}\partial_k u_k , \tag{3.15}$$

which reduce to 3.11 in the non-relativistic limit $|\vec{v}| \ll 1$. Equation 3.15 may be regarded as the definition of the shear and bulk viscosities of a relativistic fluid.

3.2.2 Diffusion coefficient

We have seen that the equations of motion of a relativistic fluid express the conservation of energy and momentum. Further conservation laws, of the form

$$\partial_\mu j^\mu = 0 , \tag{3.16}$$

exist for all other eventual conserved quantities. We consider here the case of a conserved particle number density. The current j^μ in this case is expressed as: $j^\mu = nu^\mu$, where u^μ represents the fluid four-velocity and n the particle number density in the local rest frame. The diffusion equation:

$$\partial_t n = D\,\triangle n , \tag{3.17}$$

where $\triangle = \partial_i\partial^i$, describes the evolution of the number density n, when n is low and not uniform over the fluid. In this case, the number density flux can be expressed, in the local rest frame, as:

$$j^i = -D\partial^i n , \tag{3.18}$$

which, in combination with the conservation law 3.16, implies the diffusion equation 3.17. The coefficient D is known as diffusion coefficient. Equations of the form 3.17,

3.18 describe for example the evolution of the concentration c of the solute in a weak solution ($c \ll 1$) [41]. Random walk dynamics, which may be applied to the description of Brownian motion, is also governed by the diffusion equation. It will be shown in the following that the current related to fermion number conservation (analogue to baryon number conservation in QCD) in a hot gauge theory satisfies a constitutive relation of the form 3.18.

3.3 Transport coefficients of a hot gauge theory: kinetic approach

The equilibrium state of a high temperature quantum field theory can be described as a relativistic fluid. Transport coefficients can in principle be computed, based on the dynamics of the underlying microscopic theory. This is what the authors of [37, 42] did in the case of a weakly coupled , high temperature gauge theory, both in a leading-log approximation [37] and in a full leading order treatment [42]. In this section, we describe the method used in these works to compute the transport coefficients. The analytic results given in [37], together with the coefficients in table 3.1, are the basis for our study of transport coefficients in the perturbative conformal window.

In [37, 42], a finite temperature gauge theory coupled to fermions is considered, under the assumption that the gauge coupling at the scale of the temperature is weak: $g(T) \ll 1$. The temperature is assumed to be much larger than any other mass scale in the theory, such as for example zero-temperature fermion masses, chemical potentials, or, in the case of non-Abelian gauge group, the scale at which the gauge coupling becomes strong. Under this assumption, the transport coefficients are given by a power of the temperature determined by dimensional analysis, multiplied by some function of the gauge coupling.

As explained by the authors of [37, 42], a kinetic theory approach is appropriate for computing the transport coefficients under their analysis (shear viscosity, diffusion coefficients, electrical conductivity) at leading order in the gauge coupling. We will get back to this point in the following. The kinetic theory is defined by assigning to each particle species a phase space distribution function $f^a(\vec{p}, x)$, which satisfies a Boltzmann equation of the form:

$$\left(\frac{\partial}{\partial t} + \vec{v}_{\vec{p}} \cdot \frac{\partial}{\partial \vec{x}} + \vec{F} \cdot \frac{\partial}{\partial \vec{p}}\right) f^a(\vec{p}, x) = -C_a[f](\vec{p}, x) \,, \tag{3.19}$$

where $\vec{v}_{\vec{p}}$ is the velocity of a particle with momentum $\vec{p}$, $\vec{F}$ is an external force acting on the particle species a, and $C_a[f](\vec{p}, x)$ is the collision term, describing the rate at which excitations with momentum $\vec{p}$ of the species a are lost or created due to scattering with other particles in the fluid. Typical excitations in the plasma have momentum $|\vec{p}| = \mathcal{O}(T)$ and thus are highly relativistic (in the high temperature limit), and may be treated as massless particles moving at the speed of light, with dispersion relation $p^0 = |\vec{p}|$. It follows that the velocity $\vec{v}_{\vec{p}}$ is a unit vector: $\vec{v}_{\vec{p}} = \hat{p} = \vec{p}/|\vec{p}|$.

In [37] transport coefficients are computed in the leading-log approximation,

i.e. the coefficient of the leading order result (in the gauge coupling g) is in turn expanded in powers of $1/\log g^{-1}$ and only the first term of this expansion is retained. In this approximation, it is sufficient to include in the collision term only two-body scattering processes:

$$\begin{aligned} C_a[f](\vec{p},x) = \frac{1}{4p^0}\sum_{b,c,d}^{\mathrm{f\bar{f}hc}}\int_{\vec{k},\vec{p}',\vec{k}'} \left|\mathcal{M}^{ab}_{cd}(p,k;p',k')\right|^2 (2\pi)^4\delta^4(p+k-p'-k')\times \\ \times\Big[f^a(\vec{p},x)f^b(\vec{k},x)[1\pm f^c(\vec{p}',x)][1\pm f^d(\vec{k}',x)]- \\ - f^c(\vec{p}',x)f^d(\vec{k}',x)[1\pm f^a(\vec{p},x)][1\pm f^b(\vec{k},x)]\Big]\,, \end{aligned} \tag{3.20}$$

where $\mathcal{M}^{ab}_{cd}$ is the scattering amplitude for the process $ab\leftrightarrow cd$, and the sum extends to flavours (f), anti-flavours ($\bar{\mathrm{f}}$), helicities (h) and colours (c) of the particles b, c and d. The shorthand notation $\int_{\vec{p}}\equiv\int \mathrm{d}^3p/\big(2p^0(2\pi)^3\big)$ is introduced for the momentum integrals, and in the final-state statistical factors $[1\pm f]$ the upper sign applies to bosons and the lower to fermions. The energy momentum tensor of the fluid formed by the excitations distributed according to f^a is given by:

$$T^{\mu\nu}(x) = \sum_a^{\mathrm{f\bar{f}hc}}\int\frac{\mathrm{d}^3p}{(2\pi)^3p^0}p^\mu p^\nu f^a(\vec{p},x)\,, \tag{3.21}$$

while other conserved currents are given by:

$$j^\mu(x) = \sum_a^{\mathrm{f\bar{f}hc}}\int\frac{\mathrm{d}^3p}{(2\pi)^3p^0}p^\mu q^a f^a(\vec{p},x)\,, \tag{3.22}$$

where q^a is the corresponding charge carried by the species a.

The next step in the computation of transport coefficients is the linearisation of the Boltzmann equation in the case of small deviations from local equilibrium. Equilibrium solutions of the Boltzmann equation are given by:

$$f^a_{eq}(\vec{p}) = \frac{1}{\exp[\beta(-u_\mu p^\mu-\mu_\alpha q^a_\alpha)]\mp 1}\,, \tag{3.23}$$

where $\beta=1/T$, u^μ is the fluid four-velocity, $\{\,q^a_\alpha\,\}$ a set of conserved charges and $\{\,\mu_\alpha\,\}$ the related chemical potentials. As before, the upper sign applies to bosons and the lower to fermions, and this convention will hold through all the following derivation. In order to study small deviations from local equilibrium, relevant for the computation of transport coefficients, the phase space distribution can be written as:

$$f^a(\vec{p},x) = f^a_0(\vec{p},x)+\delta f^a(\vec{p},x)\,, \tag{3.24}$$

where $f^a_0(\vec{p},x)$ is a local equilibrium solution, i.e. of the form 3.23 but with β, u_μ, μ_α possibly depending on space-time coordinates. The deviation from local

equilibrium δf^a can be rewritten in a form that will simplify the expression of the linearised collision term:

$$\delta f^a(\vec{p}, x) = f_0^a(\vec{p}, x)[1 \pm f_0^a(\vec{p}, x)] f_1^a(\vec{p}, x) \, . \tag{3.25}$$

The Boltzmann equation can be linearised by retaining only terms of first order in the deviation from equilibrium. In particular, only terms that are linear in either f_1^a, the external force $\vec{F}$ or the gradients of β, u_μ, μ_α are retained. Products of f_1^a with gradients or $\vec{F}$, as well as derivatives of f_1^a, are among the discarded terms. As a result, the Boltzmann equation becomes a linear integral equation in f_1^a:

$$\left(\frac{\partial}{\partial t} + \hat{p} \cdot \frac{\partial}{\partial \vec{x}} + \vec{F} \cdot \frac{\partial}{\partial \vec{p}} \right) f_0^a(\vec{p}, x) = -(\mathcal{C} f_1)^a(\vec{p}, x) \, , \tag{3.26}$$

where the linearised collision integral is given by:

$$\begin{aligned} (\mathcal{C} f_1)^a(\vec{p}, x) = \frac{1}{4p^0} \sum_{b,c,d}^{\mathrm{f\bar{f}hc}} \int_{\vec{k},\vec{p}',\vec{k}'} & \left| \mathcal{M}_{cd}^{ab}(p, k; p', k') \right|^2 (2\pi)^4 \delta^4(p + k - p' - k') \times \\ & \times f_0^a(\vec{p}, x) f_0^b(\vec{k}, x)[1 \pm f_0^c(\vec{p'}, x)][1 \pm f_0^d(\vec{k'}, x)] \times \\ & \times \left[f_1^a(\vec{p}, x) + f_1^b(\vec{k}, x) - f_1^c(\vec{p'}, x) - f_1^d(\vec{k'}, x) \right] . \end{aligned} \tag{3.27}$$

In order to obtain this result, the fact that the collision term vanishes in the case of a local equilibrium distribution, $C_a[f_0] = 0$, has been used.

In this setup, transport coefficients can be computed by applying the following program:

- the collision integrals 3.27 must be computed for all the relevant particle species, at the desired order in the gauge coupling g
- an appropriate "driving term" (left-hand-side of 3.26) must be chosen, which allows to compute the desired transport coefficient
- the deviations from local equilibrium f_1^a must be computed for all relevant particle species by solving the integral equations 3.26
- the phase space distributions $f^a = f_0^a + \delta f^a$ must be inserted in the relevant conserved current (3.21 or 3.22). Transport coefficients can be read off from the resulting equation.

Here we don't aim at describing the full procedure in detail. We will just give a sketch of point two of the above program, and further on we will briefly discuss which approximations are applied in the collision integrals in order to obtain leading-log results for transport coefficients.

The form of the local equilibrium distribution f_0 can be chosen appropriately for the computation of a specific transport coefficient. In the case of viscosity, the temperature and chemical potentials are constant, while the flow velocity varies as a function of space. In the case of a diffusion coefficient, some chemical potential μ_α is chosen as varying in space, while all other parameters are constant. In both

cases the external force $\vec{F}$, which would be relevant for the calculation of electrical conductivity, can be set to zero. Derivatives of f_0^a can be written as:

$$\mathrm{d}f_0^a(\vec{p},x) = f_0^a(\vec{p},x)[1 \pm f_0^a(\vec{p},x)]\mathrm{d}[\beta u_\mu p^\mu + \beta q_\alpha^a \mu_\alpha] \,, \tag{3.28}$$

from which the left-hand-side of equation 3.26 can be expressed as (we limit ourselves to the forms of f_0 relevant for viscosity and diffusion coefficients):

$$\hat{p}\cdot\frac{\partial}{\partial\vec{x}} f_0^a(\vec{p},x) = \beta f_0^a(\vec{p},x)[1 \pm f_0^a(\vec{p},x)] q^a I_{i\ldots j}(\hat{p}) X_{i\ldots j}(x) \,, \tag{3.29}$$

where the term $\hat{p}\cdot\partial/\partial\vec{x}\,[u_\mu p^\mu + q_\alpha^a\mu_\alpha]$ has been split in a part depending only on spacial coordinates:

$$X_{i\ldots j}(x) = \begin{cases} \frac{\partial}{\partial x^i}\mu_\alpha & \text{(diffusion coefficient)} \\ \frac{1}{\sqrt{6}}\left(\frac{\partial}{\partial x^i}u_j + \frac{\partial}{\partial x^j}u_i - \frac{2}{3}\delta_{ij}\frac{\partial}{\partial x^k}u_k\right) & \text{(shear viscosity)} \end{cases} \tag{3.30}$$

and one depending only on the direction of the momentum $\hat{p}$:

$$I_{i\ldots j}(\hat{p}) = \begin{cases} \hat{p}_i & \text{(diffusion coefficient)} \\ \sqrt{\frac{3}{2}}\left(\hat{p}_i\hat{p}_j - \frac{1}{3}\delta_{ij}\right) & \text{(shear viscosity)} \,. \end{cases} \tag{3.31}$$

In equation 3.29, q^a is the relevant conserved charge, and it stands for either q_α^a (for the diffusion coefficient) or $|\vec{p}|$ (for shear viscosity).

We now assume to be in the local rest frame of the fluid. In this frame, at any point x, $f_0(\vec{p},x)$ depends only on $p^0 = |\vec{p}|$, and all the angular dependence in 3.29 comes from the function $I_{i\ldots j}(\hat{p})$. The linearised collision operator $\mathcal{C}$, in the local rest frame at x, is rotationally invariant and independent of x, therefore the dependence of f_1^a on $\hat{p}$ and x is the same as the one of the driving term 3.29. As a consequence, the deviation from local equilibrium f_1^a can be expressed as:

$$f_1^a(\vec{p},x) = \beta^2 X_{i\ldots j}(x) I_{i\ldots j}(\hat{p}) \chi^a(|\vec{p}|) \,, \tag{3.32}$$

where $\chi^a(|\vec{p}|)$ is an unknown function, which must be determined by solving the integral equation 3.26. The phase space distributions $f^a(\vec{p},x)$ thus obtained should then be used to compute the energy momentum tensor 3.21 and the conserved current 3.22. In the case of the energy momentum tensor, the forms of $X_{i\ldots j}(x)$ and $I_{i\ldots j}(\hat{p})$ relevant for the computation of shear viscosity must be chosen. It can be seen that the deviation from local equilibrium δf contributes to $T^{\mu\nu}$ with a term of the form

$$\eta\left(\frac{\partial u_j}{\partial x^i} + \frac{\partial u_i}{\partial x^j} - \frac{2}{3}\delta_{ij}\frac{\partial u_k}{\partial x^k}\right) \,, \tag{3.33}$$

where the coefficient η, representing the shear viscosity, can be computed once the functions $\chi^a(|\vec{p}|)$ are known for all relevant particle species. In the case of the diffusion coefficient, it can be seen that the current 3.22 is of the form 3.18, once the term $\partial\mu_\alpha/\partial x^i$ is rewritten as:

$$\frac{\partial \mu_\alpha}{\partial x^i} = \left(\frac{\partial n_\alpha}{\partial \mu_\alpha}\right)^{-1} \frac{\partial n_\alpha}{\partial x^i} \,. \tag{3.34}$$

In fact, in the local rest frame, only the deviation from local equilibrium δf gives a nonzero contribution to the spacial components j^i. The diffusion coefficient D_α, relative to the conserved charge q_α, can be computed once the functions $\chi^a(|\vec{p}|)$ are determined by solving the linearised Boltzmann equation 3.26 in the presence of the appropriate driving term.

The kinetic theory approach is not appropriate for describing all the excitations of a high temperature gauge theory. The authors of [37, 42] argue that soft excitations with momentum $\mathcal{O}(gT)$ or less cannot be described in terms of quasiparticles with purely local collisions. These long-wavelength fluctuations must be treated as classical gauge field fluctuations, and an effective theory can be constructed in which the high-momentum excitations propagate in a slowly varying classical background field. The method described above for the computation of transport coefficients is valid only for those quantities that are not dominantly sensitive to soft excitations. This is true for shear viscosity and diffusion coefficients, but not for bulk viscosity, which would require a more refined treatment [37].

3.3.1 Leading-log and next-to-leading-log results

In [37], leading-log results are provided for shear viscosity, fermion number diffusion coefficient and electrical conductivity. The leading-log approximation is obtained by restricting to a specific interval the integration over the transfer momentum in the collision integral 3.27. In a process with ingoing momenta $\vec{p}$, $\vec{k}$ and outgoing momenta $\vec{p'}$, $\vec{k'}$, the transfer momentum can be defined as $\vec{q} = \vec{p'} - \vec{p}$. The leading-log approximation amounts to extracting the small $|\vec{q}|$ contribution to the collision integral ($|\vec{q}| \ll T$). In this approximation, the integration over $q \equiv |\vec{q}|$ results in a factor:

$$\int_{gT}^{T} \frac{\mathrm{d}q}{q} = \log g^{-1} \,. \tag{3.35}$$

The lower bound at $q = gT$ is due to the fact that some of the tree-level diagrams, which contribute at leading order in g to the collision integral, are divergent at small q. As a consequence, the collision integral is logarithmically divergent. The infrared divergences disappear when self-energy contributions are included in the exchange lines in the diagrams. The approach assumed in [37] is not to include the self-energy contributions, and to cut down the integration at $q \sim gT$, where the self-energy corrections to the propagators start becoming important. This way leading-log results are obtained.

We report here the results for shear viscosity and fermion number diffusion coefficient, which are relevant for our study in the conformal window. The leading-log shear viscosity reads [37]:

$$\eta \simeq 270\, d[G] \zeta(5)^2 \left(\frac{2}{\pi}\right)^5 (v^T c^{-1} v) \frac{T^3}{g^4 \log(g^{-1})} \,, \tag{3.36}$$

where

$$c = (d[G]C_2[G] + N_f d[r]C_2[r]) \begin{pmatrix} d[G]C_2[G] & 0 \\ 0 & \frac{7}{4}N_f d[r]C_2[r] \end{pmatrix} + \\ + \frac{9\pi^2}{128} N_f d[r]C_2^2[r]d[G] \begin{pmatrix} 1 & -1 \\ -1 & 1 \end{pmatrix} , \tag{3.37}$$

$$v = \begin{pmatrix} d[G] \\ \frac{15}{8}N_f d[r] \end{pmatrix} . \tag{3.38}$$

In the previous equations, N_f denotes the number of fermions, r the representation of the gauge group acting on the fermion fields and G the adjoint representation. The definition of the group factors d and C_2 can be found in appendix A.1.3. In equation 3.36, the $\simeq$ sign is due to the fact that this is an approximate result. Specifically, the results of [37, 42] are obtained by converting the solution of the integral equation 3.26 in a variational problem, corresponding to the maximisation of a functional of $\chi^a(|\vec{p}|)$ (see equation 3.32). The maximisation is performed by expanding $\chi^a(|\vec{p}|)$ over a finite basis of functions, and maximising within this variational subspace. The analytic expression 3.36 is found by cutting to one the number of elements in the functional basis, and it approximately reproduces results obtained numerically by using a larger basis [37].

The diffusion coefficient for the net number density of the fermion flavour a reads, at the leading-log level [37]:

$$D_a \simeq \frac{6^5\zeta(3)^2}{\pi^3 C_2[r_a]} \left[\sum_b^{f\bar{f}h} T[r_b]\lambda_b + \frac{3\pi^2}{8} C_2[r_a] \right]^{-1} \frac{T^{-1}}{g^4 \log(g^{-1})} , \tag{3.39}$$

where the sum extends over all flavours (f), anti-flavours ($\bar{\text{f}}$) and helicities (h) of particles of species b that a can scatter with in the process $ab \to ab$ mediated by a gauge boson. Specifically, a factor of four appears for every Dirac fermion, and a factor of two for every gauge boson. The factor λ_b is equal to one if the particle b is a fermion, and to two if it is a boson. The definition of the group factors T and C_2 can be found in appendix A.1.3. This result is again obtained by using a one-function basis for the expansion of $\chi^a(|\vec{p}|)$. In the case of an SU(N) gauge theory with N_f Dirac fermions, all in the same representation r, the diffusion coefficient is equal for all fermion species, and it reads:

$$D \simeq \frac{6^5\zeta(3)^2}{\pi^3 C_2[r]} \left[4N_f T[r] + 4N + \frac{3\pi^2}{8} C_2[r] \right]^{-1} \frac{T^{-1}}{g^4 \log(g^{-1})} . \tag{3.40}$$

In [42], a full leading-order computation of transport coefficients is performed, and the convergence of the expansion in inverse powers of $\log g^{-1}$ is analysed. The authors show that the leading-order transport coefficients can in turn be expanded according to:

$$D \sim \frac{1}{g^4 T} \sum_{n=1}^{\infty} D_n(\mu) \left(\log \frac{\mu}{m_D} \right)^{-n} , \tag{3.41}$$

$$\eta \sim \frac{T^3}{g^4} \sum_{n=1}^{\infty} \eta_n(\mu) \left(\log \frac{\mu}{m_D} \right)^{-n} , \tag{3.42}$$

where μ is an arbitrary energy scale, which should be chosen to be $\mathcal{O}(T)$, and m_D is the Debye mass:

$$m_D^2 = \frac{1}{3} \left(C_2[G] + N_f C_2[r] \frac{d[r]}{d[G]} \right) g^2 T^2 . \tag{3.43}$$

The coefficients η_1 and D_1 are independent of μ. The leading-log approximation corresponds to truncating the series 3.41, 3.42 at $n = 1$.

The scale μ can be chosen such that the $n = 2$ term in the expansion vanishes: $D_2(\mu^*) = 0$, $\eta_2(\mu^*) = 0$. With this choice, the next-to-leading-log transport coefficients are given by:

$$D_{NLL} = \frac{1}{g^4 T} \left(\frac{D_1}{\log(\mu^*/m_D)} \right) , \qquad \eta_{NLL} = \frac{T^3}{g^4} \left(\frac{\eta_1}{\log(\mu^*/m_D)} \right) . \tag{3.44}$$

We rename $\mu^* = AT$ in the case of shear viscosity, and $\mu^* = BT$ for the diffusion coefficient, and we find the next-to-leading-log results:

$$\eta \simeq 270\, d[G] \zeta(5)^2 \left(\frac{2}{\pi} \right)^5 (v^T c^{-1} v) \frac{T^3}{g^4 \log(AT/m_D)} , \tag{3.45}$$

$$D \simeq \frac{6^5 \zeta(3)^2}{\pi^3 C_2[r]} \left[4 N_f T[r] + 4N + \frac{3\pi^2}{8} C_2[r] \right]^{-1} \frac{T^{-1}}{g^4 \log(BT/m_D)} , \tag{3.46}$$

where the matrix c and the vector v are always given by equations 3.37, 3.38. The coefficients A and B, for an SU(3) gauge group and different values of N_f in the perturbative conformal window (plus $N_f = 6$), have kindly been provided to us by G. D. Moore. Their values are reported in table 3.1.

The convergence of the inverse-log expansion is studied in [42]: the coefficients $D_n(\mu^*)$, $\eta_n(\mu^*)$ are found to decrease with increasing n until $n = 4$, while subsequent coefficients appear to grow. The authors prove that the expansions 3.41, 3.42 are asymptotic expansions with zero radius of convergence. By comparing full-leading-order results with truncated expansions, they find that the next-to-leading-log result is very close to the full leading order provided $m_D/T \leq 1$, while going beyond the order $n = 2$ in the inverse-log expansion has little practical utility.

3.4 Application to theories in the conformal window

We consider SU(N) gauge theories in the perturbative conformal window, i.e. with a number N_f of fermion flavours such that: $N_f \lesssim N_f^{AF}$ (see equation 3.4). For these theories, we study the shear viscosity and fermion number diffusion

N_f	A	B
6	2.918	3.064
14	2.878	3.135
15	2.873	3.172
16	2.869	3.176
16.25	2.867	3.177

Table 3.1: Values of the coefficients A and B [43] appearing in the next-to-leading-log expressions of the shear viscosity and the fermion number diffusion coefficient, for $N = 3$ and different values of N_f.

coefficient, as defined in equations 3.45, 3.46. More specifically, we concentrate on the dimensionless quantities η/s and DT, s being the entropy density, i.e. we drop the overall temperature dependence, which, in a hot gauge theory, is simply determined by dimensional analysis. We consider the IR-fixed-point values of η/s and DT, and we study their dependence on the number of flavours for a fixed value of N. Moreover, we study the temperature dependence of η/s and DT, due to the running of the gauge coupling, for different choices of N and N_f within the perturbative conformal window.

We start by considering the dimensionless ratio η/s. We determine the entropy density s via its relation with the free energy density f:

$$s = -\frac{\mathrm{d}f}{\mathrm{d}T} \ . \tag{3.47}$$

The free energy density of a high temperature SU(N) gauge theory with N_f fermion flavours is known up to the order $g^6 \log(1/g)$ [44], but for our study it is sufficient to retain only terms up to order g^2:

$$\frac{f}{\pi^2 T^4} = -\frac{d[G]}{9}\left[\frac{1}{5} + \frac{7}{20}\frac{d[r]}{d[G]}N_f - \left(C_2[G] + \frac{5}{2}T[r]N_f\right)\frac{g^2}{(4\pi)^2}\right] \ , \tag{3.48}$$

where r is the representation of the gauge group acting on the fermions, G the adjoint representation and the group theory factors d, T and C_2 are defined appendix A.1.3. The free energy of hot gauge theories in the perturbative conformal window has been studied in [45]. One of the interesting results of this work is a good estimate of the lower boundary of the conformal window, obtained by studying the order-$g^6 \log(1/g)$ free energy density evaluated at the IR fixed point.

In order to obtain the fixed-point value of an observable, the gauge coupling g must be traded for its value at the fixed point: $g = g_{FP}$. The shear viscosity-to-entropy density ratio at a generic fixed point reads:

$$\left(\frac{\eta}{s}\right)^{FP} = \frac{\mathcal{A}(N_f, N)}{g_{FP}^4 \ln[\mathcal{B}(N_f, N) g_{FP}^{-1}]} \ , \tag{3.49}$$

with $\mathcal{A}(N_f, N)$ and $\mathcal{B}(N_f, N)$ calculable definite positive and smooth functions of the number of colours and flavours. At non-interacting fixed points, such as the UV

fixed point ($g_{FP} = 0$), the ratio diverges. On the other hand, at the interacting IR fixed point $g_{FP} = g^*$ (see equation 3.5) the ratio approaches a finite value controlled by a small non-vanishing $\delta = N_f^{AF} - N_f$.

In the upper panel of figure 3.2, we plot η/s evaluated the the IR fixed point, $(\eta/s)^{IR}$, as function of the number of flavours, for fermions in the fundamental representation and $N = 3$. We express the coefficient A of equation 3.45 as a continuous function of the number of fermions via a linear fit of the values given in table 3.1. When decreasing the number of flavours below the asymptotically free boundary, where the shear viscosity diverges, we observe an abrupt decrease of η/s, while still remaining above the bound $\eta/s \geq 1/(4\pi)$ conjectured by AdS/CFT [46]. We expect that, when further decreasing the number of flavours, the IR ratio would decrease to reach a minimum value at the lower boundary of the conformal window. Below this critical number of flavours we expect the onset of chiral symmetry breaking and the theory in the deep IR becomes a theory of non-interacting pions with again a divergent value of η/s.

In the lower panel of figure 3.2, we present the temperature dependence of the shear viscosity over entropy density for several values of N_f. η/s depends on the temperature over a reference scale Λ via the gauge coupling. The reference energy scale is chosen such that the beta function reaches a minimum at $T = \Lambda$, between the UV and IR fixed points:

$$g^2(\Lambda) = \frac{3}{5}(g^*)^2 \,. \tag{3.50}$$

For $N_f = 6$, where theory does not display an IR perturbative fixed point, Λ is taken to be the scale at which the one-loop gauge coupling diverges. The ratio η/s decreases with decreasing temperature. For $N_f = 15$, we observe that a minimum develops at around $T = \Lambda$. This happens because for this value of N_f there exists a temperature such that $4 \ln (AT/m_D) = 1$, which corresponds to a minimum for the function $g^{-4} \ln (AT/m_D)^{-1}$.

We repeat the above analysis for the fermion number diffusion coefficient. In the upper panel of figure 3.3, we plot the value of the dimensionless quantity $(TD)^{IR}$ as a function of N_f, for fermions in the fundamental representation and $N = 3$. We linearly interpolate the values given in table 3.1 in order to express B as a continuous function of N_f. As for the case of the shear viscosity-to-entropy density ratio, we observe that $(TD)^{IR}$ diverges as the number of flavours approaches the asymptotic freedom boundary, corresponding to $g^* \to 0$. In the lower panel of figure 3.3, we plot TD as a function of the temperature for different values of N_f in the perturbative conformal window and for $N_f = 6$.

One comment has to be made about the applicability of the next-to-leading-log approximation for transport coefficients in the conformal window. The presence of a perturbative IR fixed point allows us to apply the next-to-leading-log results in the whole energy range, from the UV (high temperature), where the theory is asymptotically free, down to the IR (low temperature). However, particular care has to be taken to decide whether the values obtained in the deep IR can be trusted. We chose to illustrate the results for the case of three colours and for different values of the number of flavours within the perturbative conformal window. $N_f = 15$ is the last value at which we can observe the expected behaviour

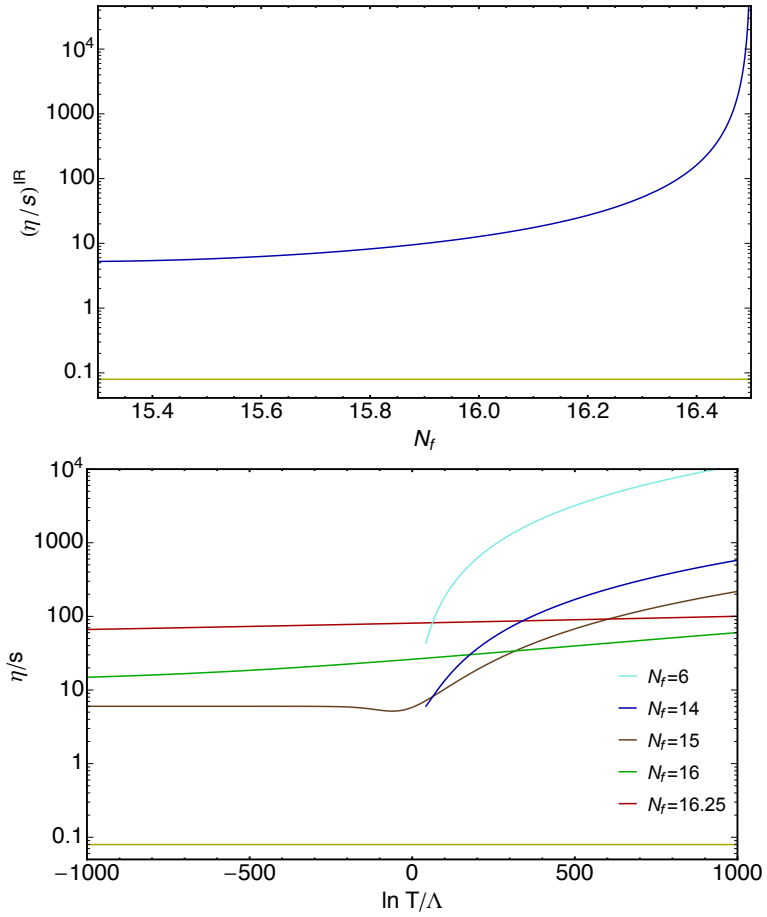

Figure 3.2: Upper panel: η/s evaluated at the IR fixed point, as a function of the number of flavours, for fermions in the fundamental representation and $N = 3$ colours. Lower panel: η/s as function of the temperature over the RG scale Λ for different values of N_f in the conformal window and one outside corresponding to $N_f = 6$, for $N = 3$ colours. Although $N_f = 14$ still displays a potential IR fixed point, the IR dynamics of η/s cannot be accessed perturbatively. The horizontal line at the bottom is the conjectured AdS/CFT bound. This picture has already been published in [36].

of the transport coefficients as functions of the temperature, i.e., to run from a divergent value in the UV down to a constant finite value in the IR. For $N_f = 14$, the next-to-leading-log expression of the transport coefficients does not stabilise at a finite value in the IR, but instead diverges at low energies, showing that the next-to-leading-log approximation cannot be trusted even qualitatively. In fact, following [42], one can argue that the next-to-leading-log result is very close to the full-leading-order result (and therefore trustable) as long as $m_D/T \leq 1$. This requirement is satisfied in our analysis provided $N_f \geq 16.25$, thus further limiting the window of applicability of the perturbative results. The values of m_D/T at the IR fixed point for $N = 3$ and the values of N_f within the conformal window considered in this study are reported in table 3.2.

To conclude, we summarise the salient points of our analysis. We determined the

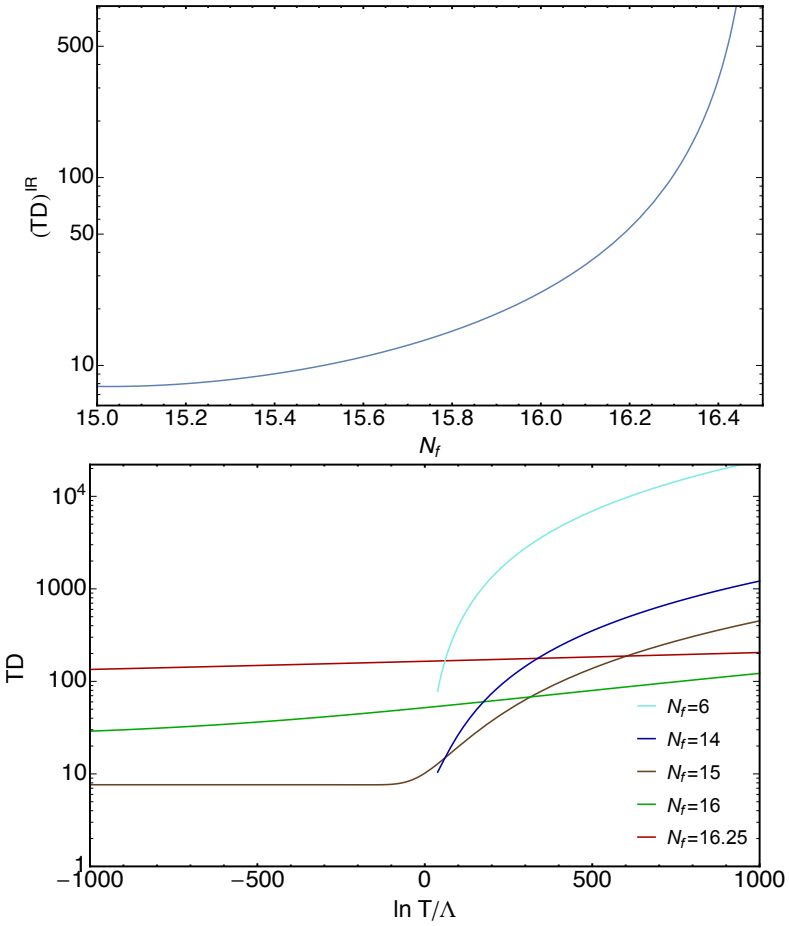

Figure 3.3: Upper panel: $(TD)^{IR}$ as a function of the number of flavours, for fermions in the fundamental representation and $N = 3$. Lower panel: TD as a function of the temperature, for different values of N_f and $N = 3$. This picture has already been published in [36].

shear viscosity-to-entropy density ratio and the fermion number diffusion coefficient (multiplied by the temperature) within the perturbative regime of the conformal window. This provides a theoretically relevant example in which the perturbative estimate of the transport coefficients can be used along the entire RG flow from the UV to the IR without losing validity. We determined the range of applicability of those results within the conformal window of QCD-like theories. In the case $N = 3$, we found out that already at $N_f = 14$ the next-to-leading-log results cannot be trusted even qualitatively. The ratio η/s at the IR fixed point drops significantly when going from 16.25 to 15 flavours showing that a modest change in the number of flavours dramatically affects the dynamics of the theory encoded in the transport coefficients. Higher-order corrections are needed to reach lower values of N_f within the conformal window for the transport coefficients. In contrast, at zero temperature one observes that perturbation theory allows to go quite low in the number of flavours within the conformal window [47, 48, 49, 50]. Although unproven, it is reasonable to expect that the minimum of η/s as function of temperature in QCD lies below the lowest value of η/s obtained at the bottom of the conformal window,

N_f	$(m_D/T)^{IR}$
14	3.41
15	2.51
16	1.38
16.25	0.97

Table 3.2: Values of the ratio m_D/T evaluated at the IR fixed point for $N = 3$ and different values of N_f in the conformal window. It can be observed that the constraint $m_D/T \leq 1$ is respected only in the case $N_f = 16.25$.

and therefore lower than the one obtained near 15 flavours.

Conclusions

Appendix A

A.1 General conventions and definitions

In this appendix we introduce the general notations and conventions used in the thesis.

A.1.1 Metric and units

We use the following convention for Minkowski metric:

$$(\eta_{\mu\nu}) = \mathrm{diag}[1, -1, -1, -1]\,. \tag{A.1}$$

As for the unit system, we use natural units, where the speed of light c, the reduced Planck constant $\hbar$ and the Boltzmann constant k_B are all set to unity.

A.1.2 Gamma matrices

Gamma matrices appear in the Dirac Lagrangian: $\mathcal{L}_D[\bar{\psi}, \psi] = \bar{\psi}(i\gamma^\mu D_\mu - m\mathbb{1})\psi$, and fulfil the following relations:

- Clifford algebra: $\left\{\gamma^\mu, \gamma^\nu\right\} = 2\mathbb{1}\eta^{\mu\nu}$
- Relation with the hermitian conjugate: $\gamma^\mu = \gamma^0(\gamma^\mu)^\dagger\gamma^0$.

As a consequence, the following equations hold:

- $(\gamma^0)^2 = \mathbb{1}$, $(\gamma^i)^2 = -\mathbb{1}$, $i = 1, 2, 3$
- $(\gamma^0)^\dagger = \gamma^0$, $(\gamma^i)^\dagger = -\gamma^i$, $i = 1, 2, 3$
- $\left\{\gamma^\mu, \gamma^\nu\right\} = 0$ if $\mu \neq \nu$.

γ_5 is defined by: $\gamma_5 = i\gamma^0\gamma^1\gamma^2\gamma^3$, and it has the following properties: $(\gamma_5)^2 = \mathbb{1}$, $(\gamma_5)^\dagger = \gamma_5$, $\left\{\gamma_5, \gamma^\mu\right\} = 0$. There exist multiple representations of the gamma matrices, and physical results do not depend on the choice of the representation. In this thesis we use the chiral representation:

$$\gamma^0 = \begin{pmatrix} 0 & \mathbb{1}_{2\times2} \\ \mathbb{1}_{2\times2} & 0 \end{pmatrix}, \qquad \gamma^i = \begin{pmatrix} 0 & \sigma^i \\ -\sigma^i & 0 \end{pmatrix}, \qquad \gamma_5 = \begin{pmatrix} -\mathbb{1}_{2\times2} & 0 \\ 0 & \mathbb{1}_{2\times2} \end{pmatrix}, \tag{A.2}$$

where σ^i, $i = 1, 2, 3$, are the Pauli matrices.

Gamma matrices are involved in the definition of the Lorentz group representation acting on Dirac spinors. In particular, the generators of Lorentz transformations are defined by: $J^{\mu\nu} = -i/4[\gamma^\mu, \gamma^\nu]$. Moreover, the parity transformation of a Dirac spinor is defined by:

$$\psi(\mathbf{x}, t) \to \psi'(\mathbf{x}, t) = \gamma^0 \psi(-\mathbf{x}, t) \,, \tag{A.3}$$

and the transformation under charge conjugation by:

$$\psi(x) \to \psi^C(x) = C\bar{\psi}(x)^T \,, \tag{A.4}$$

where the charge conjugation operator is $C = i\gamma^2\gamma^0$.

γ_5 appears in the definition of the chirality projectors:

$$P_L = \frac{\mathbb{1} - \gamma_5}{2} \,, \qquad P_R = \frac{\mathbb{1} + \gamma_5}{2} \,, \tag{A.5}$$

which have the following properties: $P_{R,L}^2 = P_{R,L}$, $P_R P_L = P_L P_R = 0$, $P_L + P_R = \mathbb{1}$, and are used to define left- and right-handed spinors:

$$\psi(x) = \psi_L(x) + \psi_R(x) \,, \qquad \psi_L(x) = P_L\psi(x) \,, \qquad \psi_R(x) = P_R\psi(x) \,. \tag{A.6}$$

The Dirac Lagrangian can be rewritten in terms of left- and right-handed Dirac spinors as follows:

$$\mathcal{L}_D = \bar{\psi}_L(i\gamma^\mu D_\mu)\psi_L + \bar{\psi}_R(i\gamma^\mu D_\mu)\psi_R - m(\bar{\psi}_L\psi_R + \bar{\psi}_R\psi_L) \,. \tag{A.7}$$

The Dirac Lagrangian in Euclidean space is: $\mathcal{L}_D^E[\bar{\psi}, \psi] = \bar{\psi}(\gamma_\mu^E D_\mu + m\mathbb{1})\psi$, where the relation between Minkowskian and Euclidean gamma matrices is:

$$\gamma_0^E = \gamma_0 \,, \qquad \gamma_i^E = i\gamma_i = -i\gamma^i \,. \tag{A.8}$$

Euclidean gamma matrices have the following properties:

- $\left\{\gamma_\mu^E, \gamma_\nu^E\right\} = 2\mathbb{1}\delta_{\mu\nu} \Rightarrow (\gamma_\mu^E)^2 = \mathbb{1}$
- $(\gamma_\mu^E)^\dagger = \gamma_\mu^E$

Euclidean γ_5 is defined by: $\gamma_5^E = \gamma_1^E\gamma_2^E\gamma_3^E\gamma_0^E$, and has analogue properties to Minkowskian γ_5: $(\gamma_5^E)^2 = \mathbb{1}$, $(\gamma_5^E)^\dagger = \gamma_5^E$, $\left\{\gamma_5^E, \gamma_\mu^E\right\} = 0$.

Euclidean gamma matrices in the chiral representation are given by:

$$\gamma_0^E = \begin{pmatrix} 0 & \mathbb{1}_{2\times2} \\ \mathbb{1}_{2\times2} & 0 \end{pmatrix} , \qquad \gamma_i^E = \begin{pmatrix} 0 & -i\sigma^i \\ i\sigma^i & 0 \end{pmatrix} , \qquad \gamma_5^E = \begin{pmatrix} \mathbb{1}_{2\times2} & 0 \\ 0 & -\mathbb{1}_{2\times2} \end{pmatrix} . \tag{A.9}$$

In this thesis we always omit the superscript E in gamma matrices, and we implicitly assume that every time we discuss a lattice model, which requires the Euclidean version of the action, gamma matrices assume their Euclidean form.

r	$T[r]$	$C_2[r]$	$d[r]$
$\square$	$\frac{1}{2}$	$\frac{N^2-1}{2N}$	N
G	N	N	N^2-1

Table A.1: Values of d, T and C_2 for the fundamental ($\square$) and adjoint (G) representation of SU(N).

A.1.3 SU(N) generators

We denote the generators of the representation r of SU(N) by T_r^a, with $a = 1, \ldots, N^2-1$. The generators are normalised as:

$$\mathrm{tr}\left[T_r^a T_r^b\right] = T[r]\delta^{ab} \,. \tag{A.10}$$

The quadratic Casimir $C_2[r]$ is defined by:

$$\sum_{a=1}^{N^2-1} T_r^a T_r^a = C_2[r]\mathbb{1} \,, \tag{A.11}$$

and it is related to $T[r]$ and the dimension of the representation $d[r]$ by:

$$C_2[r]d[r] = T[r]d[G] \,, \tag{A.12}$$

where G denotes the adjoint representation. The values of d, T and C_2 for the fundamental and adjoint representation are listed in table A.1.

A.2 Lattice Fourier transforms

In this appendix we define Fourier transforms on the lattice. The lattice Λ is defined as:

$$\Lambda = \{\, x_\mu = n_\mu a \mid n_\mu = 0, \ldots, L_\mu - 1,\ \mu = 0, \ldots, 3 \,\} \ , \tag{A.13}$$

where a is the lattice spacing and L_μ the number of lattice points in direction μ. The total number of lattice points V is given by: $V = \prod_{\mu=0}^{3} L_\mu$.

We consider a function $f(x)$ defined on the lattice, and we define its Fourier transform as:

$$\begin{aligned} f(x) &= \frac{1}{\sqrt{V}} \sum_{p \in \tilde{\Lambda}} \tilde{f}(p) e^{ip\cdot x} \\ \tilde{f}(p) &= \frac{1}{\sqrt{V}} \sum_{x \in \Lambda} f(x) e^{-ip\cdot x} \end{aligned} \tag{A.14}$$

where $\tilde{\Lambda}$ denotes the momentum space. Since the space-time has a finite volume, the momenta belong to a discrete set. Specifically, if periodic boundary conditions are imposed in direction μ, i.e. $f(x + aL_\mu\hat{\mu}) = f(x)$, then p_μ takes values in the discrete

set $\{\, p_\mu = \frac{2\pi}{aL_\mu} k_\mu \mid k_\mu \in \mathbb{Z} \,\}$. While in the case of anti-periodic boundary conditions, $f(x + aL_\mu \hat{\mu}) = -f(x)$, p_μ belongs to $\{\, p_\mu = \frac{2\pi}{aL_\mu}(\frac{1}{2} + k_\mu) \mid k_\mu \in \mathbb{Z} \,\}$. Moreover, since the coordinates x_μ of each lattice point are represented by integer numbers of lattice spacings, the momenta are periodic: $\tilde{f}(p) = \tilde{f}(p + \frac{2\pi}{a}\hat{\mu})$. Therefore, the momentum space is defined as:

$$\tilde{\Lambda} = \{\, p_\mu = \frac{2\pi}{aL_\mu}(k_\mu + \theta_\mu) \mid k_\mu = -\frac{L_\mu}{2} + 1, \ldots, \frac{L_\mu}{2},\ \mu = 0, \ldots, 3 \,\} \ , \tag{A.15}$$

where $\theta_\mu = 0$ corresponds to periodic boundary conditions in direction μ, and $\theta_\mu = 1/2$ to anti-periodic ones.

The lattice delta functions are defined as:

$$\begin{aligned} \delta(x - x') &= \delta_{n_0,n_0'}\delta_{n_1,n_1'}\delta_{n_2,n_2'}\delta_{n_3,n_3'} = \frac{1}{V}\sum_{p\in\tilde{\Lambda}} e^{ip\cdot(x-x')} \\ \delta(p - p') &= \delta_{k_0,k_0'}\delta_{k_1,k_1'}\delta_{k_2,k_2'}\delta_{k_3,k_3'} = \frac{1}{V}\sum_{x\in\Lambda} e^{i(p-p')\cdot x} \ . \end{aligned} \tag{A.16}$$

A.3 Hybrid Monte Carlo and the detailed balance relation

In this appendix we show that the HMC algorithm respects the detailed balance relation 1.15. We consider a scalar field theory with action $S[\phi]$. According to equation 1.54, the expectation value of an observable O is given by:

$$\langle O \rangle = \frac{\int \prod_x \mathrm{d}\phi(x)\mathrm{d}\pi(x)\, O[\phi] e^{-H[\pi,\phi]}}{\int \prod_x \mathrm{d}\phi(x)\mathrm{d}\pi(x)\, e^{-H[\pi,\phi]}} \ , \tag{A.17}$$

where the Hamiltonian is defined by: $H[\pi, \phi] = \frac{1}{2}\sum_x \pi(x)^2 + S[\phi]$.

The HMC algorithm consists of the following steps:

- The momenta $\pi(x)$ are extracted from a Gaussian distribution, with probability $P[\pi(x)] \propto \exp[-\pi(x)^2/2]$. This way an initial configuration of the momenta is defined

- Starting from the initial configuration (π, ϕ), the system evolves to a new state (π', ϕ') along a molecular dynamics trajectory which is a numerical solution of Hamilton's equations 1.55

- The final configuration (π', ϕ') is accepted or rejected in a Metropolis step, according to the transition probability

$$W_M(\pi, \phi \to \pi'\phi') = \min\left[1, \frac{e^{-H[\pi',\phi']}}{e^{-H[\pi,\phi]}}\right] . \tag{A.18}$$

We denote by $W_{\rm md}(\pi,\phi\to\pi',\phi')$ the probability of evolving from the state (π,ϕ) to (π',ϕ') along the molecular dynamics trajectory. We stress however that molecular dynamics is a deterministic process, and, given an initial state, all the following states in the trajectory are uniquely determined.

We further assume that the numerical integrator generating the molecular dynamics trajectory fulfils the following conditions:

- Preservation of the integration measure: $\prod_x \mathrm{d}\phi(x)\mathrm{d}\pi(x) = \prod_x \mathrm{d}\phi'(x)\mathrm{d}\pi'(x)$
- Reversibility: $W_{\rm md}(\pi,\phi\to\pi',\phi') = W_{\rm md}(-\pi',\phi'\to-\pi,\phi)$.

The probability to evolve from a scalar field configuration ϕ to ϕ' in one HMC step is given by:

$$W(\phi\to\phi') = \int\prod_x \mathrm{d}\pi(x)\mathrm{d}\pi'(x) W_M(\pi,\phi\to\pi',\phi') W_{\rm md}(\pi,\phi\to\pi',\phi') e^{-\sum_x \pi(x)^2/2} \,. \tag{A.19}$$

We rewrite Metropolis transition probability as follows:

$$\begin{aligned} W_M(\pi,\phi\to\pi',\phi') &= \min\left[1,\frac{e^{-H[\pi',\phi']}}{e^{-H[\pi,\phi]}}\right] = \frac{e^{-H[\pi',\phi']}}{e^{-H[\pi,\phi]}}\min\left[1,\frac{e^{-H[\pi,\phi]}}{e^{-H[\pi',\phi']}}\right] = \\ &= \exp\left[-\frac{1}{2}\sum_x \pi'(x)^2 - S[\phi'] + \frac{1}{2}\sum_x \pi(x)^2 + S[\phi]\right] W_M(\pi',\phi'\to\pi,\phi) \,, \end{aligned} \tag{A.20}$$

and we insert this expression in equation A.36:

$$\begin{aligned} W(\phi\to\phi') = \int\prod_x \mathrm{d}\pi(x)\mathrm{d}\pi'(x) W_M(\pi',\phi'\to\pi,\phi) W_{\rm md}(\pi,\phi\to\pi',\phi')\times \\ \exp\left[-\frac{1}{2}\sum_x \pi'(x)^2 - S[\phi'] + S[\phi]\right] . \end{aligned} \tag{A.21}$$

We now use the reversibility of the molecular dynamics trajectory, together with the fact that $W_M(\pi,\phi\to\pi',\phi')$ is quadratic in π and π':

$$\begin{aligned} W(\phi\to\phi') &= \exp\big[-S[\phi'] + S[\phi]\big] \int\prod_x \mathrm{d}\pi(x)\mathrm{d}\pi'(x) W_M(-\pi',\phi'\to-\pi,\phi)\times \\ &\qquad W_{\rm md}(-\pi',\phi'\to-\pi,\phi)\exp\big[-\sum_x \pi'(x)^2/2\big] = \\ &= \exp\big[-S[\phi'] + S[\phi]\big] W(\phi'\to\phi) \,, \end{aligned} \tag{A.22}$$

where in the last step we used the fact that the integration measure $\int\prod_x \mathrm{d}\pi(x)\mathrm{d}\pi'(x)$ and the factor $\exp\big[-\sum_x \pi'(x)^2/2\big]$ are invariant under a change of sign of π and π'. The detailed balance relation follows directly from equation A.37:

$$\exp\big[-S[\phi]\big]W(\phi\to\phi') = \exp\big[-S[\phi']\big]W(\phi'\to\phi)\,. \tag{A.23}$$

In the above proof we used explicitly the reversibility of the molecular dynamics process. The preservation of the integration measure $\prod_x \mathrm{d}\phi(x)\mathrm{d}\pi(x) = \prod_x \mathrm{d}\phi'(x)\mathrm{d}\pi'(x)$ is also required, because it ensures that in the path integral $\int \prod_x \mathrm{d}\phi(x)\mathrm{d}\pi(x)\, e^{-H[\pi,\phi]}$ each configuration is actually weighted by $e^{-H[\pi,\phi]}$, without the appearance of an extra Jacobian determinant.

A.4 Scalar quartic potential in an SU(2) gauge theory

We consider a theory of gauge-interacting scalars in the fundamental representation of the gauge group SU(2). We discuss which terms are allowed by colour and flavour symmetries in the quartic potential. In the case of a theory with a single scalar field, we also discuss the possibility of spontaneous flavour symmetry breaking due to a scalar condensate.

A.4.1 Single scalar field

We first consider the case of one single scalar field ϕ. A gauge transformation is given by:

$$\phi \to \phi' = U\phi \tag{A.24}$$

where $U \in \mathrm{SU}(2)$=Sp(2) is characterised by:

$$\begin{cases} U^\dagger U = \mathbb{1} \\ U^T \epsilon U = \epsilon \end{cases}, \tag{A.25}$$

ϵ being the two-dimensional antisymmetric tensor:

$$\epsilon = \begin{pmatrix} 0 & 1 \\ -1 & 0 \end{pmatrix}. \tag{A.26}$$

We can construct a field $\tilde{\phi} = -\epsilon\phi^*$ which transforms in the same way as ϕ under a gauge transformation: $\tilde{\phi} \to \tilde{\phi}' = U\tilde{\phi}$. We define a matrix S

$$S = (\phi, \tilde{\phi}) \tag{A.27}$$

which transforms as: $S \to S' = US$. The relation $\tilde{\phi} = -\epsilon\phi^*$ is translated in a relation between S and S^*:

$$S^* = -\epsilon S E\,, \tag{A.28}$$

where

$$E = \begin{pmatrix} 0 & 1 \\ -1 & 0 \end{pmatrix}. \tag{A.29}$$

Eq. A.28 can be verified as follows: we write the entries of S as S_{ia}, where $i = 1, 2$ is the colour index and $a = 1, 2$ is the flavour index, then we have $S_{i1} = \phi_i$, $S_{i2} = -\epsilon_{ij}\phi_j^* = -\epsilon_{ij}S_{j1}^*$. It follows that:

$$\begin{aligned}(\epsilon SE)_{i1} &= \epsilon_{ij}S_{ja}E_{a1} = -\epsilon_{ij}S_{j2} = -\epsilon_{ij}(-\epsilon_{jk}S_{k1}^*) = -\delta_{ik}S_{k1}^* = -S_{i1}^* \\ (\epsilon SE)_{i2} &= \epsilon_{ij}S_{ja}E_{a2} = \epsilon_{ij}S_{j1} = -S_{i2}^*\end{aligned} . \tag{A.30}$$

The kinetic term of the scalar Lagrangian is expressed in terms of S as follows:

$$\mathcal{L}_{kin} = \frac{1}{2}\mathrm{Tr}\big[(D_\mu S)^\dagger (D^\mu S)\big] . \tag{A.31}$$

Given a matrix $M \in \mathrm{U}(2)$ we define a flavour transformation

$$S \to S' = SM , \tag{A.32}$$

and we work out the conditions under which it is a symmetry of the kinetic term A.31. If we require $S'^* = -\epsilon S'E$, it follows that M must fulfil the following constraint:

$$EM^* = ME , \tag{A.33}$$

which, together with the fact that M is a unitary matrix, implies:

$$E = MEM^T . \tag{A.34}$$

The flavour symmetry group is therefore Sp(2)=SU(2).

The possible terms which are quartic in the field ϕ and symmetric under colour and flavour transformations are the following:

$$\begin{matrix}\big(\mathrm{Tr}\big[S^\dagger S\big]\big)^2 \\ \mathrm{Tr}\big[S^\dagger S S^\dagger S\big] \\ \big(\mathrm{Tr}\big[S^T \epsilon SE\big]\big)^2 \\ \mathrm{Tr}\big[S^T \epsilon SE S^T \epsilon SE\big]\end{matrix} . \tag{A.35}$$

The last two terms in A.35 can be shown to be equal to the first ones by applying equation A.28:

$$\begin{aligned}\big(\mathrm{Tr}\big[S^T \epsilon SE\big]\big)^2 &= \big(\mathrm{Tr}\big[S^T(-S^*)\big]\big)^2 = \big(-\mathrm{Tr}\big[(S^\dagger S)^*\big]\big)^2 \\ &= \big(\mathrm{Tr}\big[(S^\dagger S)\big]\big)^2\end{aligned} , \tag{A.36}$$

$$\begin{aligned}\mathrm{Tr}\big[S^T \epsilon SE S^T \epsilon SE\big] &= \mathrm{Tr}\big[S^T(-S^*)S^T(-S^*)\big] = \mathrm{Tr}\big[(S^\dagger S)^*(S^\dagger S)^*\big] \\ &= \mathrm{Tr}\big[S^\dagger S S^\dagger S\big] .\end{aligned} \tag{A.37}$$

The first and the second term in equation A.35 are not linearly independent when only one scalar field is present. To show this we start by explicitly writing $S^\dagger S$:

$$
\begin{aligned}
&S^\dagger S = \begin{pmatrix} \phi^\dagger\phi & \phi^\dagger\tilde{\phi} \\ \tilde{\phi}^\dagger\phi & \tilde{\phi}^\dagger\tilde{\phi} \end{pmatrix} \\
&\phi^\dagger\tilde{\phi} = -\phi_i^*\epsilon_{ij}\phi_j^* = 0 \qquad\qquad \Rightarrow S^\dagger S = \phi^\dagger\phi\,\mathbb{1}\,. \\
&\tilde{\phi}^\dagger\phi = -\epsilon_{ij}\phi_j\phi_i = 0 \\
&\tilde{\phi}^\dagger\tilde{\phi} = -\epsilon_{ij}\phi_j(-\epsilon_{ik}\phi_k^*) = \delta_{jk}\phi_j\phi_k^* = \phi^\dagger\phi
\end{aligned} \tag{A.38}
$$

It follows that: $(\mathrm{Tr}[S^\dagger S])^2 = 4(\phi^\dagger\phi)^2$, $\mathrm{Tr}[S^\dagger S S^\dagger S] = 2(\phi^\dagger\phi)^2$. In conclusion, the most general quartic potential for one single scalar field ϕ is given by:

$$
V = \lambda(\mathrm{Tr}[S^\dagger S])^2\,. \tag{A.39}
$$

We now consider gauge-symmetric scalar bilinears, which may cause spontaneous flavour symmetry breaking:

$$
\mathcal{S}_1 = \langle S^\dagger S\rangle\,, \qquad \mathcal{S}_2 = \langle S^T\epsilon S\rangle\,. \tag{A.40}
$$

Under the flavour transformation $S \to SM$, $M \in \mathrm{Sp}(2)$, they transform as:

$$
\mathcal{S}_1 \to M^\dagger\mathcal{S}_1 M\,, \qquad \mathcal{S}_2 \to M^T\mathcal{S}_2 M\,. \tag{A.41}
$$

In the following, we show that both $\mathcal{S}_1$ and $\mathcal{S}_2$ are symmetric under this transformation, and therefore there cannot be spontaneous flavour symmetry breaking in a theory with a singe scalar field. In the case of $\mathcal{S}_1$, this follows directly from equation A.38:

$$
\mathcal{S}_1 = \langle\phi^\dagger\phi\rangle\mathbb{1} \to M^\dagger\mathcal{S}_1 M = \langle\phi^\dagger\phi\rangle M^\dagger M = \mathcal{S}_1\,. \tag{A.42}
$$

We rewrite $\mathcal{S}_2$ as:

$$
\begin{aligned}
&(S^T\epsilon S)_{11} = \epsilon_{ij}\phi_i\phi_i = 0 \\
&(S^T\epsilon S)_{22} = -\epsilon_{ij}\phi_i^*\phi_j^* = 0 \qquad\qquad \Rightarrow \mathcal{S}_2 = \langle\phi^\dagger\phi\rangle\,E\,, \\
&(S^T\epsilon S)_{12} = -(S^\dagger\epsilon S)_{21} = \delta_{ij}\phi_i\phi_j^* = \phi^\dagger\phi
\end{aligned} \tag{A.43}
$$

implying that also $\mathcal{S}_2$ is symmetric under flavour transformations:

$$
\mathcal{S}_2 = \langle\phi^\dagger\phi\rangle E \to M^T\mathcal{S}_2 M = \langle\phi^\dagger\phi\rangle M^T E M = \mathcal{S}_2\,. \tag{A.44}
$$

A.4.2 Multiple scalar fields

In the case of N_S scalar fields ϕ_1, ϕ_2, … ϕ_{N_S} we define the $2 \times 2N_S$ matrix S as:

$$
S = (\phi_1, \tilde{\phi}_1, \ldots, \phi_{N_S}, \tilde{\phi}_{N_S})\,. \tag{A.45}
$$

A gauge transformation is expressed as:

$$
S \to S' = US\,, \quad \text{with} \quad U \in \mathrm{SU}(2)\,. \tag{A.46}
$$

S and S^* are related to each other by:

$$S^* = -\epsilon S E \tag{A.47}$$

where, in this case:

$$E = \mathrm{diag}(\epsilon, \ldots, \epsilon)\,. \tag{A.48}$$

The kinetic term is expressed as: $\mathcal{L}_{kin} = \frac{1}{2}\mathrm{Tr}\big[(D_\mu S)^\dagger (D^\mu S)\big]$. The constraint A.47 restricts flavour transformation to be: $S \to S' = SM$, with $M \in \mathrm{Sp}(2N_S)$. Given these definitions, the same arguments of equations A.35, A.36, A.37 apply, to show that the most general quartic potential for N_S scalar fields is:

$$V = \lambda_1 \big(\mathrm{Tr}\big[S^\dagger S\big]\big)^2 + \lambda_2 \mathrm{Tr}\big[S^\dagger S S^\dagger S\big]\,. \tag{A.49}$$

Bibliography

[1] N. Metropolis, A. W. Rosenbluth, M. N. Rosenbluth, A. H. Teller, and E. Teller, "Equation of state calculations by fast computing machines," *J. Chem. Phys.*, vol. 21, pp. 1087–1092, 1953.

[2] K. G. Wilson, "Confinement of Quarks," *Phys. Rev.*, vol. D10, pp. 2445–2459, 1974. [,319(1974)].

[3] K. G. Wilson, "Quarks and Strings on a Lattice," in *New Phenomena in Subnuclear Physics: Proceedings, International School of Subnuclear Physics, Erice, Sicily, Jul 11-Aug 1 1975. Part A*, p. 99, 1975. [,0069(1975)].

[4] F. Sannino, A. Strumia, A. Tesi, and E. Vigiani, "Fundamental partial compositeness," *JHEP*, vol. 11, p. 029, 2016.

[5] M. Hansen, T. Janowski, C. Pica, and A. Toniato, "SU(2) with fundamental fermions and scalars," *EPJ Web Conf.*, vol. 175, p. 08010, 2018.

[6] D. J. E. Callaway, "Triviality Pursuit: Can Elementary Scalar Particles Exist?," *Phys. Rept.*, vol. 167, p. 241, 1988.

[7] G. Degrassi, S. Di Vita, J. Elias-Miro, J. R. Espinosa, G. F. Giudice, G. Isidori, and A. Strumia, "Higgs mass and vacuum stability in the Standard Model at NNLO," *JHEP*, vol. 08, p. 098, 2012.

[8] L. Susskind, "Dynamics of Spontaneous Symmetry Breaking in the Weinberg-Salam Theory," *Phys. Rev.*, vol. D20, pp. 2619–2625, 1979.

[9] M. E. Peskin and D. V. Schroeder, *An Introduction to quantum field theory*. Reading, USA: Addison-Wesley, 1995.

[10] S. Weinberg, "Implications of Dynamical Symmetry Breaking," *Phys. Rev.*, vol. D13, pp. 974–996, 1976. [Addendum: Phys. Rev.D19,1277(1979)].

[11] B. Holdom, "Raising the Sideways Scale," *Phys. Rev.*, vol. D24, p. 1441, 1981.

[12] K. Yamawaki, M. Bando, and K.-i. Matumoto, "Scale Invariant Technicolor Model and a Technidilaton," *Phys. Rev. Lett.*, vol. 56, p. 1335, 1986.

[13] D. D. Dietrich, F. Sannino, and K. Tuominen, "Light composite Higgs from higher representations versus electroweak precision measurements: Predictions for CERN LHC," *Phys. Rev.*, vol. D72, p. 055001, 2005.

[14] T. Appelquist and Y. Bai, "A Light Dilaton in Walking Gauge Theories," *Phys. Rev.*, vol. D82, p. 071701, 2010.

[15] D. B. Kaplan, H. Georgi, and S. Dimopoulos, "Composite Higgs Scalars," *Phys. Lett.*, vol. 136B, pp. 187–190, 1984.

[16] D. B. Kaplan and H. Georgi, "SU(2) x U(1) Breaking by Vacuum Misalignment," *Phys. Lett.*, vol. 136B, pp. 183–186, 1984.

[17] G. Cacciapaglia and F. Sannino, "Fundamental Composite (Goldstone) Higgs Dynamics," *JHEP*, vol. 04, p. 111, 2014.

[18] R. Arthur, V. Drach, M. Hansen, A. Hietanen, C. Pica, and F. Sannino, "SU(2) gauge theory with two fundamental flavors: A minimal template for model building," *Phys. Rev.*, vol. D94, no. 9, p. 094507, 2016.

[19] S. Dimopoulos and L. Susskind, "Mass Without Scalars," *Nucl. Phys.*, vol. B155, pp. 237–252, 1979. [2,930(1979)].

[20] E. Eichten and K. D. Lane, "Dynamical Breaking of Weak Interaction Symmetries," *Phys. Lett.*, vol. 90B, pp. 125–130, 1980.

[21] D. B. Kaplan, "Flavor at SSC energies: A New mechanism for dynamically generated fermion masses," *Nucl. Phys.*, vol. B365, pp. 259–278, 1991.

[22] C. Pica and F. Sannino, "Anomalous Dimensions of Conformal Baryons," *Phys. Rev.*, vol. D94, no. 7, p. 071702, 2016.

[23] G. Cacciapaglia, H. Gertov, F. Sannino, and A. E. Thomsen, "Minimal Fundamental Partial Compositeness," *Phys. Rev.*, vol. D98, no. 1, p. 015006, 2018.

[24] F. Sannino, P. Stangl, D. M. Straub, and A. E. Thomsen, "Flavor Physics and Flavor Anomalies in Minimal Fundamental Partial Compositeness," *Phys. Rev.*, vol. D97, no. 11, p. 115046, 2018.

[25] F. F. Hansen, T. Janowski, K. Langæble, R. B. Mann, F. Sannino, T. G. Steele, and Z.-W. Wang, "Phase structure of complete asymptotically free SU(N_c) theories with quarks and scalar quarks," *Phys. Rev.*, vol. D97, no. 6, p. 065014, 2018.

[26] L. Del Debbio, A. Patella, and C. Pica, "Higher representations on the lattice: Numerical simulations. SU(2) with adjoint fermions," *Phys. Rev.*, vol. D81, p. 094503, 2010.

[27] I. P. Omelyan, I. M. Mryglod, and R. Folk, "Optimized verlet-like algorithms for molecular dynamics simulations," *Phys. Rev. E*, vol. 65, p. 056706, May 2002.

[28] I. Omelyan, I. Mryglod, and R. Folk, "Symplectic analytically integrable decomposition algorithms: classification, derivation, and application to molecular dynamics, quantum and celestial mechanics simulations," *Computer Physics Communications*, vol. 151, no. 3, pp. 272 – 314, 2003.

[29] W. Caudy and J. Greensite, "On the ambiguity of spontaneously broken gauge symmetry," *Phys. Rev.*, vol. D78, p. 025018, 2008.

[30] E. H. Fradkin and S. H. Shenker, "Phase Diagrams of Lattice Gauge Theories with Higgs Fields," *Phys. Rev.*, vol. D19, pp. 3682–3697, 1979.

[31] K. Osterwalder and E. Seiler, "Gauge field theories on a lattice," *Annals of Physics*, vol. 110, no. 2, pp. 440 – 471, 1978.

[32] M. Wurtz and R. Lewis, "Higgs and W boson spectrum from lattice simulations," *Phys. Rev.*, vol. D88, p. 054510, 2013.

[33] S. Elitzur, "Impossibility of Spontaneously Breaking Local Symmetries," *Phys. Rev.*, vol. D12, pp. 3978–3982, 1975.

[34] W. Langguth and I. Montvay, "Two State Signal at the Confinement Higgs Phase Transition in the Standard SU(2) Higgs Model," *Phys. Lett.*, vol. 165B, pp. 135–139, 1985.

[35] F. Sannino, "Dynamical Stabilization of the Fermi Scale: Phase Diagram of Strongly Coupled Theories for (Minimal) Walking Technicolor and Unparticles," 2008.

[36] A. Toniato, F. Sannino, and D. H. Rischke, "Viscous Conformal Gauge Theories," *Phys. Rev.*, vol. D96, no. 1, p. 016020, 2017.

[37] P. B. Arnold, G. D. Moore, and L. G. Yaffe, "Transport coefficients in high temperature gauge theories. 1. Leading log results," *JHEP*, vol. 11, p. 001, 2000.

[38] T. Banks and A. Zaks, "On the Phase Structure of Vector-Like Gauge Theories with Massless Fermions," *Nucl. Phys.*, vol. B196, pp. 189–204, 1982.

[39] A. J. Hietanen, J. Rantaharju, K. Rummukainen, and K. Tuominen, "Spectrum of SU(2) lattice gauge theory with two adjoint Dirac flavours," *JHEP*, vol. 05, p. 025, 2009.

[40] M. Hansen, V. Drach, and C. Pica, "SU(3) sextet model with Wilson fermions," *Phys. Rev.*, vol. D96, no. 3, p. 034518, 2017.

[41] L. Landau and E. Lifshitz, *Fluid Mechanics*. No. v. 6, Elsevier Science, 2013.

[42] P. B. Arnold, G. D. Moore, and L. G. Yaffe, "Transport coefficients in high temperature gauge theories. 2. Beyond leading log," *JHEP*, vol. 05, p. 051, 2003.

[43] G. D. Moore. Private communication.

[44] K. Kajantie, M. Laine, K. Rummukainen, and Y. Schroder, "The Pressure of hot QCD up to g6 ln(1/g)," *Phys. Rev.*, vol. D67, p. 105008, 2003.

[45] M. Mojaza, C. Pica, and F. Sannino, "Hot Conformal Gauge Theories," *Phys. Rev.*, vol. D82, p. 116009, 2010.

[46] P. Kovtun, D. T. Son, and A. O. Starinets, "Viscosity in strongly interacting quantum field theories from black hole physics," *Phys. Rev. Lett.*, vol. 94, p. 111601, 2005.

[47] C. Pica and F. Sannino, "Beta Function and Anomalous Dimensions," *Phys. Rev.*, vol. D83, p. 116001, 2011.

[48] C. Pica and F. Sannino, "UV and IR Zeros of Gauge Theories at The Four Loop Order and Beyond," *Phys. Rev.*, vol. D83, p. 035013, 2011.

[49] T. A. Ryttov and R. Shrock, "Higher-Loop Corrections to the Infrared Evolution of a Gauge Theory with Fermions," *Phys. Rev.*, vol. D83, p. 056011, 2011.

[50] T. A. Ryttov and R. Shrock, "Infrared Zero of β and Value of γ_m for an SU(3) Gauge Theory at the Five-Loop Level," *Phys. Rev.*, vol. D94, no. 10, p. 105015, 2016.